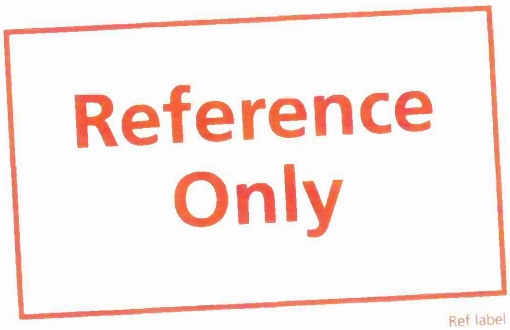

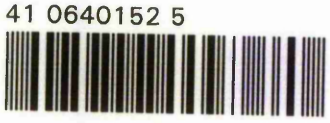

Measurement of Surface-Protein Interactions on Novel Surfaces

Paul Roach

A thesis submitted in partial fulfilment of the requirements of The Nottingham Trent University for the degree of Doctor of Philosophy

This research programme was carried out in collaboration with Smith and Nephew Ltd

The Nottingham Trent University October 2005

Abstract

This thesis is concerned with the fundamental principles affecting protein adsorption. The effects of surface chemistry and topography on protein adsorption characteristics have been identified and quantified. Particular attention has been made to understand how the conformation of surface-bound proteins was affected by the surface onto which they adsorbed.

Quartz crystal microbalance (QCM), UV-Vis spectroscopy and fluorometry were used to assess protein-surface affinity and amounts of protein adsorbed at surface saturation levels. Infrared spectroscopy was used to quantify protein conformational changes incurred upon adsorption. A fluorescent assay protocol was developed for use as an external calibration method for the quantification of adsorbed protein an d the results obtained were compared with QCM and an amido black protein assay of the same systems. Model experiments were performed using bovine fibrinogen (an elongated molecule) and albumin (a globular molecule) adsorbing onto flat hydrophilic (OH terminated) and hydrophobic (CH_3 terminated) surfaces in the first instance, but later superhydrophilic and superhydrophobic surfaces were also studied. Surface curvature on the nano-scale was used to model topography, wherein protein molecules adsorbed onto spherical substrates (15-165 nm diameter) having chemically defined surfaces.

Results obtained indicate that both proteins exhibit a less organised secondary structure upon adsorption onto hydrophobic compared to hydrophilic surfaces, with this effect being greatest for albumin. Adsorption rates and binding affinities were found to be higher on hydrophobic surfaces although the amounts adsorbed at saturation were lower. Supporting spectroscopic data suggests that proteins undergo surface induced deformation upon adsorption. Topography was shown to compound the effects of surface chemistry, with fibrinogen being more denatured on surfaces presenting high surface curvature whereas albumin was more denatured on larger substrates. These effects are most probably due to the differing size and shape of the proteins investigated.

This study highlights the possibility of using tailor-made surfaces to influence binding rates and the conformation of bound proteins through protein-surface interactions. The data presented in this thesis demonstrates our ability to control protein adsorption characteristics through careful consideration of the underlying surface, which may facilitate the development and fabrication of materials / surface coatings with tailored bioactivity.

Acknowledgements

I would like to thank Prof. Carole C. Perry for her support, guidance and never-ending patience throughout my time at The Nottingham Trent University.

I am deeply indebted to past and present members of the inorganic chemistry research group who have always supplied good humour and interesting debate, especially over morning coffee. I particularly wish to thank Dr N.J. Shirtcliffe, Dr S.V. Patwardhan, Dr. K. Shafran and Dr D. Belton.

Staff members across the faculty of science at The Nottingham Trent University have been very kind and helpful. I thank all of those who have allowed me to use their equipment and lab space over the past years, especially David Chambers-Asman.

I gratefully acknowledge financial support from Smith and Nephew and support and kindness from the research centre in York, particularly Mr D. Farrar.

I would also like to give a special thanks to Lucy who has helped me so much. I thank you for putting up with me, especially over the past three years.

Mostly I owe thanks to my parents John and Madeline Roach and my brother David who have given me the support and encouragement to get me where I am today.

Contents

Abbreviations

A	Surface area
ATR	Attenuated total reflectance
BSA	Bovine serum albumin
C	BET constant
c	Concentration of adsorbing species
CA	Contact angle
CD	Circular dichroism
d	Thickness of substrate
d_p	Penetration depth of radiation into substrate
ε	Molar extinction coefficient
f	Fraction of surface area in contact with liquid
f_0	Fundamental resonant frequency
Fg	Fibrinogen
FTIR	Fourier transform infrared spectroscopy
G	Gibbs free energy
γ	Surface energy
GA	Grazing angle
H	Enthalpy of adsorption
h	Planck's constant
I	Intensity of radiation
IRE	Internal reflection element
φ_x	Surface fraction having contact angle 'q_x'
k	Affinity constant
l	Pathlength of radiation through sample
M	Added mass of adsorbing layer
m	Mass change per unit area
MTEOS	Methyl triethoxysilane
MW	Molecular weight
m_x	Sheer modulus of mass 'x'
N	Avogadro's number
NMR	Nuclear magnetic resonance

n_x	Refractive index of material 'x'
PBS	Phosphate buffered saline
P_a	Ambient pressure
Q	Adsorbate surface concentration
QCM	Quartz crystal microbalance
Q_m	Maximum adsorbate binding capacity
r_p	Average pore radius
ρ_x	Density of mass 'x'
S	Entropy of adsorption
SAM	Self assembled monolayer
SEM	Scanning electron microscopy
SPR	Surface plasmon resonance
T	Absolute temperature
t	Adsorbed layer thickness
TEM	Transmission electron microscopy
t_q	Thickness of quartz
v	Frequency of radiation
V_{ads}	Volume of nitrogen adsorbed
V_{liq}	Volume of liquid nitrogen
V_p	Average pore volume
W_m	Mass of adsorbing monolayer
v_q	Velocity of the shear wave in quartz

List of Figures

List of Tables

Chapter 1

Introduction

1.1 Biomaterials

There have been many definitions proposed for the term 'biomaterial' usually pertaining to any natural or synthetic substance (or combination of substances) that can be used for any period of time to treat, augment or replace any tissue, organ or function within the body. A more up-to-date definition has broadened to include advances in technology such as biosensors[1,2] and drug delivery systems: 'substances other than food or drugs which are contained in therapeutic or diagnostic systems.'[3]

Approximately 300,000 hip and knee implants and between 100,000 and 300,000 dental implants are used, along with many other medical implants, each year in the US alone,[4] making the biomaterials market hugely profitable, Table 1.1. The objective of modern implantology is to design devices that accommodate accelerated and controlled healing. Research aimed towards surface modification of implants to induce protein and cell adhesion would not only lead to rapid healing and faster recuperation of the patient, but also allow stable fixation between the implant and

surrounding tissue leading to early loading of the device. The latter point is important in terms of decreased patient morbidity and health care costs.

Table 1.1. European Market for Orthopedic Biomaterials, statistics from 2001. Source, Millennium Research Group.

Product	2001 Market Value / US$M	Compound Annual Growth Rate (2002-2006) / %
Bone Graft Substitutes	44.6	13.2
Growth Factors	0.5	114.0
Bone Cements	46.8	4.0
Resorbable Tissue Fixation Devices	19.9	8.6
Autologous Chondrocyte Implantation	7.4	23.2
Hyaluronic Acid Viscosupplementation (Biopolymer)	69.9	8.2
TOTAL	186.1	12

Events leading to the integration of an implant into the surrounding tissue and hence determining its performance take place at the tissue-implant interface.[5-7] Development of this interface is key in the modification and improvement of such devices; to integrate them into the body, such that they prove to be biocompatible.

1.2 Biocompatibility

The general definition of biocompatibility describes the performance of a biomaterial within its intended biological environment, 'the ability of a material to perform with an appropriate host response in a specific application.' The broadness of the definition is necessary because of the two main points which one must take into account: '*appropriate host response*' and '*specific application.*' The nature of any material is governed by its purpose and intended working environment. Depending on where a specific material is implanted these two points may relate to very different requirements. For instance a biomaterial intended for a hip replacement would require substantial protein and cell attachment allowing it to be incorporated into the body and function properly. If this same material were used to produce vascular stents such results would not be desirable as a vascular stent is required to hold open a blood vessel

and definitely does not require attachment of any bodily tissues as these would result in the vessel being blocked.

Several other issues describing the properties of a biomaterial and / or an implant device can be addressed. Blood compatibility – thrombus formation should always be minimised. Inflammation – this is usually involved during a natural wound healing process, although it should be controlled. Tissue encapsulation – the result of an active immune response to a foreign material is not desired as it can lead to expulsion of the material. Toxicity – obviously not desired unless the device (such as a drug delivery system) is intended to provide such an effect. Physical and mechanical properties – if a biomaterial or device fails either physically or mechanically it can be termed non-biocompatible.

1.3 The Tissue-Implant Interface

It has been suggested that biological tissues interact with only the outermost atomic layers of an implant.[7] Consequently much research has been devoted to methods that modify the surfaces of existing biomaterials to achieve more desirable biological integration by changing morphological,[8,9] physiochemical[10-12] or biochemical parameters[13-15].

Biocompatibility is closely related to cell behaviour in contact with surfaces and can be described by the response of the host to implantation and the response of the biomaterial to the host. On implantation, foreign materials are conditioned with biological fluid components creating the tissue-implant interface which can change with response of the host organism and degradation of the implant material.[16] Vigorous immunological events may arise which aim to destroy any potential pathogens and foreign bodies. The precise nature of the immune response is a consequence of the type of material implanted and is an important factor to consider in the design of such devices. For a material to be successful at an implantation site, the ensuing immune reaction should be localised and not result in a reaction that will damage the material or the host.

During any operation to implant a foreign material into a host body numerous responses occur as a result of the surgical trauma and reaction of the host to the implanted material. The body uses very specific cell signalling to heal wounds which is usually disrupted by the implantation of a foreign material. The adsorption of a protein

layer on the surface of the material is the first stage of integration although depending on the characteristics of the protein layer the immune system may be alerted to a foreign invader and trigger a cascade of reactions.[17] Biological surface science is therefore a very complex and diverse field, the aim being to initiate normal wound healing responses by the control of protein adsorption, conformation and orientation.

The role of protein adsorption and subsequent cell adhesion to biomaterials is key in terms of the performance of an implant; from the time of implantation and throughout its lifetime. Before providing detail about protein adsorption, the importance of protein structure and function in relation to protein composition will be described.

1.4 Diversity of Proteins

Proteins are complex structures consisting of one or more polypeptide strands, each constructed from amino acids. There are 20 common amino acids having differing chemical natures dependant on their side chains, Table 1.2.

Table 1.2. Amino acids

Amino Acid	Abbreviations	Molecular structure	Character
Alanine	ALA A		Non-polar. Hydrophobic.
Isoleucine	ILE I	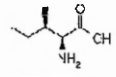	
Leucine	LEU L	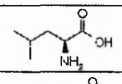	
Methionine	MET M	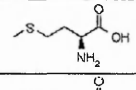	
Phenylalanine	PHE F	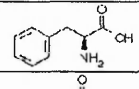	
Proline	PRO P		
Tryptophan	TRP W	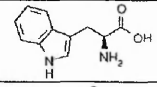	
Valine	VAL V	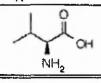	

Table 1.2 Continued. Amino Acids

Amino Acid	Abbreviations	Molecular structure	Character
Asparagine	ASN N	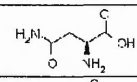	Polar. Neutral. Hydrophilic.
Cysteine	CYS C	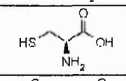	
Glutamine	GLN Q	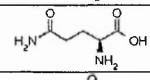	
Glycine	GLY G	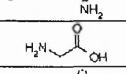	
Serine	SER S	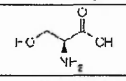	
Threonine	THR T	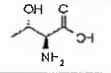	
Tyrosine	TYR Y	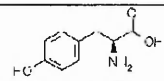	
Aspartic acid	ASP D	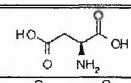	Polar. Negative. Hydrophilic.
Glutamic acid	GLU E	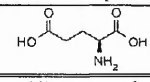	
Arginine	ARG R	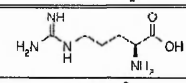	Polar. Positive. Hydrophilic.
Histidine	HIS H	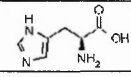	
Lysine	LYS K	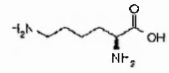	

Glycine is the simplest and smallest amino acid with a hydrogen atom side chain, allowing much more conformational flexibility compared to other amino acids. Alanine has a methyl group side chain giving it hydrophobic character, along with the larger non-polar amino acids, valine, leucine, ioleucine and tryptophan. These interact with other hydrophobic groups rather than with water and so tend to play important roles in holding protein chains together by hydophobic bonding, stabilising the folded conformations of proteins. Conversely, polar side chains, such as those in serine and threonine, convey hydrophilic character.

Each protein differs from another by the composition and length of its amino acid backbone, termed its primary structure. The polypeptide chain can fold and turn to interact with itself or, if present, another polypeptide chain within the same protein. The specific secondary structure is therefore determined by protein composition with each amino acid allowing a degree of flexibility of the backbone, although segments brought

together by polypeptide folds may interact with each other. Secondary structure elements are local spatial structures which occur due to interactions between differing segments of the backbone, giving rise to helix, sheet, random coil or extended chain structures, Figure 1.1. The tertiary structure is the overall shape of the protein, formed as a result of interaction between secondary structure elements. Electrostatic forces, Van der Waals interactions, hydrogen bonding and hydrophobic interactions are all factors involved in the stabilisation of the protein structure.

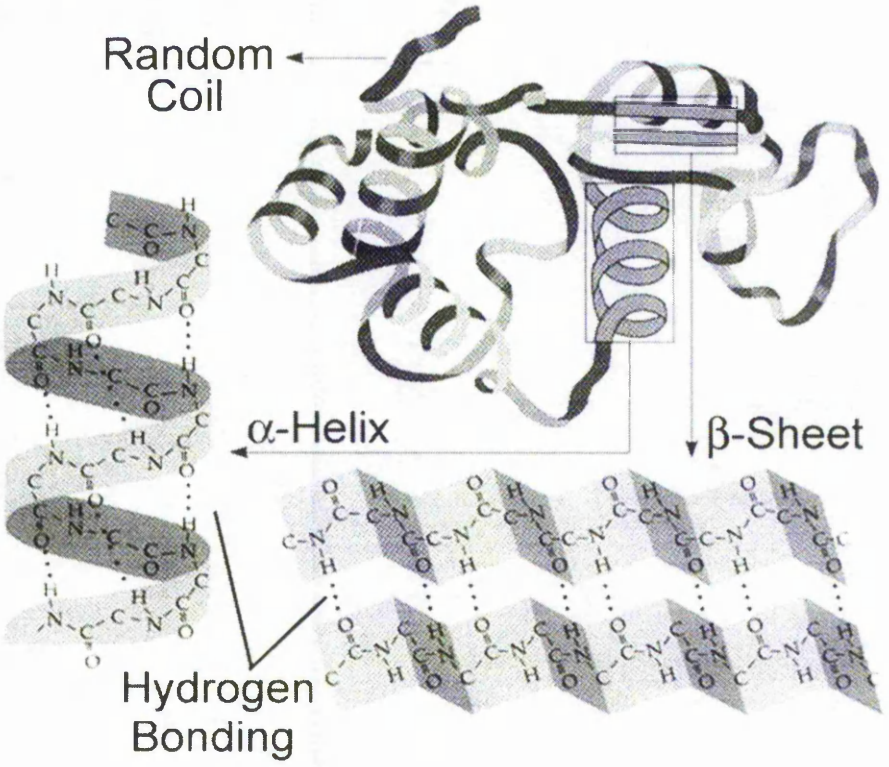

Figure 1.1. Schematic of protein secondary structure elements.

The diversity of proteins is apparent when considering the number of differing amino acid sequence lengths and combinations, giving rise to the unique features exhibited by different proteins. The spatial arrangement of each individual amino acid within a protein has a relative effect on its properties. Residues pointing outward would be available for surface interaction whereas those in the core would not. Unfolding, or denaturing of the protein would allow the inner residues to become accessible to the external environment thereby making them available to take part in outwardly

interactions. Such a deformation may be induced by the protein interacting with a surface.

1.5 Protein Adsorption

The adsorption of proteins to surfaces can be defined as the accumulation of protein at a solid-liquid interface. Driven by thermodynamics, Equation 1.1, a spontaneous adsorption process reduces the overall energy of the system, releasing energy as proteins move from an aqueous environment onto a solid surface.

$$\Delta G_{ads} = \Delta H_{ads} - T\Delta S_{ads} \qquad \text{Equation (1.1)}$$

Where 'G' is the Gibbs free energy of the system, 'H' is the enthalpy of adsorption, 'T' is absolute temperature and 'S' is the entropy of the adsorption process. For the process to be spontaneous the overall free energy must be negative. This may be realised by taking into account several factors:[18-21]

- Electrostatic interactions between protein and adsorbate surface, possibly along with co-adsorption of ions. The most favourable situation for protein adsorption is that of charge neutralisation without ion incorporation.

- Dehydration (and / or changes in the hydration state) of the adsorbate surface and regions of the protein. Hydrophobic residues are normally hidden within the interior of the proteins structure but still a large fraction of the outer surface of proteins can be hydrophobic which is unfavourable if the protein is in aqueous medium.

- Structural rearrangements of the protein can be both entropically and enthalpically favourable for protein adsorption, due to the decrease in ordered secondary structure and increase in intramolecular hydrogen bonding respectively. Bonding between neighbouring protein molecules can allow hydrophobic regions to be shielded from the aqueous phase, due to the increase in flexibility of the polypeptide backbone brought about by loss of secondary structure. Van der Waals, electrostatic and hydrogen bonds can also form which are enthalpically favourable.

o Dispersion interactions – always favourable but are lower with lower molecular weight proteins and an increase in distance between protein and the surface.

All these factors may contribute to the adsorption process although dehydration and structural rearrangements of the protein are thought to be the dominant factors.

Depending on the protein solution concentration and particular protein-surface interactions a maximum surface concentration is reached which can be in the order of 1000 times greater than the concentration of the bulk.[17] At higher concentrations a limiting value is reached, which is generally assumed to be that of a monolayer of adsorbed protein, although a protein multilayer may accumulate at a surface due to specific or non-specific interactions between surface-bound proteins and 'free' proteins in solution. Protein-surface interactions are very important factors when considering the adsorbed state. If the interaction is very high it is thought that protein deformation occurs, either on adsorption or some time thereafter due to surface rearrangement, a process sometimes termed '*relaxation*'. This probably involves the protein spreading to increase its interaction with the surface and / or to decrease its interaction with the aqueous phase, resulting in the immobilisation of proteins (those less likely to desorb). Similarly, differing protein-surface interactions could force protein molecules to adopt specific orientations. As a result the protein may lose the specific structure required for activity, or functional sites may become obscured due to conformational / orientational rearrangements that hinder protein function, e.g. antibody binding, Figure 1.2.

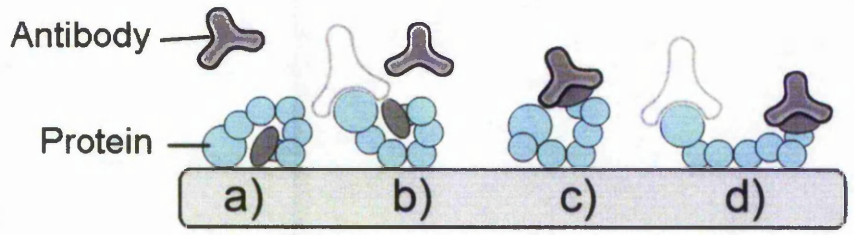

Figure 1.2. Schematic of protein conformational / orientational change upon adsorption that may hinder normal function: a) no antibody binding, b) and c) restricted binding of one antibody and d) both antibodies may bind, due to a) orientational and b-d) conformational control.

Protein adsorption occurs almost immediately on implantation of biomaterials,[22,23] a process affected by many factors including temperature, protein concentration, pH, ionic strength and solution composition and functional groups of proteins and substrates[6,24-26].

On implantation a material is conditioned in several stages by biological fluids and components therein.[5,27] Firstly a water layer will form on the surface and accommodate ions from the bioliquid. Shortly after, blood proteins and other macromolecules (e.g. lipids and sugars) arrive at the surface. Since blood contains many hundreds of differing proteins competition for the surface ensues. After a complex process of adsorption, desorption and surface rearrangement, wherein the protein layer composition changes dramatically over time, equilibrium is reached at the interface. It is generally accepted that the more abundant small proteins will adsorb first due to their rapid transport to the surface. Over time these are then replaced by larger proteins with a greater affinity towards the surface. The '*surface enrichment*' of fibrinogen was first observed by Vroman and Adams and is generally termed the 'Vroman effect'.[28] The protein layer may then susequently mediate cell attachment and progressively the material is integrated into the biological system.[29,30]

To briefly summarise, proteins adsorb in differing quantities, densities, conformations, and orientations, depending on the chemical and physical characteristics of the surface.[25,26,31-33] Although surface-protein interactions are not well understood, surface chemistry has been shown to play a fundamental role in protein adsorption.[25,26,33] Moreover, the properties of protein over-layers can be altered by the underlying surface chemistry, which directly impinges on control of conformation and/or orientation.[25,26]

1.6 Cell Adhesion

Cells are complex, self sustaining units that interact and communicate intracellularly via receptors located on their outer walls. Specific binding of antibodies or antigens to these receptors creates a receptor response, which starts a chain reaction of events within the cell leading to an appropriate trigger response. One such class of cell receptors called 'integrins' bind specifically to an arginine-glycine-aspartic acid (RGD) tripeptide found in cell adhesive proteins such as fibronectin,[30] vitronectin and

laminin, which in turn can attach to solid surfaces. Therefore it has been suggested that adsorbed proteins may act as pilots for cell adsorption if they have the correct geometry to mediate attachment,[34,35] Figure 1.3.

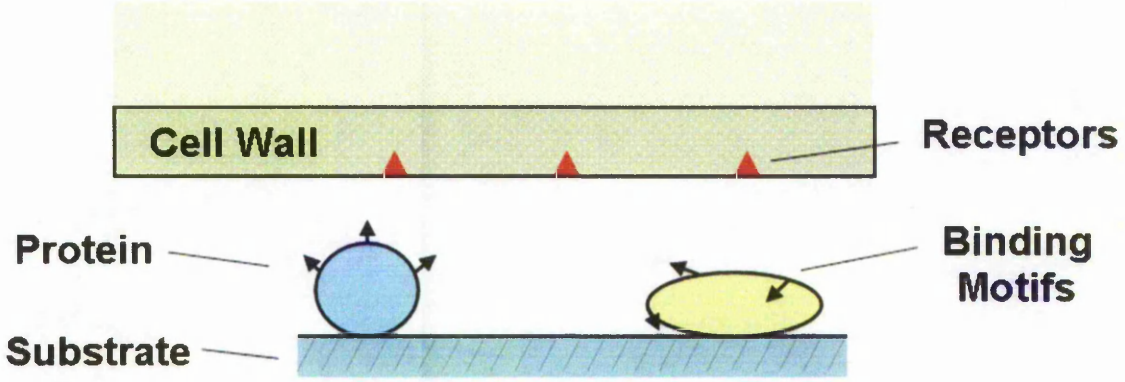

Figure 1.3. Model showing cell-surface attachment mediated through pre-adsorbed proteins.

Cells sense their surroundings using protrusions termed '*lamellipodia*' in epithial cells and fibroblasts, or '*pseudopodia*' in amoebae and neutrophils. These are micron sized sheet-like structures composed of an actin filament mesh which lies parallel to the surface but can be pushed back across the cell if attachment to the surface is not possible. On the ends of these, smaller hair-like protrusions termed '*filopodia*', composed of long, thin actin filament bundles act as feelers to sense the extracellular matix and substrate surface. When the *filopodia* find a suitable binding site, such as the lock and key integrin binding sites discussed earlier, a feedback signalling pathway within the cell allows more integrin receptors to be localised in that region of the cell. By progressively sending out *lamellipodia* along the leading edge of the cell focal contacts can then be made allowing the cell to adhere and move across a surface. In fact cells crawl across a surface allowing them to proliferate and spread. Non-adhesion of cells is fatal, likewise, if cells adhere too tightly to a surface they cannot proliferate and also die. A solution between these extremes is therefore the most desirable situation for healthy, confluent cell cultures.

In a physiological environment cell adhesion always follows protein adsorption. Although cell-surface interactions are understood to be affected by underlying surface chemistry, structural information on surface bound protein conformations and

geometries governing cell adhesion have not yet been elucidated. The ability of antibody binding assays to detect the availability of specific binding sites provides indirect evidence of protein conformational or orientational change upon adsorption, although no structural information can be obtained from such investigations.[36] Other analytical tools have been used to study protein adsorption[25,32,37-42] yet only generalized information on the adsorbed protein has been presented, implying conformational change and detailed secondary structure analysis of the adsorbed proteins has not been reported.

1.7 Surface Control

1.7.1 Chemistry

It has been demonstrated that the surface chemistry of an implanted material, that is the chemical environment at the molecular level, is important and can be altered to induce protein[31,32,40,43-50] and cell[51-55] adhesion, although the specific mechanism is still unknown. There is great interest in this field with a number of review articles being published in recent years.[5,6,27,56]

It is possible to control cell movement and growth by chemically patterning surfaces, Figure 1.4. Hydrophobic regions hinder cell attachment and spreading although neighbouring hydrophilic regions allow cells to attach and spread.[51,52,57-59] More recently control of cell signalling by surface chemistry has been directly demonstrated – an extremely important break-through highlighting the importance of protein adhesion control for cell binding.[60]

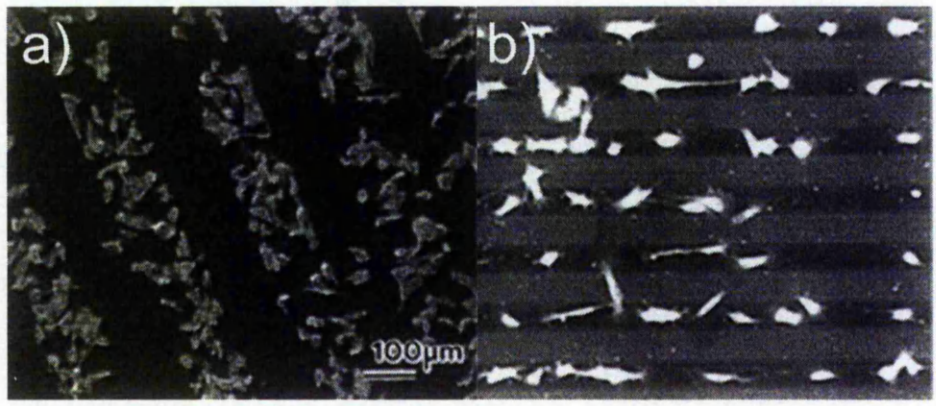

Figure 1.4. Cell attachment to chemically modified surfaces, a) osteoblasts on mercaptopropanol / octanethiol patterned surfaces with cells attaching preferentially to hydrophilic surfaces[51] and b) astroglial cells bind to N1[3-(trimethoxysilyl)propyl]diethylenetriamine but not to octadecyltrichlorosilane functionalised surfaces.[52]

There are several proposed mechanisms by which cells are thought to 'observe' surface characteristics; cells may reach the surface by protrusions though the protein layer or by consuming pre-adsorbed proteins altogether.[17] This may be possible in the later stages of cell adhesion, although it is more likely that adsorbed proteins themselves convey the underlying chemistry through their specific geometry and conformation.[60]

It has been demonstrated that proteins adsorb in varying amounts depending on the functional groups presented at the surface of a material,[32,46,47,51,52] Figure 1.5a. The chemical nature of the surface can be modified to induce greater protein-surface affinity by either electrostatic or hydrophobic interaction. The outer shell of adsorbing proteins is therefore an important factor in determining how proteins bind, but generally hydrophobic bonding is a major factor which induces rapid adsorption compared to that observed on hydrophilic surfaces.[31,61]

Although it is well know that the extent of protein adhesion can be directed by surface chemical patterning, Figure 1.5b, the degree of control over the conformation and orientation of adsorbed proteins remains largely unknown. It has been suggested that protein-surface interactions induce deformation of an adsorbing protein molecule but many of the techniques used to examine such ultrathin layers of adsorbed proteins

only imply conformational / orientational change rather than providing an absolute measure of protein structure.

A large number of investigations examining bound proteins have used techniques that give limited information: fluorescence,[62,63] atomic force microscopy,[64-66] mass spectrometry,[67] zeta potential,[68] Nuclear magnetic resonance (NMR),[69] ellipsometry,[70-71] circular dichroism[62] and antibody or platelet binding[72-74]. Most of the analytical tools used have given results where generalised information on the adsorbed protein was obtained or conformational changes were implied and were not measured or quantified at all. Examination of the ease of protein removal from surfaces has been suggested by authors to provide evidence of protein structural change, although such studies only show that conformational and / or orientation change could be occurring.

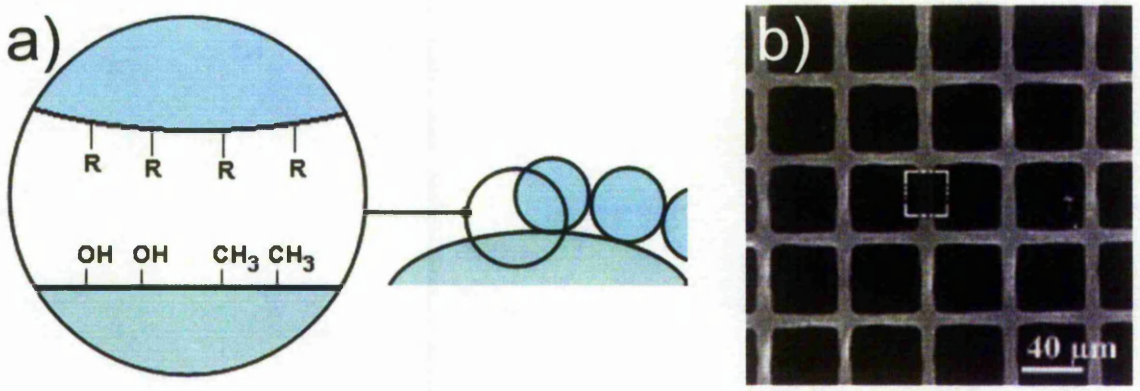

Figure 1.5. Protein adsorption a) schematic of protein-surface interactions and b) adsorption onto a biotinylated stripes which appear white, whilst adsorption is hindered on square oligo-ethylene-glycol regions.[75] The white box indicates an intentionally photo bleached area.

Circular dichroism (CD) is one of the more common methods used to study protein adsorption onto colloidal particles and although changes in secondary structure can be followed, this technique has inherent inconsistency problems in absolute secondary structure determination due to variation in the deconvolution of CD specta.[76] Colloidal scattering also restricts the size of substrates that can be used which obviously limits the range of investigations using this technique.[77] Some interesting studies have, however, been reported showing that protein stability is controlled by the chemistry of the substrate.[78] Infrared spectroscopy allows a more thorough examination of the bound

protein secondary structure[26] - a method also not constrained by substrate size or material. Previous infrared studies have shown that surface chemistry affects protein conformation although investigations have focussed on hydrophilic versus hydrophobic polymers, taking little account of the surface chemistry on the molecular level, nor the surface roughness on the nano-scale which can be experienced by adsorbing proteins. Separating chemical and topographical effects is difficult since most topographical variations are accompanied by chemical heterogeneities.[79]

1.7.2 Topography

Many studies have examined cell-surface interactions with respect to topography[53-55] e.g. a study of cell adhesion on polymethylmethacrylate (PMMA) with varying degrees of roughness in the micron range has shown that cell adhesion is related to the degree of surface roughness.[55] Studies of cell attachment to micron-sized topographic features have demonstrated that cell growth can be guided across a surface, Figure 1.6.[80,81] So-called 'contact guidance' has also been shown to occur on grooved surfaces, Figure 1.6b.[5,9] The importance of surface features above 0.5 μm in height has been highlighted for the control of cell-surface interactions.[79] Below this feature size it has been suggested that the chemical nature of the surface takes precedence.[82] Other studies report, however, that the surface densities of adsorbed protein layers are governed by surface topographical features as small as 3-4 nm.[83]

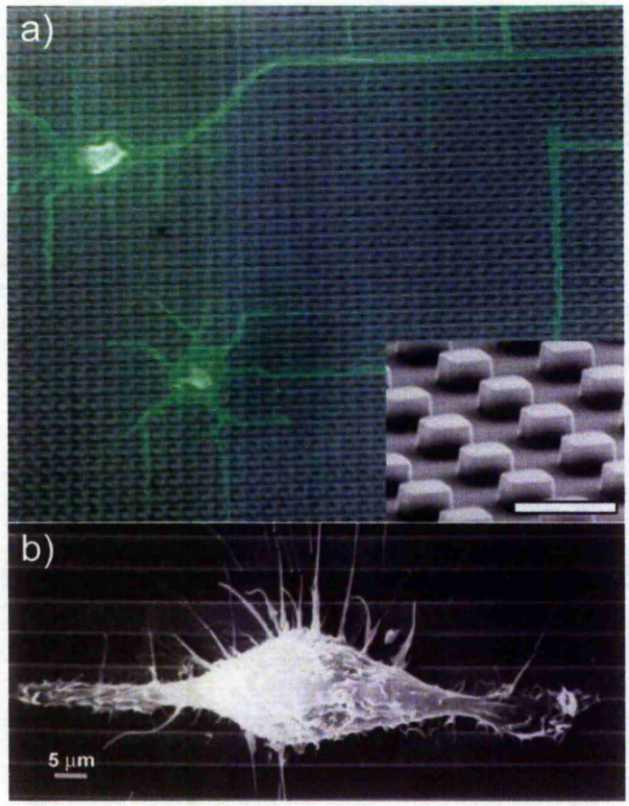

Figure 1.6. Cell attachment controlled by micron-sized surface topography: a) hippocampal neurons on silicon pillars. Insert shows example 1 micron high features, scale bar -4 μm[80] b) well-spread macrophage on micro-grooved substratum, groove depth 71 nm.[81]

Micron-sized features are far too large for individual protein molecules to observe. However, if surface features are produced on the same length scale as the proteins themselves then the architecture of the surface may be used to manipulate protein shape and form upon adsorption. Can protein molecules mould around surface curvature? Can packing density and / or arrangement be controlled by surface features? These questions are a topic of much interest at present – the answers may allow one to predict or even control the structure and therefore the activity of surface-bound proteins.

It has been shown that protein adsorption characteristics can be controlled by changing substrate surface parameters: chemistry,[78,84] colloidal substrate size and curvature[77,85]. Researchers have investigated the effects of surface curvature as a means to model topography, wherein protein molecules adsorb onto colloidal substrates of varying size. Conformational assessment of surface-bound proteins has shown that

lysozyme and human carbonic anhydrase, two small globular proteins, display native-like secondary structures when bound to spherical substrates with radii <15-20 nm but exhibit a loss of ordered structure upon binding to larger substrates.[69,77,85] Albumin has also been shown to change conformation when adsorbed and desorbed from nano-sized particles.[86] Activity of proteins was reduced upon adsorption, which also suggests a conformational change[77,87] The extent to which the surface chemistry and topography contributes to the control of conformation and thus the activity of surface-bound proteins is not fully understood.

Furthermore, studies examining the effect of surface topography have focussed only on small globular proteins such as lysosyme (MW=14.5 kDa 4.5 by 3.5 by 3.5 nm),[77,88] human carbonic anhydrase (MW = 28.7 kDa,[89] ca. spherical protein with diameter ~4.5 nm)[69,85] and cytochrome C (MW = 15 kDa, 2.5 by 2.5 by 3.7 nm)[84,90]. Other larger proteins which would dominate the implant-interface at realistic timescales of implantation have been overlooked.

There have been no studies that examine the effects of surface chemistry with and without surface topography on the adsorption and surface-bound characteristics of small globular, compared to larger non-globular proteins. Two such proteins that have been used in investigations reported in this thesis are albumin and fibrinogen.

1.8 Aims

Previous research has shown that both surface chemistry and topography can control cell-surface interactions although it is unclear if these changes are actually being imposed on the protein layer, which then mediates cell attachment. Surface chemistry can be used to control rates of protein adsorption and the amounts adsorbed, allowing proteins to be patterned on surfaces. The structural differences between proteins adsorbed onto differing surface chemistries are however largely unknown. Many studies have suggested surface chemistry can induce conformational and / or orientational changes of adsorbed proteins, but structural characterisation of surface-bound proteins has not been critically conducted.

Micron-sized surface features used to guide cell growth are too large to affect protein molecules, although smaller features, comparable to the protein length scale

may offer some control over protein adsorption characteristics. Few reports have shown variation in adsorbed protein conformation with respect to nano-scale surface curvature. These studies are in their infancy, covering a very small length-scale range and have focussed only on small globular proteins.

The aim of this study was to gain a deeper understanding of protein-surface interactions. Structural differences between proteins adsorbed onto differing surface chemistries have been investigated to understand the impact of surface chemistry on surface-bound protein conformation. Protein adsorption onto model hydrophilic and hydrophobic surfaces was compared to understand the differing interactions between the proteins and the two surface chemistries. The use of albumin and fibrinogen, two proteins found in high abundance in serum, were used to ascertain the impact of surface chemistry on the likely performance of biomaterials. Comparison of these two proteins having very different dimensions has allowed insight into the importance of surface chemistry with regard to protein size and shape.

A quartz crystal microbalance was used to examine differing protein adsorption rates and surface saturation amounts over a range of protein concentrations. Infrared spectroscopy allowed investigation of the secondary structure of surface-bound proteins. Furthermore topographical effects have been investigated, with and without the effects of surface chemistry. Nano-sized substrates were used to present varying degrees of surface curvature as a model for surface topography. Silica spheres were produced and chemically modified to again compare hydrophilic and hydrophobic surface chemistry effects on protein adsorption.

A fluorometric assay was also used to quantitatively assess the amount of protein adsorbed onto surfaces of differing chemistry. This method was compared to quartz crystal microbalance (QCM) which does not allow an absolute measurement of adsorbed protein but a value relating to the total mass of an adsorbing layer (including entrapped water) and also viscoelastic contributions. A comparison of protein adsorption characteristics onto superhydrophobic and superhydrophilic surfaces were also examined using this fluorometric assay.

1.9 References

1. A.F. Collings; F. Caruso, "Biosensors: Recent Advances," *Biosensors Bioelectronics, Rep. Prog. Phys.*, **1997**, 60, 1397-1445
2. H.A. Fishman; D.R. Greenwald; R.N. Zare, "Biosensors in Chemical Separations," *Annual Rev. Biophys. Biomolec. Struct.*, **1998**, 27, 165-198
3. N.A. Peppas; R. Langer, "New Challenges in Biomaterials," *Science*, **1994**, 5154, 1715-1720
4. B. Kasemo, "Biological surface science," *Surface Science*, **2002**, 500, 1-3, 656-677
5. K. Anselme, "Osteoblast Adhesion on Biomaterials," *Biomaterials*, **2000**, 21, 7, 667-681
6. D.A. Puleo; A. Nanci, "Understanding and Controlling the Bone-Implant Interface," *Biomaterials*, **1999**, 20, 2311, 2321
7. B. Kasemo; J. Lausmaa, "*Surface Aspects on Inorganic Biomaterials. CRC Critical Review on Biocompatibility*," **1986**, 2, 335-380
8. V.A. DePalma; R.E. Baier; J.W. Ford; V.L Gott; A. Feruse, "Investigation of Three-Surface Properties of Several Metals and Their Relation to Blood Compatibility," *J. Biomed. Mater. Res. Symp.*, **1972**, 3, 6(4) 37-75
9. D.M. Brunette, "The Effects of Surface Topography on the Behaviour of Cells on Implants", *Int. J. Oral Maxillofac. Implantology*, **1998**, 3, 231-246
10. N. Hamamoto; Y. Hamamoto; T. Nakajima; H. Ozawa, "Histological, Histocytochemical and Ultrastructural Study on the Effects of Surface Charge on Bone Formation in the Rabbit Mandible," *Archives of Oral Biology*, **1995**, 40(2), 97-106
11. M. Krukowski; R.A. Shively; P. Osdoby; B.L Eppley, "Stimulation of Craniofacial and Intramedullary Bone Formation By Negatively Charged Beads," *J. Oral Maxillofa. Surg.*, **1990**, 48, 468-475
12. S.D. Bruck; S. Rabin; R.S. Ferguson, "Evaluation of Biocompatible Materials," *Biomater. Med. Devices Artif. Organs*, **1973**, 1, 191-222
13. A. Hunter; C.W. Archer; P.S. Walker; G. W. Blunn, "Attachment and Proliferation of Osteoblasts and Fibroblasts on Biomaterials For Orthopaedic Use," *Biomaterials*, **1995**, 16, 287-95

14. J.C. Keller; C.M. Stanford; J.P. Wightman; R.A. Draughn; R. Zaharias, 'Characterizations of Titanium Implant Surfaces. III," *J. Biomed. Mater. Res*, **1994**, 28, 939-946
15. Y. Ito; M. Kajihara; Y. Imanishi; "Materials For Enhancing Cell Adhesion By Immobilization of Cell-Adhesive Peptide," *J. Biomed. Mater. Res.*, **1991**, 25, 1325-1337
16. B. D. Ratner; A.S. Hoffman; F.J. Schoen; J.E. Lemons (ed), "*Biomaterials Science*," Elsevier Academic Press, **2004**
17. T.A. Horbett; B.D. Ratner; J.M. Schakenraad; F.J. Schoen, "*Biomaterials Science*," **1996**, p133-164, Academic Press Inc,
18. J. Lyklema; (A. Baszkin, W. Norde Ed.) "*Physical Chemistry of Biological Interfaces*," **2000**, p1-47, Marcel Dekker Inc., New York
19. W. Norde ; (J.D. Andarde Ed.) "*Surface and Interfacial Aspects of Biomedical Polymers*," **1985**, 2nd Ed., Plenum Press, New York
20. C.A. Haynes; W. Norde, "Globular Proteins at Solid / Liquid Interfaces, " *Colloid Surf. Sci. B*, **1994**, 2, 517-566
21. R.A. Latour Jr; L.L. Hench, "A Theoretical Analysis of the Thermodynamic Contributions for the Adsorption of Individual Protein Residues on Functionalized Surfaces," *Biomaterials*, **2002**, 23, 23, 4633-4648
22. J.D. Andrade, "*Surface and Interfacial Aspects of Biomedical Polymers,* " **1985**, p. 1-80, New York: Plenum Press
23. T.A. Horbett; J.L. Brash, "*Proteins at Interfaces: Physiochemical and Biochemical Studies,* " **1987**, p. 1-33, Washington, DC: American Chemical Society
24. B.W. Morrissey; R.R. Stromberg, "Conformation of Adsorbed Blood Proteins by Infrared Bound Fraction Measurements," *J. Colloid Int. Sci.*, **1974**, 46(1) 152-164
25. M. Taborelli; L. Eng; P. Descouts; J.P. Ranieri; R. Bellamkonda; P. Aebischer, "Bovine Serum Albumin Conformation on Methyl and Amine Functionalized Surfaces Compared by Scanning Force Microscopy," *J. Biomed. Mater. Res.*, **1995**, 29(6), 707-714

26. T.J. Lenk, T.A. Horbett, B.D. Ratner, K.K. Chittur, "Infrared Spectroscopic Studies of Time-Dependent Changes in Fibrinogen Adsorbed to Polyurethanes," *Langmuir*, **1991**, 7(8) 1755-1764
27. B. Kasemo; J. Gold, "Implant Surfaces and Interface Processes," *Adv. Dental Res.*, **1999**, 13, 8-20
28. L. Vroman; A.L. Adams, "Identification of Rapid Changes at Plasma-Solid Interfaces," *J. Biomed. Mater. Res.*, **1969**, 3, 43-67
29. F. Grinnell; M.K. Feld, "Adsorption Characteristics of Plasma Fibronectin in Relationship to Biological Activity," *J. Biomed. Mater. Res.*, **1981**, 15, 363-381
30. S. Johansson; G. Svineng; K. Wennerberg; A. Armulik; L. Lohikangas; "Fibronectin-Integrin Interactions," *Front. Biosci. 2.*, **1997**, 126-146
31. W.G. Pitt; S.L. Cooper, "Albumin Adsorption on Alkyl Chain Derivatized Polyurethanes: I. The Effect of C-18 Alkylation," *J. Biomed. Mater. Res.*, **1988**, 22(5) 359-382
32. G.B. Sigal; M. Mrksich; G.M. Whitesides, "Effect of Surface Wettability on the Adsorption of Proteins and Detergents," *J. Am. Chem. Soc.*, **1998**, 120(14), 3464-3473
33. T.C. Ta; M.T. McDermott, "Mapping Interfacial Chemistry Induced Variations in Protein Adsorption with Scanning Force Microscopy," *Anal. Chem.*, **2000**, 72, 2627-2634
34. F. Grinnel, "Cellular Adhesiveness and Extracellular Substrata," *Int. Rev. Cytol*, **1978**, 53, 65-144
35. D. Thom; A.J. Powell; D.A. Rees, "Mechanisms of Cellular Adhesion. IV. Role of Serum Glycoproteins in Fibroblast Spreading on Glass," *J. Cell, Sci.*, **1979**, 35, 281-305
36. D. Kiaei; A.S. Hoffman; T.A. Horbett; K.R. Lew, "Platelet and Monoclonal Antibody Binding to Fibrinogen Adsorbed on Glow-Discharge-Deposited Polymers," *J. Biomed. Mater. Res.* **1995**, 29(6), 729-39
37. F. Höök; M. Rodahl; P. Brzezinski; B. Kasemo, "Energy Dissipation Kinetics for Protein and Antibody-Antigen Adsorption under Shear Oscillation on a Quartz Crystal Microbalance," *Langmuir*, **1998**, 14(4) 729-734
38. F. Höök; B. Kasemo, "Variations in Coupled Water, Viscoelastic Properties, and Film Thickness of a Mefp-1 Protein Film During Adsorption and Cross-Linking:

a Quartz Crystal Microbalance With Dissipation Monitoring, Ellipsometry, and Surface Plasmon Resonance Study," *Anal. Chem.*, **2001**, 73(24) 5796-5804

39. F. Caruso; D.N. Furlong; P. Kingshott, "Characterization of Ferritin Adsorption onto Gold," *J. Colloid Int. Sci.*, **1997**, 186, 129-140
40. S. Kidoaki; T. Matsuda, "Adhesion Forces of the Blood Plasma Proteins on Self-Assembled Monolayer Surfaces of Alkanethiolates with Different Functional Groups Measured by an Atomic Force Microscope," *Langmuir*, **1999**, 15(22) 7639-7646
41. K.K. Chittur, "FTIR/ATR for protein adsorption to biomaterial surfaces," *Biomaterials*, **1998**, 19(4-5), 357-369
42. Y. Wu; K. Murayama; B. Czarnik-Matusewicz; Y. Ozaki, "Two-Dimensional Attenuated Total Reflection/Infrared Correlation Spectroscopy Studies on Concentration and Heat-Induced Structural Changes of Human Serum Albumin in Aqueous Solutions," *Appl. Spectrosc.*, **2002**, 56(9), 1186-1193
43. B.R. Young; W.G. Pitt; S.L. Cooper, "Protein Adsorption on Polymeric Biomaterials. II. Adsorption Kinetics," *J. Colloid and Int. Sci.*, **1988**, 125(1) 246-260
44. W.G. Pitt; D.R. Weaver; S.L. Cooper, "Fibronectin Adsorpton Kinetics on Phase Segregated Polyurethaneureas," *J. Biomater. Sci. Polymer Edn.*, **1993**, 4(4) 337-346
45. U. Jönsson; B. Ivarsson; I. Lundström; L. Berghem, "Adsorption Behavior of Fibronectin on Well-Characterized Silica Surfaces," *J. Colloid and Int. Sci.*, **1982**, 90(1) 148-163
46. F. Höök; M. Rodahl; P. Brzezinski; B. Kasemo, "Measurements using the Quartz Crystal Microbalance Technique of Ferritin Monolayers on Methyl-Thiolated Gold: Dependence of Energy Dissipation and Saturation Coverage on Salt Concentration," *J. Colloid and Int. Sci.*, **1998**, 208, 63-67
47. C.G. Marxer; M.C. Coen; L. Schlapbach, "Study of Adsorption and Viscoelastic Properties of Proteins With a Quartz Crystal Microbalance by Measuring the Oscillation Amplitude," *J. Colloid and Int. Sci.*, **2003**, 261, 291-298
48. M. Lestelius; B. Liedberg; P. Tengvall; "In Vitro Plasma Protein Adsorption on Functionalized Alkanethiolate Self-Assembled Monolayers," *Langmuir*, **1997**, 13(22), 5900-5908

49. S.S. Cheng; K.K. Chittur; C.N. Sukenik; L.A. Culp; K. Lewandowska, "The Conformation of Fibronectin on Self-Assembled Monolayers with Different Surface Composition: An FTIR/ATR Study," *J. Colloid Int. Sci.*, **1994**, 162(1), 135-43
50. J. Buijs; V. Hlady, "Adsorption Kinetics, Conformation, and Mobility of the Growth Hormone and Lysozyme on Solid Surfaces, Studied with TIRF," *J. Colloid Int. Sci.*, **1997**,190(1), 171-181
51. C.A. Scotchford; C.P. Gilmore; E. Cooper; G.J. Leggett; S. Downes, "Protein Adsorption and Human Osteoblast-Like Cell Attachment and Growth on Alkylthiol on Gold Self-Assembled Monolayers," *J. Biomed Mater. Res.*, **2002**, 59(1) 84-99
52. P.M. St. John; L. Kam; S.W. Turner; H.G. Craighead; M. Issacson; J.N. Turner; W. Shain, "Preferential Glial Cell Attachment to Microcontact Printed Surfaces," *J. Neurosci. Methods*, **1997**, 75(2) 171-177
53. K.D. Chesmel; C.C. Clark; C.T. Brighton; J. Black, "Cellular Responses to Chemical and Morphologic Aspects of Biomaterial Surfaces. II. The Biosynthetic and Migratory Response of Bone Cell Populations," *J. Biomed. Mater. Res.*, **1995**, 29(9), 1101-1110
54. C Fredriksson; S. Khilman; B. Kasemo; D.M. Steel, "In Vitro Real-Time Characterization of Cell Attachment and Spreading," *J. Mater. Res.:Mat. Res.*, **1998**, 9(12), 785-788
55. M. Lampin; R. Warocquier-ClИrout; C. Legris; M. Degrange; M.F. Sigot-Luizard; "Correlation Between Substratum Roughness and Wettability, Cell Adhesion, and Cell Migration," *J. Biomed. Mater. Res.*, **1997**, 36(1) 99-108
56. B. Kasemo, "Biological Surface Science," *Current Opinion in Solid State and Materials Sci.*, **1998**, 3, 451-459
57. H. Zreiqat; C.R. Howlett, "Titanium Substrata Composition Influences Osteoblastic Phenotype: In Vitro Study," *J. Biomed. Mater. Res.*, **1999**, 47(3) 360-366
58. H. Zreiqat; P. Evans; C.R. Howlett, "Effect of Surface Chemical Modification of Bioceramic on Phenotype of Human Bone-Derived Cells," *J. Biomed. Mater. Res.*, **1999**, 44(4) 389-396

59. K.E. Healy; C.H. Thomas; A. Rezania; J.E. Kim; P.J. McKeown; B. Lom; P.E. Hockberger; "Kinetics of Bone Cell Organization and Mineralization on Materials With Patterned Surface Chemistry," *Biomaterials*, **1996**, 17, 195-208
60. B.G. Keselowsky; D.M. Collard; A.J. Garcia, "Integrin Binding Specificity Regulates Biomaterial Surface Chemistry Effects on Cell Differentiation," *PNAS*, **2005**, 102(17) 5953-5957
61. G.K. Iwamoto; L.C. Winterton; R.S. Stoker; R.A. Van Wagenen; J.D Andrade; D.F. Mosher, "Fibronectin Adsorption Detected by Interfacial Fluorescence," *J. Colloid Int. Sci.*, **1985**, 106(2) 459-464
62. C.Yongli; Z. Xiufang; G. Yandao; Z. Nanming; Z. Tingying; S. Xinqi, "Conformational Changes of Fibrinogen Adsorption onto Hydroxyapatite and Titanium Oxide Nanoparticles," *J. Colloid Int. Sci.*, **1999**, 214(1)38-45
63. M. Prokopowicz; J. L-Tukasiak; B. Banecki; A. Przyjazny,"In Vitro Measurement of Conformational Stability of Fibrinogen Adsorbed on Siloxane," *Biomacromolecules*, **2005**, 6(1) 39-45
64. A. Agnihotri; C.A. Siedlecki, "Time-Dependent Conformational Changes in Fibrinogen Measured by Atomic Force Microscopy," *Langmuir*, **2004**, 20(20) 8846-8852
65. K.L Marchin; C.L. Berrie, "Conformational Changes in the Plasma Protein Fibrinogen upon Adsorption to Graphite and Mica Investigated by Atomic Force Microscopy," *Langmuir*, **2003**, 19(23) 9883-9888
66. P. Cacciafesta; A.D.L Humphris; K.D. Jandt; M.J. Miles, "Human Plasma Fibrinogen Adsorption on Ultraflat Titanium Oxide Surfaces Studied with Atomic Force Microscopy," *Langmuir*, **2000**, 16(21) 8167-8175
67. N. Xia; D.G. Castner, "Preserving the Structure of Adsorbed Protein Films for Time-of-Flight Secondary Ion Mass Spectrometry Analysis," *J. Biomed. Mater. Res.*, **2003**, 67A(1) 179-190
68. C. Werner; R. Zimmermann; T. Kratzmüller; "Streaming Potential and Streaming Current Measurements at Planar Solid / Liquid Interfaces for Simultaneous Determination of Zeta Potential and Surface Conductivity," *Colloids and Surfaces A: Physiochem. Eng. Aspects*, **2001**, 192(1-3) 205-213

69. M. Lundqvist; I. Sethson; B-H Jonsson, "High-Resolution 2D 1H-15N NMR Characterization of Persistent Structural Alterations of Proteins Induced by Interactions with Silica Nanoparticles," *Langmuir*, **2005**, 21, 5974-5979
70. B.W. Morrissey; L.E. Smith; C.A. Fenstermaker; R.R. Stromberg; W.H. Grant, "Conformation of Adsorbed Blood Proteins," *NBS Special Publication (US)* **1975**, 415, 83-90
71. P. Tengvall; I. Lundström; B. Leidberg; "Protein Adsorption Studies on Model Organic Surfaces: An Ellipsometric and Infrared Spectroscopic Approach," *Biomaterials*, **1998**, 19(4-5) 407-422
72. J.M. Grunkemeier; T.A. Horbett; "Fibrinogen Adsorption to Receptor-Like Biomaterials Made by Pre-Adsorbing Peptides to Polystyrene Substrates," *J. Mol. Rec.*, **1996**, 9(3) 247-257
73. V. Balasubramanian; N.K. Grusin; R.W. Bucher; V.T. Turitto; S.M. Slack; "Residence-Time Dependent Changes in Fibrinogen Adsorbed to Polymeric Biomaterials," *J. Biomed. Mater. Res.*, **1999**, 44(3) 253-260
74. W.-B.Tsai; J.M. Grunkemeier; T.A. Horbett; "Human Plasma Fibrinogen Adsorption and Platelet Adhesion to Polystyrene," *J. Biomed. Mater. Res.*, **1999**, 44(2) 130-139
75. C. Grunwald; W. Eck; N. Opitz; J. Kuhlmannc; C. Wölla, "Fabrication of 2D-Protein Arrays Using Biotinylated Thiols: Results From Fluorescence Microscopy and Atomic Force Microscopy," *Phys. Chem. Chem. Phys.*, **2004**, 6, 4358-4362
76. B. Dalmas; W.H. Bannister, "Prediction of Protein Secondary Structure From Circular Dichroism Spectra: An Attempt to Solve the Problem of the Best-Fitting," *Anal. Biochem.*, **1995**, 225, 39-48
77. A.A. Vertegal; R.W. Siegel; J.S. Dordick, "Silica Nanoparticle Size Influences the Structure and Enzymatic Activity of Adsorbed Lysozyme," *Langmuir*, **2004**, 20, 6800-6807
78. S. Srivastava; A. Verma; B.L. Frankamp; V.M. Rotello, "Controlled Assembly of Protein-Nanoparticle Composites Through Protein Surface Recognition," *Adv. Mater.*, **2005**, 17(5) 617-621
79. A. Curtis; C. Wilkinson, "Topographical Control of Cells," *Biomaterials*, **1997**, 18(24) 1573-1583

80. N.M. Dowell-Mesfin; M.-A. Abdul-Karim; A.M.P. Turner; S. Schanz; H.G Craighead; B. Roysam; J.N. Turner; W. Shain, "Topographically Modified Surfaces Affect Orientation and Growth of Hippocampal Neurons," *J. Neural Eng. 1*, **2004**, 78–90
81. B. Wójciak-Stothard; A. Curtis; W. Monaghan; K. MacDonald; C. Wilkinson, "Guidance and Activation of Murine Macrophages by Nanometric Scale Topography," *Exp. Cell Res.*, **1996**, 223, 426–435
82. S. Britland; C. Perridge; M. Deyner; H. Morgan; A. Curtis; C. Wilkinson, "Morphogenetic Guidance Cues Can Interact Synergistically and Hierarchically in Steering Nerve Cell Growth," *Exp. Biol. Online (EBO)*, **1996**, 1:2
83. G.C. Marxer; M.C. Coen; R. Hauert; V.L Katanaev; P. Groning; L. Schlapbach, "Creation of Nanostructures to Study the Topographical Dependency of Protein Adsorption," *Colloids and Surfaces, B: Biointerfaces*, **2002**, 26(3), 255-267
84. L.-C. Huang, H.-C. Chang, "Adsorption and Immobilization of Cytochrome c on Nanodiamonds," *Langmuir*, **2004**, 20(14) 5879-5884
85. M. Lundqvist; I. Sethson; B.-H. Jonsson; "Protein Adsorption onto Silica Nanoparticles: Conformational Changes Depend on the Particles' Curvature and the Protein Stability," *Langmuir*, **2004**, 20(24) 10639-10647
86. Z.G. Peng; K. Hidajat; M.S. Uddin, "Conformational Change of Adsorbed and Desorbed Bovine Serum Albumin on Nano-Sized Magnetic Particles," *Colloids and Surfaces B: Biointerfaces*, **2004**, 33(1) 15-21
87. A. Kondo; F. Murakami; M. Kawagoe; K. Higashitani, "Kinetic and Circular Dichroism Studies of Enzymes Adsorbed on Ultrafine Silica Particles," *Appl. Microbiol. Biotechnol.*, **1993**, 39(6) 726-731
88. M. Tian; W.-K. Lee; M.K. Bothwell; J. McGuire, "Structural Stability Effects on Adsorption of Bacteriophage T4 Lysozyme to Colloidal Silica," *J. Colloid Int. Sci.*, **1998**, 200(1) 146-154
89. M. Jonsson; E. Pettersson, "Isoelectric Fractionation, Analysis, and Characterization of Ampholytes in Natural pH Gradients. VI. Isoelectric Spectrum of Bovine Carbonic Anhydrase B," *Acta Chem. Scand*, **1968**, 22(2) 712
90. X. Jiang; J. Jiang; Y. Jin; E. Wang; S. Dong, "Effect of Colloidal Gold Size on the Conformational Changes of Adsorbed Cytochrome C: Probing by Circular

Dichroism, UV-Visible, and Infrared Spectroscopy," *Biomacromolecules*, **2005**, 6(1) 46-53

Chapter 2:

Materials and Methods

The adsorption characteristics and surface bound conformation of proteins adsorbing onto various chemically and topographically modified surfaces have been investigated. This chapter covers experimental theory and explains exact experimental details of all techniques used to prepare and characterise the materials used within the investigations described in this thesis.

2.1 Contact Angle Measurements

When a liquid droplet rests on a solid surface thermodynamics dictates that the total energy of the system 'E' be minimized. This can be expressed as,

$$E = A_{SV}\gamma_{SV} + A_{SL}\gamma_{SL} + A_{LV}\gamma_{LV} \qquad \text{Equation (2.1)}$$

where 'A' is the area, 'γ' is the surface energy and the three distinct interfaces are accounted for: 1) the solid-liquid interface 'SL', 2) the solid-vapour interface 'SV' and 3) the liquid-vapour interface 'LV'. By considering the geometry of the interfaces included in Equation 2.1, the Young equation can be obtained.[1]

$$\frac{\gamma_{SV} - \gamma_{SL}}{\gamma_{LV}} = \cos\theta_T \qquad \text{Equation (2.2)}$$

A drop resting on a solid therefore rests with an equilibrium contact angle, the angle 'θ' that the tangent to the liquid surface makes with the solid at the three phase boundary measured through the liquid, Figure 2.1. The energetics of the system therefore govern the droplet shape allowing characterisation of a surfaces' wettability to be analysed via the angle at which the droplet rests on the surface. Depending on the properties of the three phases the liquid may spread or remain near-spherical. A small angle (<90°), attained when water spreads over a surface, shows that the system is stablised when having a high solid-water interfacial area, i.e. the surface is hydrophilic. Conversely, high water contact angles (≥90°) are observed on hydrophobic surfaces.

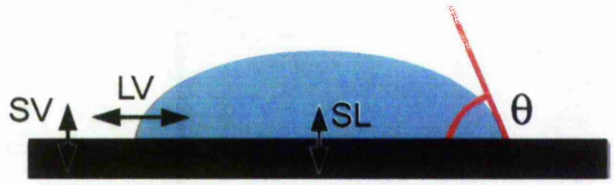

Figure 2.1. Forces acting at a solid-liquid interface.

The main characteristic that dictates wettability is surface chemistry, although surface roughness can emphasize the effects of hydrophobicity or hydrophilicity giving rise to superhydrophobic and superhydrophilic surfaces respectively.[2-3] A superhydrophobic surface is defined as one which has a greater water contact angle than that which is possible for any perfectly smooth surface, i.e. teflon is hydrophobic with a water contact angle of ~90°, but by making the surface rough this angle can be increased to >150° – a superhydrophobic surface. Wenzel was the first to establish the effect of surface roughness on liquid contact angles.[4] The 'specific surface' or 'roughness factor' which is defined as 'r', the ratio between the actual surface area (including microscopic topography) and the apparent macroscopic surface area, can then be taken into account. Modifying the surface energy components of each interface to accommodate differences between the actual and apparent surface area, i.e. the surface energy of the solid-liquid interface becomes $r\gamma_{SL}$, etc and the modified Young equation is then,

$$\frac{r(\gamma_{SV} - \gamma_{SL})}{\gamma_{LV}} = \cos\theta \qquad \text{Equation (2.3)}$$

Heterogeneity of the surface is a problem not allowed for in Equation 2.3. Indeed the chemical nature of the surface was recognized to be the only factor affecting contact angle variation prior to Wenzels investigations. Cassie-Baxter derived a two-phase equation which compensated for differing surface chemistry,[5]

$$\cos\theta = \varphi_1 \cos\theta_{T1} + \varphi_2 \cos\theta_{T2} \qquad \text{Equation (2.4)}$$

where again 'θ' is the observed contact angle and 'φ_1' and 'φ_2' are fractions of the surface having 'real' contact angles 'θ_1' and 'θ_2' respectively.

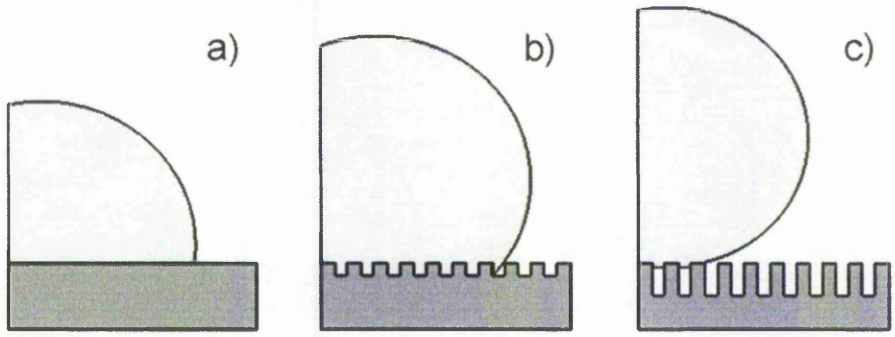

Figure 2.2. Schematic of wetting on a) flat hydrophobic, b) wetting rough and c) non-wetting rough surfaces.

Porous materials, or surfaces with high aspect ratio features will either fill with liquid or hold the liquid on the surface such that it bridges across the surface protrusions, Figure 2.2. In the latter case the fraction of the surface in contact with the liquid can be termed '*f*' and so the air gap under the droplet is '(1-*f*)'. Substituting these values into Equation 2.4 gives rise to the Cassie-Baxter equation which describes contact angles on such surfaces,[6]

$$\cos\theta = f\cos\theta_S + (1-f)\cos\theta_V \qquad \text{Equation (2.5)}$$

where 'θ_S' is the contact angle of the liquid on a smooth surface of the solid and 'θ_V' is the contact angle of the liquid on air which is assumed to be 180° for a suspended droplet.

Experimentally, contact angles are measured by capturing an image of the liquid droplet parallel to the interface using a camera, with the drop being back-lit to define its edges, Figure 2.3. Tangents can then be drawn to find the contact angle at each edge of the drop or the whole drop-shape can be fitted to a curve.

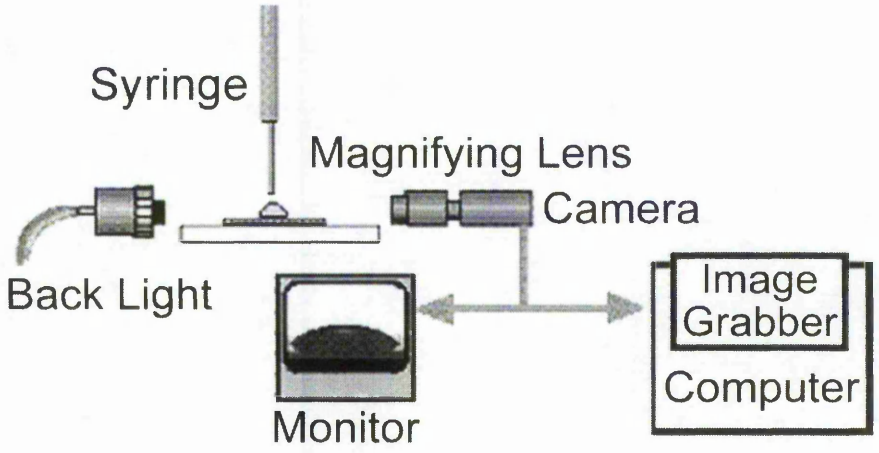

Figure 2.3. Schematic of contact angle measurement capture.

2.1.1 Experimental Details - Contact Angle Measurement

The wettability of surfaces prepared in this study was characterised by taking images of 5µl water droplet equilibrium contact angles on a Krüss DSA10. Droplets were applied to the surface by a microsyringe with a hydrophobised needle and images were taken immediately to eliminate drying effects. Generally angles can be measured with an accuracy of ±1.0° so any given contact angle reported in this thesis is an average of at least 3 drops, i.e. 6 contact angle measurements.

2.2 Quartz Crystal Microbalance (QCM)

The piezoelectric effect is the ability of a material to develop a net dipole moment when it is mechanically deformed in certain directions with respect to its atomic arrangement. The structure of quartz, one such piezoelectric material, consists of helical chains of silicon tetrahedra which spiral along one axis of the crystal. In its natural state the positive and negative ions are uniformly distributed, but upon deformation the ions are displaced and the centres of charge no longer coincide, giving

rise to an overall dipole.[7] Piezoelectric materials lack a centre of symmetry else the arrangement of ions would cause a cancellation of individual dipoles.

Conversely, an applied electric potential across a piezoelectric material results in its mechanical deformation in a specific direction and by reversing the direction of this potential but keeping its level constant, deformation of the same magnitude will occur in the opposite direction. An alternating current will therefore excite the crystal into a vibration state, oscillating in a particular manner depending on how the crystal was cut and the electrodes are applied.

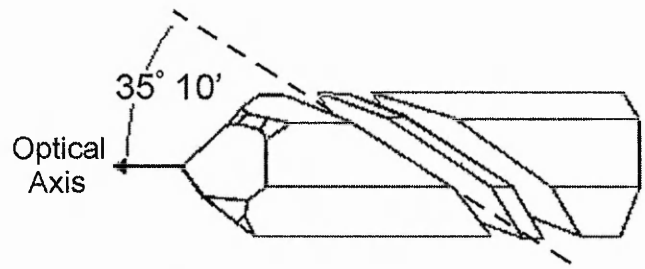

Figure 2.4. Schematic of AT-cut quartz crystal.

A quartz crystal microbalance uses AT-cut quartz (defined as a crystal cut at an angle ~35° to the crystal axis) and operates in a thickness-shear mode, Figure 2.4. The shear wave, traveling in the direction perpendicular to the faces bounces back and forth such that the top and bottom surfaces experience no shear force. The crystal will vibrate at its resonant frequency only when the shear wave has a pathlength equal to twice the thickness of the crystal or its multiples.[8] An expression for this can be written as,

$$t_q = \frac{\lambda_q}{2} \qquad \text{Equation (2.6)}$$

And by substituting $v = f\lambda$ the equation can be rearranged;

$$t_q = \frac{v}{2f} \qquad \text{Equation (2.7)}$$

where 't_q' is the thickness of the crystal, 'v' is the velocity of the shear wave in quartz and 'f' is the fundamental frequency.

Mass loading can be assumed to be an increase in the thickness of the crystal if the layer is thin compared to the wavelength of oscillation. This thickness change can be related to the change in frequency by first considering the properties of the overlayer and vibration;

$$t = \frac{M}{A\rho} \qquad \text{Equation (2.8)}$$

where 't' is the added thickness, 'M' is the added mass, 'A' is the area covered by the added layer and 'ρ' is density, and the velocity of vibration through quartz which is governed by the density 'ρ_q' and shear modulus 'μ_q';

$$v = \sqrt{\left(\frac{\mu_q}{\rho_q}\right)} \qquad \text{Equation (2.9)}$$

By substitution of Equations 2.7 to 2.9 into a simple expression relating frequency change to an increase in crystal thickness, Equation 2.10, the Sauerbrey equation[9] can be derived, Equation 2.11.

$$\frac{df_q}{f_q} = -\frac{dt_q}{t_q} \qquad \text{Equation (2.10)}$$

$$\Delta f = -\frac{2f^2}{\sqrt{\rho_q \mu_q}} \Delta m \qquad \text{Equation (2.11)}$$

where 'Δf'' is the change in frequency observed in Hz and 'm' is the change in mass per unit area of the crystal surface, given in g cm^{-2}.

Sauerbrey was the first to acknowledge the usefulness of piezoelectric quartz for the detection of mass-loading.[9] The main assumption is that the added overlayer is of negligible thickness and rigid and so such devices have been mostly used in the study of gaseous systems.[8,10,11] The Sauerbrey relationship predicts a 1 Hz frequency shift for a mass loading of 17.7 ng cm^{-1} for a crystal having a fundamental frequency of 5 MHz, (where 'ρ_q' and 'μ_q' are 2.648 gcm^{-3} and 2.947×10^{11} g cm^{-1} s^{-2} respectively.)

When using QCM for liquid studies one must be aware of deviations from the Sauerbrey equation, due to liquid density and viscosity factors. QCM measurements in

liquids were first examined by Glassford[12] and later by Kanazawa and Gordon,[13] who put forward a model to predict changes in frequency when a crystal was immersed in viscous liquids, Equation 2.12. Although such equations take into consideration the viscous medium, properties of an adsorbing layer having viscoelastic properties are difficult to model.

$$\Delta f = -f_U^{3/2}\sqrt{\frac{\rho_L \eta_L}{\pi \rho_q \mu_q}} \qquad \text{Equation (2.12)}$$

where 'f_U' is the frequency of the unloaded crystal and 'ρ_L' and 'η_L' are the density and viscosity of the liquid.

When studying protein adhesion from an aqueous environment it should be noted that the frequency change includes the mass of entrapped water,[14] viscoelastic effects of the protein[14-18] and overlayer slippage effects[14,17-19]. For the above reasons QCM results in this thesis are stated as changes in frequency, which, although they only give an indication of apparent mass-loading are uncomplicated by numerous assumptions.

2.2.1 Experimental Details - QCM Experiments

Quartz crystal microbalance measurements were made using a Maxtek PLO10 oscillator. Dual piston liquid pumps (Waters 590) were used to linearly flow solutions at a rate of three volume changes per minute of the FC-550 flow cell over a 25 mm diameter 5 MHz crystal with Cr/Au plate electrodes, Figure 2.5. A steady frequency was obtained using phosphate buffered saline (PBS) as a background solution after which a protein solution was flowed over the crystal, pumped by a second pump at the same flow rate as background. Frequency changes were monitored by a frequency counter linked to a computer, acquiring data using LabVIEW 4.0 G-programming software. The temperature was kept constant throughout each experiment using a water bath fitted with heating and chilling units. All solutions used during the experiment were thermally equilibrated in the water bath for at least 30 minutes prior to use. The temperature was continuously monitored using a thermosensor immersed in the water bath.

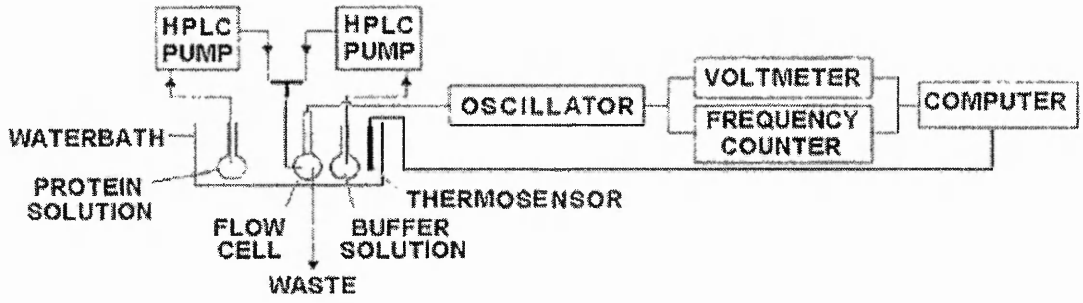

Figure 2.5. Schematic of QCM experimental set-up.

2.3 Fourier Transform Infrared Spectroscopy (FT-IR)

Infrared spectroscopy is the study of the interaction between infrared radiation and matter. This covers a wide section of the electromagnetic spectrum from 14,000-10 cm^{-1}, although the most common analysis uses only the mid-IR range 4000-400 cm^{-1}. Molecular vibrations and associated rotational transitions can be detected and measured by examination of the position and intensity of absorbance bands. Covalent bonds have specific vibration frequencies within well-defined regions of an infrared spectrum determined by the specific nature of the bonds. Stronger bonds require more energy to excite them and therefore vibrate at higher frequencies. When infrared radiation passes through a sample the absorption of energy can be expressed by, $\Delta E = hv$, where 'h' is Planck's constant and 'v' is the frequency of radiation.

In a Fourier transform infrared spectrometer the infrared beam is split by a Michelson interferometer, with one part of the beam being made to travel a longer path than the other allowing interference to occur upon recombination. By changing the pathlength difference the interference patterns change giving rise to an *interferogram* dependent on the intensity of the two beams, either passing to the detector or being reflected back to the source. This can then be mathematically treated by Fourier Transform methods to reveal spectral information, converting the waveform from the time domain into the frequency domain. The advantage of Fourier Transform IR is that the whole spectrum can be measured at once, allowing rapid data collection and better signal-to-noise ratios than with single scan IR.

A number of different sampling techniques can be used, allowing samples of different kinds to be analysed or information gathered on particular aspects of samples. For example, transmission infrared spectroscopy is most commonly used for the

analysis of solid samples. The sample is ground with potassium bromide (which does not absorb infrared radiation in the mid-IR region), pressed into a disc and the beam is passed directly through the sample. High intensity signals can be achieved with adequate absorbance from the sample giving good signal / noise ratios. Transmission IR spectroscopy can be conducted on low absorbing liquids or solutions, such as organic solvents, but aqueous samples are strongly absorbing, requiring a very small pathlength (~50-100 μm). An attenuated total reflectance (ATR) accessory restricts the sampling volume so less energy can be absorbed by a solvent such as water. Surface analysis can be conducted by bouncing the beam off a sample surface. Grazing angle infrared spectroscopy uses a beam at a high incident angle to the sample surface so ultrathin films (nanometers thick) can be analysed. For powdered samples, an incident beam is scattered and has to be refocused after the sample. A diffuse reflection accessory permits such rough surfaces to be analysed. Infrared spectroscopy is a very versatile technique for chemical analysis, allowing specific data to be obtained by the use of differing accessories, chosen depending on the nature of the sample and the characteristic information required.

2.3.1 Grazing Angle (GA) Accessory for Infrared Spectroscopy

Surface films can be measured by reflecting the infrared beam off the sample surface, Figure 2.6. Thick films (microns thick) on reflective surfaces allow relatively good spectral quality. The intensity of the signal (and therefore relative quality of the spectrum) is controlled by the incident angle of the beam.[20]

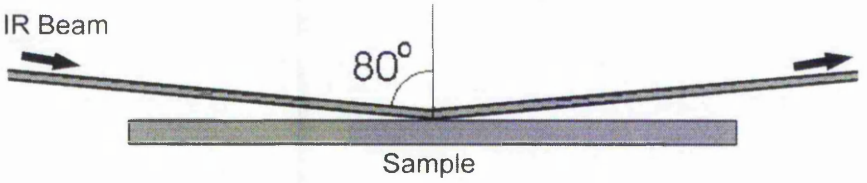

Figure 2.6. Schematic of grazing angle infrared accessory.

The required thickness 'd' of a material coated on a reflective substrate that would give rise to the same signal intensity as for a 10 mm thick sample analysed in the transmission mode can be estimated by;

$$2d = 10\cos\theta_i \qquad \text{Equation (2.13)}$$

Increasing the angle between the normal and the infrared beam increases the effective pathlength. The most important advantage of using high angles of incidence (termed grazing angles ≥80°) is that an incident beam polarized parallel to the surface can interfere with its reflected element causing an intense standing field at the surface.[20-22] This enhances the absorption signal intensity by a factor of ~20-25 relative to the adsorption of the perpendicular beam component.[21]

The use of a metal substrate also causes a signal enhancement due to the metal surface selection rules. The laws of electrostatics state that at any point near the surface of a conductor the electric field is perpendicular to the surface, whilst inside the conductor the net electric field is zero. Therefore an electric field applied parallel to the surface of a conductor will generate a field of equal strength inside the conductor but in an opposing direction, canceling each other out at the surface. If the external field is applied perpendicular to the surface the induced dipole inside the conductor is parallel to the source field, therefore the net electric field at the surface is not zero. Since an absorbance in an infrared spectrum is caused by the interaction between the infrared beam and oscillating dipoles of sample molecules, those dipoles perpendicular to a metal surface are enhanced.[20]

2.3.2 Attenuated Total Reflectance (ATR) Accessory for Infrared Spectroscopy

Attenuated total reflection is one of the most common infrared sampling techniques for liquids, especially aqueous solutions wherein water strongly absorbs beam energy. ATR solves this problem somewhat by not transmitting the beam directly through the sample. The beam is reflected by a series of mirrors through a crystal termed an *internal reflection element* (IRE). As the beam bounces though the crystal a standing wave is established at the crystal face allowing a 'tail' of electromagnetic radiation to penetrate through the crystal, termed an *evanescent wave*, Figure 2.7. The depth of penetration 'd_p' of this wave out of the crystal is governed by the radiation wavelength 'λ', the angle of incidence 'θ_i', the refractive index of the crystal 'n_c' and the external media 'n_e',

$$d_p = \frac{\lambda}{\sqrt{2\pi n_c(\sin^2\theta - n_{ec}^2)}} \qquad \text{Equation (2.14)}$$

where $n_{ec} = n_e / n_c$ ($n_e < n_c$).[23]

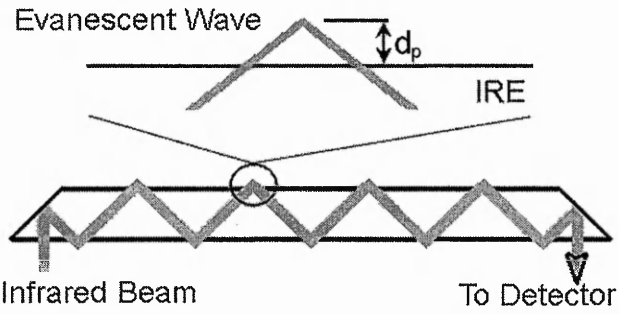

Figure 2.7. Schematic of an attenuated total reflectance crystal. Insert shows an evanescent wave.

The penetration depth for most crystals is less than 1 micron permitting only a small volume closely confined to the crystal surface to be sampled. The type of crystal chosen depends on the spectral window required and sampling conditions. Zinc selenide (ZnSe) has a wide spectral window in the mid-IR range but can easily be damaged by strong acids or alkalis so germanium is used in such cases. Diamond is an extremely good IRE due to its wide spectral range and robustness, although its cost is a major disadvantage for multi-bounce ATR cells and it is usually used only as a single-bounce crystal. A greater number of reflections, determined by the length of the ATR crystal, permits a greater volume of sample to be analysed by a passing beam giving rise to better signal to noise ratio without the need for a large number of spectra to be accumulated and then averaged. This has an advantage if changes with time are being assessed.

2.3.4 Amide I Analysis – Component Peak Fitting

Protein infrared spectra contain peaks arising mainly from amide bond vibrations. Bands due to the amide I, II, III, vibrations are sensitive to the secondary structure content of proteins, although of the three the amide I band is the most intense and also the most sensitive to secondary structure changes and has therefore received most attention for quantitative analysis.[24] The amide I band centered at ~1700-1600 cm^{-1} is largely due to C=O stretching vibrations. This band is a summation of several component bands, each arising from specific secondary structures located within the protein.

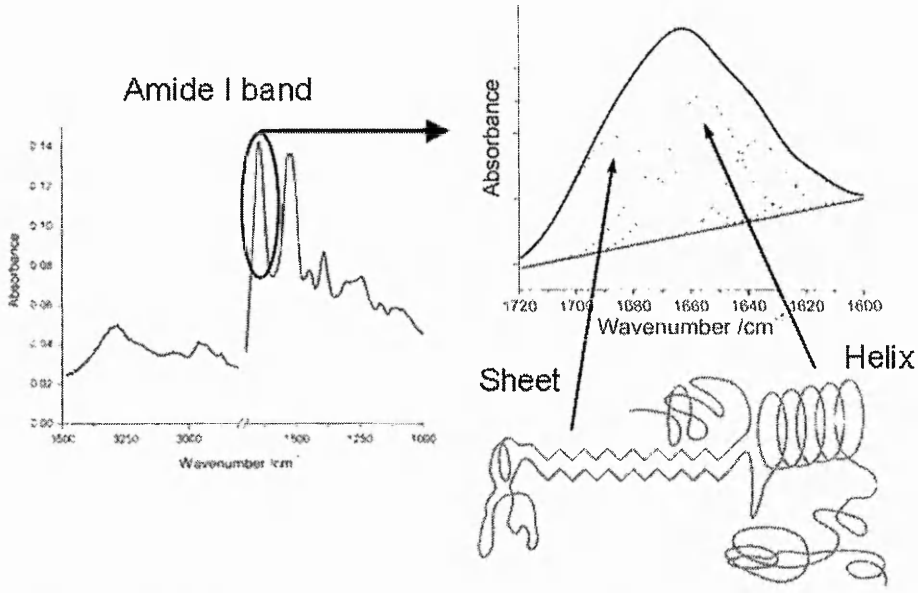

Figure 2.8. General infrared spectrum of protein highlighting amide I band.

Because the amide I band is sensitive to changes in secondary structure it has been widely used for protein conformational studies.[25-28] Amide bonds within differing secondary structures have specific vibrational frequencies, Figure 2.8. From previous studies, component bands with maxima at 1685-1663 cm^{-1} can be assigned to β-sheet structures, at 1655-1650 cm^{-1} to α-helices, at 1648-1644 cm^{-1} to random chains, at 1639-1635 cm^{-1} to extended chains and at 1632-1621 cm^{-1} to extended chains or β-sheets / turns. Bands observed at lower wavenumbers ~1616-1610 cm^{-1} are often considered to arise from intermolecular bonding.[26-28] These component bands are largely overlapping and all contribute to the characteristic broad amide I band observed in IR spectra. The overall shape of the band is therefore determined by the various secondary structure components of the protein analysed: α-helices, β-sheet, β-turn and unordered structures.[25-28]

2.3.5 Experimental Details - Fourier Transform Infrared Spectroscopy

All infrared spectroscopy measurements were conduced using a Magna IR-750 infrared spectrometer (Thermo Nicolet) either by transmission IR or using one of the following accessories: grazing angle, single-bounce ATR or multi-bounce ATR, experimental details for each set-up are given below. Spectrum collection parameters were as follows unless otherwise stated: resolution set at 4 cm^{-1}, interferometer speed

set to 0.4747 cms^{-1}, averaging 512 scans. Data was acquired using Omnic V7.1 software.

Spectra were smoothed by 9 point adjacent averaging using Origin V6.1 software and curve fitted using Galactic Grams V5.1. The fitting procedure was such that the amide I band was treated, having a linear baseline between 1720-1590 cm^{-1} fitting component peaks with a Gaussian band profile. Amide II baseline limits were set as 1590-1480 cm^{-1}. Component peak positions were determined using a number of tools. Examination of amide I band derivative spectra allows small changes in the band profile to be highlighted. Likewise Fourier deconvolution can be used – by changing bandwidth and enhancement parameters, true component peak positions can be identified. Literature values[25-28,29-31] were also considered to determine the best possible fitting of amide I bands. Although peak centres were not fixed during fitting, limit ranges of ±2.5 cm^{-1} about the estimated peak centre were set. Peak width at half height were set a maximum limit of 30 cm^{-1} for all peaks above 1620 cm^{-1} and 25 cm^{-1} for lower bands.

2.3.5.1 Grazing Angle

Infrared analysis of protein bound to flat chemically modified surfaces was conducted using an FT-80 grazing angle accessory (Thermo Nicolet) continuously purged with dry air/nitrogen for a minimum of 12 hours prior to sample analysis. A polariser, set to allow only p-polarised light to pass through the sample was used to obtain enhanced spectra. Ti/Au coated slides chemically modified using heptanethiol or mercaptoethanol (see section 2.9) were incubated in protein solutions, removed after a time, rinsed in distilled, deionised water and dried under a stream of nitrogen before immediate examination.

2.3.5.2 Single-Bounce ATR

Protein bound to the surface of silica spheres was analysed using a Golden Gate single bounce diamond ATR accessory (Graseby Specac) continuously purged with dry air for a minimum of 12 hours prior to analysis. After incubation in protein solutions, allowing proteins to adsorb on the substrate surface, sample spheres were removed by centrifugation, rinsed with distilled deionised water to remove any unbound protein and

analysed immediately. The samples were pressed onto the ATR crystal using a sapphire top-plate to ensure good contact.

2.3.5.3 Multi-bounce ATR

A germanium ATR trough accessory was plasma coated with hexane and allyl amine monomers to afford model hydrophobic and hydrophilic surfaces with defined chemistry. These were prepared at the University of Nottingham by Dr. M. Alexander and Dr. C. Fotea. After fitting the ATR into its holder the system was continuously purged with dry air for at least 3 hours prior to use (usually 12 hours). The mirror velocity was increased to 0.6329 $cm\ s^{-1}$ to maximise the rate of spectra collected, although a balance was made between the quality of spectra, speed of acquisition and the number of scans averaged. Background spectra of protein-free buffer were recorded averaging 512 scans immediately before sample spectra were taken. The background solution was quickly removed from the ATR trough and on addition of 1 $mg\ mL^{-1}$ protein solution in buffer, spectra were recorded averaging 100 scans. Spectra were continuously taken for 6 hours using a Macro Basic program designed specifically for this task. Amide I and amide II bands were analysed having a linear baseline between 1720-1480 cm^{-1}.

Macro Basic is a programming software allowing any number of data collection or data treatment steps to be automated. A number of programs were designed and built to allow spectra to be recorded at exact intervals over a number of hours, and also to treat data, assessing peak height, area, position and relative ratios of specific peaks in each infrared spectra collected.

2.4 Ultraviolet-Visible (UV-Vis) Spectroscopy

Spectra arising from the interaction of matter with ultraviolet and visible radiation are associated with transitions between electronic energy levels. These energy levels are generally between a bonding and non-bonding electron orbital, with the wavelength of excitation therefore being a measure of the orbital separation. Transitions occurring above 200 nm involve the excitation of electrons from 'p', 'd' and 'π' orbitals.[32]

The Beer-Lambert law states that the amount of energy adsorbed is independent of the incident intensity, being proportional to the number of absorbing molecules, given by;

$$\log_{10}\frac{I_o}{I} = \varepsilon \cdot c \cdot l \qquad \text{Equation (2.15)}$$

where 'I' and 'I_o' are the intensities of the transmitted and incident beams respectively, 'ε' is the molar extinction coefficient, 'c' is the concentration of adsorbing species and 'l' is the pathlength.

Stronger absorption therefore occurs when more adsorbing molecules are present, allowing concentration to be measured as a function of absorbance.

2.4.1 Experimental Details - UV-Vis Spectroscopy: Construction of Protein Adsorption Isotherms

Batch experiments were conducted at 25 °C and ambient pressure. A range of concentrations (0.1-3.0 mg mL^{-1}) of BSA and Fg in PBS were prepared. Silica spheres were sonicated in PBS to form homogeneous dispersions prior to the addition of protein. With stirring, the silica suspension was added to each protein solution to give a total substrate surface area per solution of 0.2 $m^2 mL^{-1}$. Solutions were stirred for 1 hour and left to stand for a further 2 hours to minimise any shearing effects due to stirring. After this time, solutions were centrifuged to induce sedimentation of the silica. To rule out the possibility of protein sedimentation a blank experiment with protein only was carried out. Residual protein concentration in solution was determined using a Unicam UV2 UV-Vis spectrometer using a quartz cell with 1 cm path length, measuring absorbance at 280 nm. Calibration was carried out using a series of protein solutions of known concentration, Figure 2.9. Each experiment was performed in triplicate. The silica particles were collected, rinsed with PBS to remove any excess protein solution and analysed by infrared spectroscopy immediately.

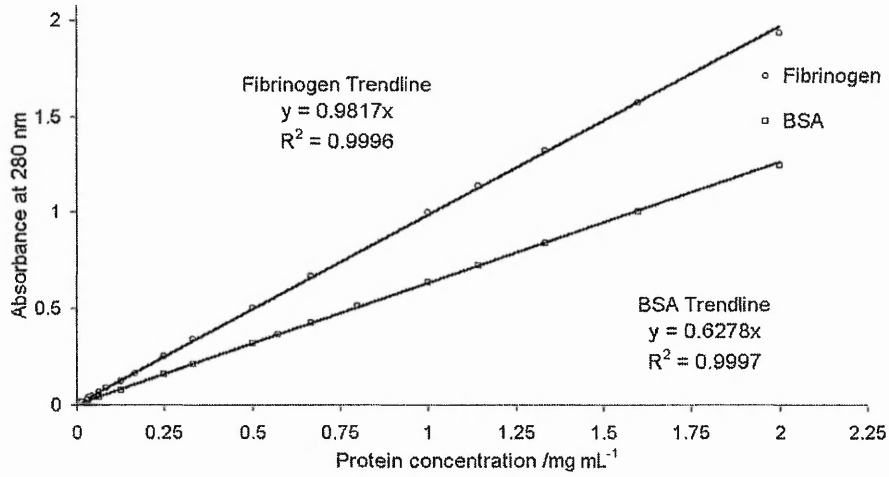

Figure 2.9. Calibration plots for BSA and bovine fibrinogen UV_{280} assay.

2.5 Surface Area and Porosity Analysis

2.5.1 Sample Characterisation by Nitrogen Adsorption

Nitrogen gas adsorption can be used for surface area analysis and can also yield information about pore structure. Samples must first be degassed by moderate heat treatment under vacuum to remove any contaminants from the surface and are then thermally equilibrated in liquid nitrogen, again under vacuum. An adsorption isotherm can then be constructed by admitting a small amount of nitrogen until a predetermined relative pressure 'P/P_0' is achieved. The inlet of nitrogen is monitored so that the exact amount of adsorbate required to reach this relative pressure is known. A range of pressures are monitored from 0 to 1 by successive injections of nitrogen. Conversely, a desorption isotherm can be constructed by sequentially lowering the relative pressure until a vacuum is reached. The shape of the isotherm is therefore dependent on the interaction between nitrogen and the sample material, giving information about energy of adsorption, surface area, the level of porosity and pore structure. Pores can be categorised depending on size: micropores ($\leq$ 20 Å diameter), mesopores (20 – 500 Å diameter) and macropores (> 500 Å diameter).

There are five classical isotherm shapes reported by Brunauer, Deming, Deming and Teller (BDDT), Figure 2.10.[33]

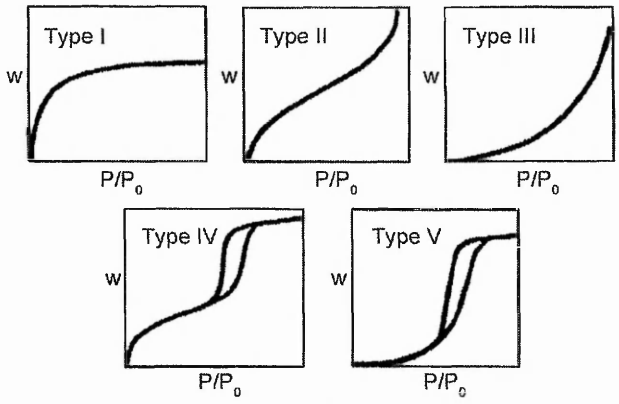

Figure 2.10. Isotherms according to BDDT.[33] 'W' is the mass of nitrogen adsorbed.

Type 1 adsorption isotherms arise from microporous solids having low surface area, which governs the total amount of adsorbate reaching a limiting value at higher partial pressures. A similar case is observed in type 2 isotherms wherein the amount adsorbed plateaus when monolayer coverage is complete but again increases due to multi-layer adsorption. These are normally observed for non-porous or macroporous materials. Type 3 isotherms are quite rare and are observed when the adsorbate-adsorbate interactions are higher than the adsorbate-adsorbent interactions. Type 4 isotherms have a steep slope at high partial pressures indicating capillary condensation in mesopores. Type 5 adsorption isotherms are also rare, similar to the type 2 but indicating the presence of mesopores.

2.5.2 BET Surface Area Measurement

From the mass of nitrogen adsorbed over a range of partial pressures the surface area of the sample can be found using the Brunauer, Emmett, Teller (BET) method,[34]

$$\frac{1}{W[(\frac{P_0}{P})-1]} = \frac{1}{W_m C} + \frac{(C-1)}{W_m C}\frac{P}{P_0} \qquad \text{Equation (2.16)}$$

Where 'W_m' corresponds to a monolayer mass of nitrogen and 'C' is the BET constant, related to the adsorbant / adsorbate interactions, 'E_a'. Large 'C' values are obtained for high affinities and low (but still positive values) for low affinities.

$$E_a = e^{\frac{E-E_l}{RT}} \qquad \text{Equation (2.17)}$$

where 'E' is the heat of monolayer adsorption, 'E_l' the heat of adsorbate liquefaction, 'R' is the gas constant and 'T' is the temperature.

By constructing an isotherm over the partial pressure range of 0.05-0.3 a plot of

$$\frac{1}{W[(P_0/P)-1]} \text{ against } \frac{P}{P_0} \text{ has a gradient } C-1/W_mC \text{ and a } y\text{-intercept } \frac{1}{W_mC},$$

allowing the BET constant and surface area to be calculated as;

$$C=\frac{Gradient}{Intercept}+1 \text{ and } W_m=\frac{1}{Gradient+Intercept} \text{ giving surface area}=\frac{W_m N A_{cs}}{M}$$

where,

N = Avogadro's number (6.023×10^{23} molecules/mole)

M = Molecular weight of nitrogen

A_{cs} = Cross sectional area of a single molecule which for nitrogen is taken to be 16.2 $Å^2$ for a hexagonal close packed monolayer at 77 K

Information about the porosity can also be gained from nitrogen adsorption isotherm shape analysis. Porous materials characteristically exhibit hysteresis where the desorption profile does not follow the path of the adsorption isotherm. Below a critical temperature nitrogen usually adsorbs to form multilayers and the presence of pores may not only effect the number of adsorbate layers, but may also induce capillary condensation. Five distinct cases have been identified, Figure 2.11.[35]

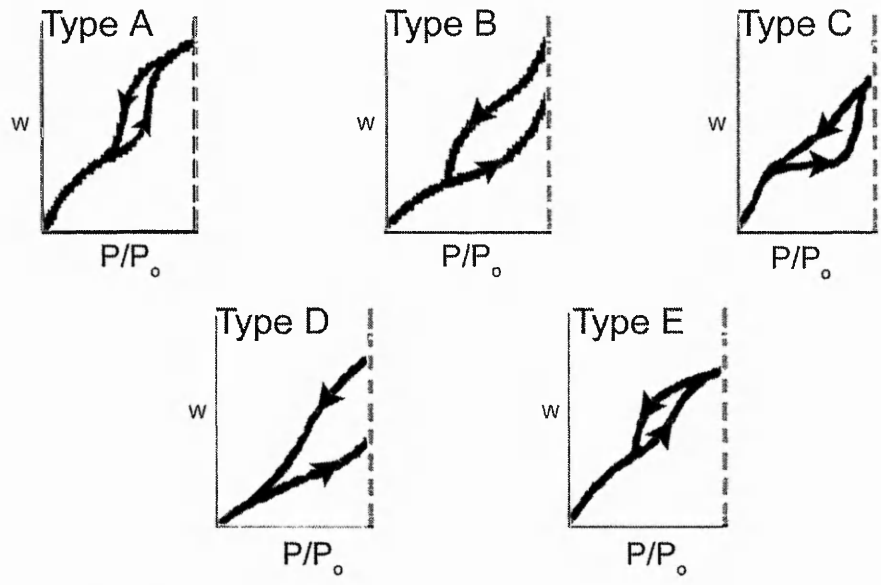

Figure 2.11. Isotherms showing hysteresis.

The differing isotherms relate to differently shaped pores, cylindrical (type A), slit-shaped (type B), wedge-shaped with open ends (type C), wedge-shaped having narrow necks at one or both ends (type D) and ink-bottle shaped (type E).

2.5.3 Total Pore Volume and Average Pore Radius

The total pore volume can be determined by the amount of vapour adsorbed at relative pressures close to unity, assuming that at this pressure all pores are filled with liquid. The volume of liquid nitrogen, 'V_{liq}' is related to the volume of nitrogen adsorbed 'V_{ads}' by the following equation;

$$V_{liq} = \frac{P_a V_{ads} V_m}{RT} \qquad \text{Equation (2.18)}$$

where 'P_a','T' and 'V_m' are the ambient pressure, temperature and molar volume of liquid nitrogen (34.7 $cm^3\,mol^{-1}$) respectively. The average pore radius, 'r_p' can then be found under the assumption that unfilled pores at this pressure have little contribution to the total pore volume.

$$r_p = \frac{2V_{liq}}{S} \qquad \text{Equation (2.19)}$$

where 'S' is the surface area.

There are many ways to assess porosity such as mercury porosimetry, electron microscopy or gas adsorption analysis. One method commonly used is that proposed by Barrett, Joyner and Halenda (BJH) which allows an estimation of pore size distribution assuming cylindrical pores.[36] At high relative pressures ~ 1 the largest filled pores of radius 'r_{pl}' are comprised of a physically adsorbed layer of thickness 't_l' and an evaporative inner layer (termed the Kelvin capillary) of radius 'r_K', Figure 2.12, the latter being reduced with a decrease in pressure.

The relationship between the pore volume 'V_{pl}' and the Kelvin capillary volume 'V_K' is given by;

$$V_{pl} = V_{Kl} \frac{r_{pl}^2}{r_{Kl}^2} \qquad \text{Equation (2.20)}$$

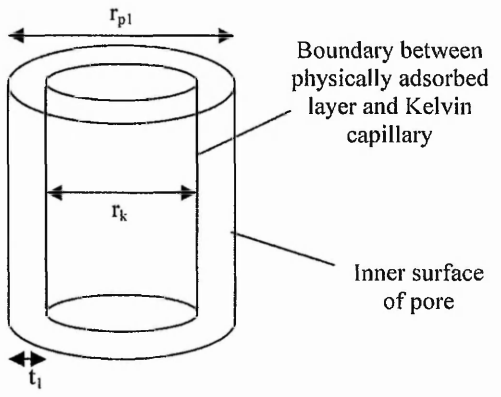

Figure 2.12. Cylindrical pore model.

By reducing the pressure the volume of the adsorbent decreases by 'ΔV_l' as the pores empty, reducing the physically adsorbed layer thickness by 'Δt_l'. Over a given decrease in pressure, if the average change in thickness is '$\Delta t_{l/2}$' the largest pore volume can be expressed as;

$$V_{pl} = \Delta V_l \left(\frac{r_{pl}}{r_{kl} + \Delta t_l / 2} \right)^2 \qquad \text{Equation (2.21)}$$

Further reduction in pressure decreases not only the liquid volume from the next largest pore but also reduces the physically adsorbed layer in the largest pores. The reduction in volume of the second largest pores can be written as;

$$V_{p2} = \left(\Delta V_2 - V_{\Delta t2}\right)\left(\frac{r_{p2}}{r_{k2} + \Delta t_2/2}\right)^2 \qquad \text{Equation (2.22)}$$

where '$V_{\Delta t2}$' is the volume desorbed by thinning of the second largest pore,

$$V_{\Delta t_2} = \Delta t_2 A c_1 \qquad \text{Equation (2.23)}$$

where 'Ac_1' is the average area exposed in the previously emptied pore by the desorption of the physically adsorbed layer. Equation (2.23) can then be written as a generalised expression of stepwise desorption of *nth* stages.

$$V_{\Delta t_2} = \Delta t_n \sum_{j=1}^{n-1} A c_j \qquad \text{Equation (2.24)}$$

Equation (2.24) includes the summation of all average areas of pores emptied excluding the final pore size. This must be included to give a complete expression, achieved by substituting Equation 2.24 into Equation 2.22 to give;

$$V_{pn} = \left(\Delta V_n - \Delta t_n \sum_{j=1}^{n-1} A c_j\right)\left(\frac{r_{pn}}{r_{kn} + \Delta t_n/2}\right)^2 \qquad \text{Equation (2.25)}$$

The area 'Ac' for any size pore is not constant, varying with each desorption step and therefore must also be evaluated.

The area 'A_p' of each pore can be calculated from the pore volume if it is assumed that cylindrical pores are present,

$$A_p = \frac{2V_p}{r_p}$$ Equation (2.26)

It is assumed that all pores with an average radius 'r_p' are emptied of their condensate during a relative pressure decrease, with an average core radius 'r_c' given by,

$$r_c = r_p - t_r$$ Equation (2.27)

where 't_r' is the thickness of the physically adsorbed layer at the corresponding value of P/P_0.

Then by letting,

$$\frac{r_c}{r_p} = \frac{r_p - t_r}{r_p} = c$$ Equation (2.28)

and substituting 'c' into Equation 2.25 gives,

$$V_{pn} = \left(\Delta V_n - \Delta t_n \sum_{j=1}^{n-1} A \left(\frac{r_p - t_r}{r_p} \right)_j \right) \left(\frac{r_{pn}}{r_{kn} + \Delta t_n / 2} \right)^2$$ Equation (2.29)

Equation (2.29) can then be used for the computation of pore size distributions.

2.5.4 Experimental Details - Nitrogen Adsorption Analysis

All nitrogen adsorption analysis was performed using a Quantachrome Nova3200 instrument and vacuum degassing of all samples for a minimum of 12 hours at 120 °C immediately prior to analysis. Sample silica spheres were dispersed by sonication in water and freeze-dried to prevent aggregation. Partial pressures in the range 0.05-1 were covered using a 56 point analysis adsorption and desorption profile. Multipoint BET analysis was conducted to assess surface area and the BJH method was used to assess pore size distribution.

2.6 Protein Adsorption

The Langmuir isotherm (Type 1) describes adsorption onto a surface with a fixed number of adsorption sites, wherein surface coverage and therefore the adsorption process is complete upon monolayer adsorption.[37] The Langmuir model describes the relationship between the adsorbate surface concentration 'Q' and the concentration in the phase adjacent to the surface 'C', written as;

$$\frac{Q}{Q_m} = \frac{K_d C}{1 + K_d C} \qquad \text{Equation (2.30)}$$

where 'Q_m' is the maximum adsorbate binding capacity and 'K_d' is a binding affinity constant. Some of the assumptions of this model are not necessarily true for protein adsorption.

Equation (2.30) can be derived by considering the adsorption of molecules 'M' onto vacant surface sites 'S' where an equilibrium constant 'k' governs S + M ⇆ SM, i.e.

$$k = \frac{[SM]}{[S][M]} \qquad \text{Equation (2.31)}$$

[SM] is proportional to the surface coverage 'θ' ($0<\theta<1$), and [S] is proportional to the number of vacant sites '$(1-\theta)$'.

$$k = \frac{\theta}{[M](1-\theta)} \qquad \text{Equation (2.32)}$$

Rearrangement and substitution of '$\theta = Q/Q_m$' gives Equation 2.30.

Deviations from the Langmuir model may be due to multiple-site binding and lateral interactions between binding species. The main assumptions within this model are that the surface is completely homogenous, with each vacant surface site filled by one adsorbing species. Proteins which spread or denature as they bind to the surface are not

accounted for. Other models such as that proposed by Freundlich incorporate parameters that try to factor in some of these problems.[38] However, these parameters must be fixed when fitting protein saturation curves to give any real meaning to the information obtained. Several previous studies have highlighted these problems.[39,40] Protein adsorption data within this thesis was found to fit well with Langmuir type curves as described above.

2.6.1 Experimental Details - Protein Adsorption

Protein adsorption was analysed by a number of techniques: QCM and UV and FTIR spectroscopy, fitting data to a Langmuir curve. See individual sections for experimental details.

2.7 Electron Microscopy

The basic principles involved in electron microscopy are that a stream of electrons are focussed and accelerated towards a sample using a series of apertures, lenses and an applied electric potential. A number of interactions can occur between the sample and the electron beam which can be measured and interpreted, yielding information about the sample, Figure 2.13. A number of interactions involve electrons being scattered, transmitted or emitted from sample can be used for sample imaging. High energy incident electrons may transfer part of their energy, and in so doing eject lower energy electrons out of sample atoms. Several of these emitted electrons, termed 'secondary electrons' can be produced by a single incident electron. Upon emission, the sample atom undergoes relaxation wherein an electron from an outer orbital moves to fill a now unfilled orbital of lower energy. Energy is given out during relaxation, usually in the form of X-rays to balance the total energy of the atom. Each element discharges X-rays having specific energy and so these can be used for elemental analysis, a method called energy dispersive X-ray analysis (EDXA).

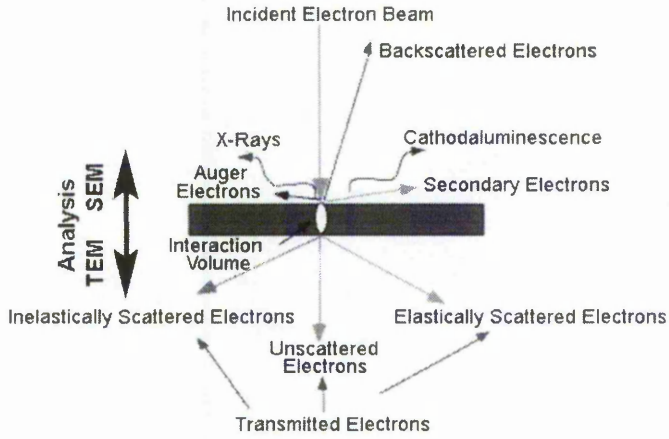

Figure 2.13. Principle interactions involved in electron microscopy.

2.7.1 Transmission Electron Microscopy (TEM)

As the electron beam interacts with the sample some electrons are transmitted directly through, depending on the density and mass of the material. This portion is focussed onto a detector affording an image relating the intensity of the transmitted beam to its spatial geometry, i.e. where the beam interacted with the sample. Transmission electron microscopy is useful for the measurement of nano-sized particles.

2.7.2 Scanning Electron Microscopy

Due to their low energy only secondary electrons arising from atoms near the sample surface (<10 nm) can be detected and again can be interpreted as intensity in relation to spatial geometry. As the beam is rastered across the sample surface any changes in topography will effect the yield of secondary electrons detected making scanning electron microscopy a useful tool to examine surface morphology.

2.8 Proteins Studied

2.8.1 Bovine Serum Albumin (BSA)

With a molecular weight of 66 kDa albumin is the most abundant protein in the circulatory system acting as a multifunctional transporter protein, having a concentration of approximately 50 mg mL^{-1} plasma. Synthesised initially as pre-proalbumin by the liver the signal peptide is removed affording proalbumin which is further processed to form albumin by removal of the six residue propeptide from the new N-terminus.

Early research led to the belief that serum albumin had an ellipsoid shape with dimensions of 14 by 4 by 4 nm although ^{1}H NMR studies indicate a heart-shaped structure[41] in good agreement with X-ray crystallographic data,[42] Figure 2.14. Data on the secondary structure of albumin is somewhat contradictory with some researchers suggesting predominantly alpha-helical (50-68%) structure with the remaining being made-up of beta-sheet (16% - 18%)[43-45] but with other research pointing towards the protein polypeptide containing no beta-sheet structure but having turns and extended flexible regions instead[46].

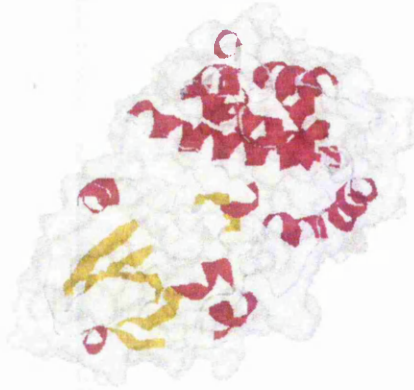

Figure 2.14. Secondary structure of BSA showing α-helixes in red and β-sheet in yellow. The outer molecular surface is shown in grey. [http://www.ncbi.nlm.nih.gov/entrez, PDB; code: 1A06]

The bovine serum albumin molecule is homologous to human serum albumin (HSA)[47] comprising three domains that are sub-divided into nine loops (L1-L9) held together by seventeen disulphide bridges. An unusual structural feature amongst extracellular proteins is the presence of a single sulfhydryl group at Cys-34. The net charge on domains I, II and III are -10, -8 and 0 respectively at neutral pH.[48] However, when in a solution with a pH below its iosoelectric point (pI=4.7) the net charge of the whole molecule is positive. Likewise above this point the net charge is negative.

2.8.2 Bovine Fibrinogen (Fg)

Fibrinogen, found in the circulatory system at a concentration of 2.6 mg mL^{-1} is the key structural glycoprotein in blood clotting which upon thrombin activation self-assembles forming a fibrin clot. Having a mass of 340 KDa the elongated molecule, 46 by 4 by 4 nm[44,49] is a genuine covalent dimer, the two halves of which have identical

sequences being linked by a central globular domain. Each monomer has three non-identical chains, Aα, Bβ and γ, connected together at the N-terminus by eleven disulphide bridges forming the 'disulphide knot'. The C-terminus of each chain is globular. Those of the β and γ chains extend forming dumbell shaped ends to the molecule termed the 'D' regions, whilst the Aα chain globular domains, termed the αC units, interact with each other at the central 'E' region, Figure 2.15. Fibrinogen is comprised of mainly helical secondary structure (35%) and beta-sheet (21%), with 13% beta turn and the remainder comprised of random chains.[50] It has an isoelectric point of pI ~5.5.

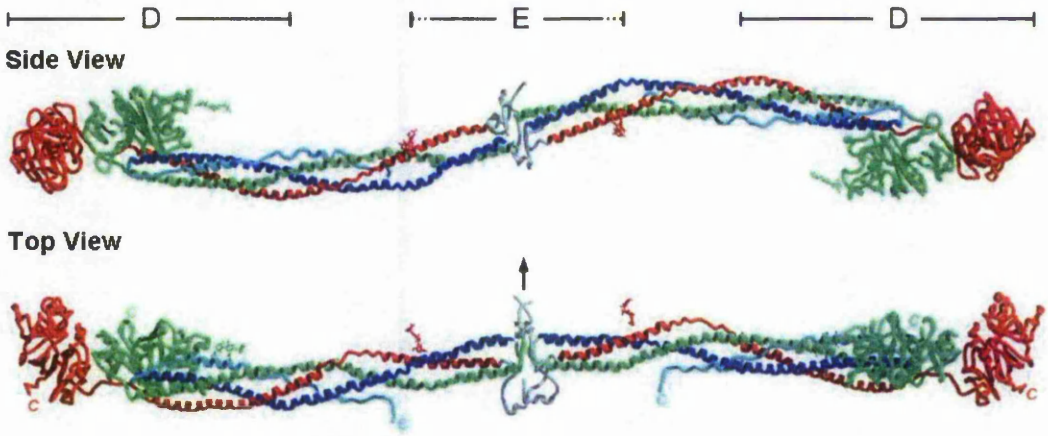

Figure 2.15. Views of the fibrinogen molecule with colour scheme – Aα-chain blue, Bβ-chain in green, γ-chain in red and anti-parallel Aα-chain in light blue. The central arrow points in the direction of axial rotation. Adapted from reference 51.

Mamalian fibrinogens principally differ only by the addition or removal of a small number of residues allowing models of fibrinogen from different sources to be used for general discussion of the structure and its characteristic properties.

2.8.3 Experimental Detail – Protein Solutions

Bovine fibrinogen (Fg, type I-S, lyophilized powder, 90%) and bovine serum albumin (BSA, fraction V, lyophilized powder, 98%) were obtained from Sigma and used as received. Phosphate buffered saline (PBS) was freshly prepared using sodium salts: NaH_2PO_4 and Na_2HPO_4 (200 mmol phosphate) and NaCl (100 mmol) obtained from Aldrich to give pH 7.4 at 25 °C. Protein solutions with concentrations in the range 6-2000 μg mL^{-1} were prepared immediately before use by dilution of a stock solution. Distilled deionised water with a conductivity of ~1 μS was used for all experiments.

2.9 Protein Assays

2.9.1 Fluorimetry - Nano Orange Fluorometric Protein Quantification

The Nano Orange protein quantification kit (Molecular probes, N6666) containing a fluorescent protein dye allows for the accurate determination of protein concentration in the range 10-0.001 μg mL^{-1}. The Nano Orange reagent is virtually non-fluorescent in aqueous solution, but upon binding to proteins the surfactant dye molecule undergoes a dramatic fluorescence enhancement,[52] having a broad excitation peak centered at 470 nm and a broad emission peak centered at 570 nm. A number of studies have examined pH,[53] contaminant,[54] and temperature affects[55] on the assay, reporting use of the fluorescent dye for up to 6 hours after addition of protein with no loss in sensitivity.

2.9.2 Amide Black Staining Assay

Naphthol blue black can be used as a protein stain to assess relative amounts of protein adhering to surfaces.[56] After protein incubation the stain is added which strongly interacts with the surface-bound protein, possibly forming a complex between a protein amine group and the sulphonic acid groups of the dye molecule.[57,58] The protein-dye interaction can then be disrupted by the addition of sodium hydroxide, allowing the dye to be recovered in solution and analysed by its characteristic absorption band at 620 nm.[59] This staining method is not directly quantitative as it requires calibration, which is difficult for surface-bound protein analysis, especially for such small quantities ~300 ng cm^{-2}.

2.9.3 Experimental Details - Protein Assay

Protein adsorption isotherms were constructed by incubating a range of protein solution concentrations over a surface, rinsing to remove any unbound protein and analysing the remaining surface-bound protein. To allow a variety of surfaces to be analysed glass rings were attached to surfaces prepared on microscope slides such that each ring defined the boundary of a well in which protein solution could be incubated. A number of adhesives were tested although polyvinyl acetate (Loctite) was found to be the best due to its lack of porosity and ease of use. In this way multi-well plates were produced specifically for each experiment, Figure 2.16.

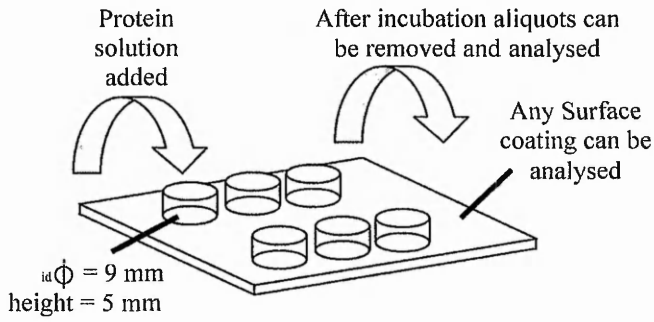

Figure 2.16. Multi-well plates fabricated to investigate any type of surface.

2.9.4 Experimental Details - Nano Orange Protein Quantification

Calibration for each protein was conducted separately, data for each concentration being collected in triplicate, Figure 2.17. The Nano Orange working solution was prepared as follows, using concentrated (500 times concentrated solution as supplied) Nano Orange protein quantitation reagent and concentrated (10X) Nano Orange protein quantitation diluent. As an example, to prepare 50 mL of Nano Orange working solution, 5 mL of 10X diluent solution was mixed with 45 mL distilled deionised water. 100 μL of the 500X Nano Orange reagent was added and the solution again mixed thoroughly. The vials were covered to prevent photodegradation.

Protein solutions were prepared in the range 6-2000 $\mu g\,mL^{-1}$ by successive dilution of a freshly prepared 2 $mg\,mL^{-1}$ stock solution. 200 μL aliquots of each solution were pipetted into Eppendorf tubes and the solvent taken to dryness using a speed vac. concentrator (Stratech Scientific, London). To each tube 300 μL of Nano Orange working solution was added and vortex stirred for 20 minutes. The samples

were heated to 96 °C for 10 minutes, allowed to cool to room temperature and again vortex stirred to ensure homogeneity. 250 µL of each sample was pipetted into a black 96-well plate and analysed using a Spectra Fluor microplate reader (Tecan), with excitation / emission wavelengths set at 485 / 595 nm, 3-10 flashes per well with 40µs integration time.

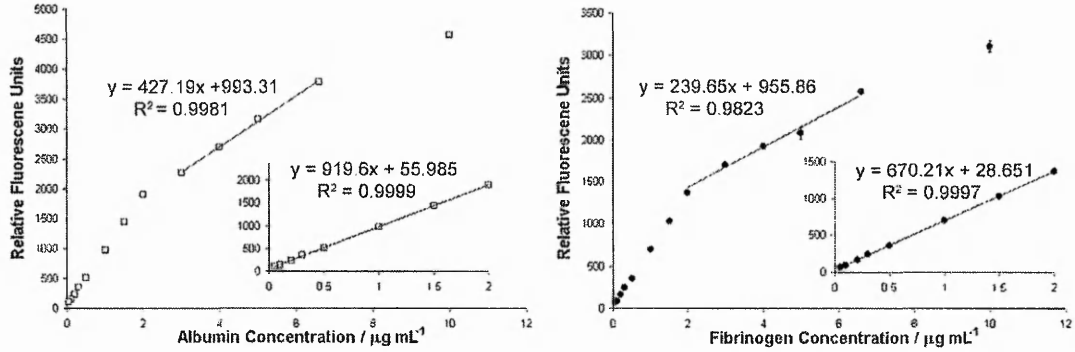

Figure 2.17. Calibration plots for A) BSA and B) bovine fibrinogen Nano Orange assay. Inserts show enlarged lower concentration range.

Protein solutions in the range 6-2000 µg mL^{-1} were incubated for 1 hour over a specific surface (either thiol self assembled monolayers or sol-gel coatings, see sections 2.10 and 2.13 respectively) in the multi-well plates prepared as above, after which time the surfaces were rinsed three times with distilled, deionised water to remove any unbound protein. Surface-bound protein was then detached by three sequential rinsing cycles using 250 µL ethanol (Haymans) and distilled deionised water. All wash solutions were collected and solvent was removed using a speed vac. concentrator (Stratech Scientific, London). Quantification of the protein removed from the surface was then conduced by fluorometric assay.

2.9.5 Experimental Details - Amido Black Staining Assay

Protein solutions in the range 6-2000 µg mL^{-1} were incubated for 1 hour over a surface in the multi-well plates prepared as above, after which time the surfaces were rinsed three times with distilled, deionised water to remove any unbound protein, Figure 2.18. 200 µL of the stain solution containing 10% methanol (Haymans), 80% distilled deionised water, 10% glacial acetic acid (Fisher) and 1% wt naphthol blue-black (Sigma) was added into each well and left for 5 mins. Surfaces were then rinsed to

remove any unbound dye using distilled deionised water followed by three rinse cycles in wash solution containing 38% methanol, 60% distilled deionised water and 2% glacial acetic acid. The bound dye was then detached into solution by placing 250 μL of the eluent solution into each well and leaving for 30 mins. The eluent solution contained 50% each ethanol (Haymans) and 50 mM sodium hydroxide (Fisher) containing 0.1 mM ethylenediaminetetraacetic acid disodium salt (EDTA) (Fisher). 200 μL was then removed from each well into a clear 96 multiwell plate and analysed in a Spectra Fluor microplate reader (Tecan) using a 620 nm incident filter with a 450 nm reference filter.

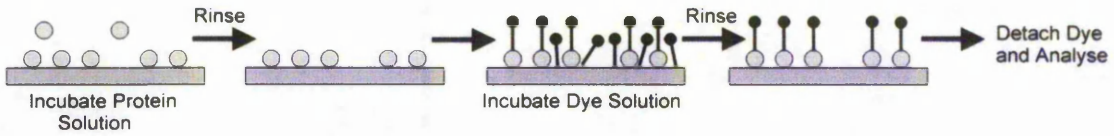

Figure 2.18. Schematic of Amide Black assay.

2.10 Self Assembled Monolayer (SAM) Formation Using Thiols

Self-assembled monolayers are a popular means of creating chemically well-defined surfaces. Due to the speed and ease of preparation and the high quality of order that can be obtained, thiols adsorbing to a gold surface are one of the most attractive systems of this kind. Formed by the interaction of a disulphide,[60] thiol (sulphydryl)[61-65] or thiolsulphate[66] with gold these monolayers can be formed from a gas or solution phase.

The formation of a monolayer occurs with the sulphur group attached to the gold and the tail group of the thiol pointing away from the surface, Figure 2.19.

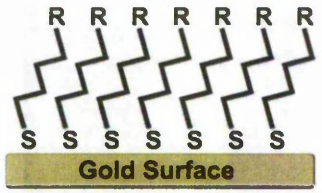

Figure 2.19. Schematic of thiol self assembled monolayer formation.

The actual reaction mechanism remains somewhat of a mystery although the generally accepted scheme is shown below, Equation 2.33.[65,67,68]

$R\text{-}S\text{-}H + Au \rightarrow R\text{-}S^{-}\text{-}Au^{+} + \frac{1}{2} H_2$ Equation (2.33)

The most common method to form thiol monolayers is by the immersion of a clean gold surface into an organic solvent containing the thiol at low concentration (typically 1-10 mM). The driving force for monolayer formation is the maximization of gold-sulphur bonds and chain-chain hydrophobic interactions, which results in a densely packed, almost crystalline monolayer.[63]

2.10.1 Experimental Details - Preparation of Thiol SAMs

Chemically defined surfaces were prepared from self assembled monolayers (SAMs) of thiols: heptanethiol and mercaptoethanol (Sigma) to give hydrophobic and hydrophilic surfaces respectively. Gold coated microscope slides and QCM crystals were incubated in 1 m M ethanolic solutions of the desired thiol, incubating for a minimum of 12 hours to ensure reproducible organised monolayer formation. After this time the surfaces were rinsed in ethanol to remove any non-bound thiols and dried under nitrogen immediately before use. Surface wettability was characterized as described in section 2.1 giving contact angles which are in good agreement with those reported previously by others.[69-71] Heptanethiol treated surfaces showed a contact angle of 94°, whereas on mercaptoethanol treated surfaces the contact angle was 48°.

2.11 Preparation of Gold-Coated Surfaces

A gold surface was required in most cases to allow chemical modification by self assembly (see above) but infrared experiments also benefited from the reflective conductive layer, giving rise to enhanced signal (see above). Substrates were prepared by sputter deposition of 30 nm gold onto glass microscope slides using 3 nm thickness titanium as an adhesive layer. This was conduced using an Emitech K575 fitted with a quartz crystal microbalance thickness monitor. The surfaces were washed in ethanol (Haymans), dried under nitrogen and stored in a desiccator before use. Quartz crystal microbalance (QCM) crystals with Cr/Au electrodes (Testbourne LTD) were cleaned before use using piranha etch solution, 37% H_2SO_4 : 98% H_2O_2 at a ratio of 3:1[72](Sigma and Fisher Chemicals respectively) rinsing thoroughly with distilled, deionised water and ethanol (Haymans) before use.

2.12 Preparation of Silica Spheres

Mono-disperse silica spheres of varying sizes were prepared by the Stöber process[73] via the condensation of silicic acid. The general reaction scheme is shown in Figure 2.20, although it should be noted that many other routes also result in the formation of silica.

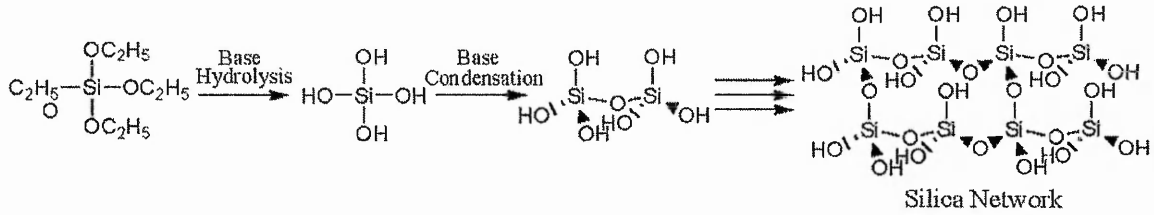

Figure 2.20. Reaction scheme of base catalysed silica formation.

Briefly, batches of spheres were prepared by the addition of ammonia to ethanolic solutions of tetraethoxyorthosilicate (Aldrich) to make a total volume of 200 mL, specific sphere sizes and preparation conditions are given in Table 2.1. These were stirred overnight and left to stand at 25 °C for more than 5 days. Spheres were collected by centrifugation and acid treated using 1M HCl (Fisher) to ensure all terminal ethoxy groups were converted to hydroxyl groups. Silica spheres were washed by repeated sonication and centrifugation cycles until the water removed had a conductivity of ~5 μS. Transmission electron microscopy (TEM) was used to measure particle size. A minimum of 40 particles for each sample were measured.

Table 2.1. Reaction conditions for sphere preparation

Surface Area /$m^2 g^{-1}$	Sphere Radius /nm	Concentration of Reactants /Mol		
		Water	TEOS	Ammonia
373	7.5 ± 0.2	6.00	0.5	0.025
350	9.6 ± 0.4	6.00	0.5	0.050
327	14.4 ± 2.1	6.00	0.5	0.070
174	41.0 ± 1.8	6.00	0.5	0.100
81	61.3 ± 3.1	6.00	0.5	0.200
65	81.8 ± 3.9	5.56	0.22	0.723

Surface area measurements were performed by nitrogen adsorption analysis as described in section 2.5, using a Quantachrome Nova3200 system after degassing the samples overnight under vacuum at 120 °C. Methyl terminated spheres were produced by silylating hydroxyl-terminated particles with a vast excess of chlorotrimethylsilane

(31.5 mmol, 98% Aldrich) in toluene (Fisher), stirring overnight and washing in toluene. The surface chemistry of the silica particles as prepared was analysed by infrared spectroscopy using a Nicolet Magna IR-750 spectrometer fitted with a Golden Gate attenuated total reflection (ATR) accessory (Thermo Nicolet). Spectra were recorded at 4 cm^{-1} resolution, averaging 256 scans. Surface wettability was characterised by measuring equilibrium water contact angles on a Krüss DSA10. A 5 µl water droplet was deposited onto loose powdered samples by microsyringe and images were taken immediately to eliminate drying effects.

2.13 Preparation of Foamed Silica Materials

Foamed silica materials were produced as bulks and surface coatings via acid hydrolysis and subsequent base condensation of methyl-triethoxysilane. The general reaction scheme is shown in Figure 2.21, although it should be noted that many other routes also result in the formation of silica.

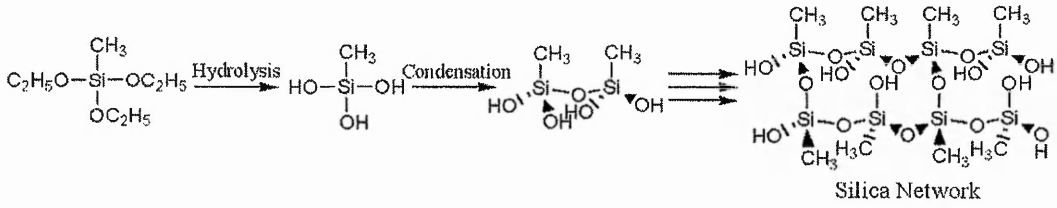

Figure 2.21. Reaction scheme of silica material production.

Sol-gel foams were prepared by mixing dimethyl formamide (DMF, Acros 99%) as solvent (2.5 mL, excess), hydrochloric acid [1.5 mL of 0.12M or 1.2M diluted from 37% HCl (Analar, Aldrich)] and methyl triethoxysilane (MTEOS, Lancaster 98%) (2.5 mL, 12.55 mmol) allowing to stir for 1 hour. After this time 1.625 mL of ammonia solution (of varying dilution, diluted from Fischer 35%) was added, the liquid mixed rapidly and then transferred to polystyrene containers to set. The materials were left sealed for 20 h to ensure complete gelation; they were not heated while wet to prevent excessive dissolution and re-deposition.[74] DMF evaporates slowly under normal conditions, so solvent exchange was necessary, achieved by placing the samples in a large volume of methanol (Haymans) and exchanging it each day for three days. Once dry the samples were placed in a Pyrex® beaker and heated to various temperatures to cross-link and eventually oxidise the materials. To avoid overheating, cracking and inconsistencies, the samples were heated at a rate of 2.5 °C min^{-1} in a Carbolite AAF

11/3 furnace and held at the maximum temperature for 100 min before cooling to room temperature at around 5 °C min^{-1}.

Flat methyl-silica films were prepared using isopropanol (2.5 mL) as solvent, hydrochloric acid (1.5 mL of 1.2M) and MTEOS (0.22 mL, 1.10 mmol).[74] After stirring for 1 hour an aliquot was spread onto a glass substrate to allow the solvent to evaporate. The film was then heated to 200 °C for 1 h (2.5 °C min^{-1}) to cross-link the unreacted silane groups.

Films of porous gels were formed by hydrolysing MTEOS in DMF and adding ammonia solution as above. DMF was chosen as it has a relatively high boiling point and is miscible with water. Tests using propan-2-ol as co-solvent were unsuccessful as evaporation of the solvent during gelation caused the gels to show radial structure.[75] After adding ammonia solution, 0.4 mL of the mixture were placed onto a microscope slide (76.2 by 25.4 mm) and a hydrophobic plate placed on top. These were prepard by incubating microscope slides in 1:20 diluted 'Extreme Wash-In Solution' (Grangers) in deionised water for 10 mins, rinsing in deionised water and heating to 100 °C on a hotplate for 5 min. Glass coverslips were used as spacers to ensure reproducibility of film thickness, Figure 2.22. Gelation was allowed to proceed for at least 4 hours, after which time the hydrophobic slip was removed using forceps. DMF was replaced with methanol as for the preparation of the bulk materials and the gel was allowed to air dry.

Figure 2.22. Production of porous films.

Films were heat treated at a rate of 2.5 °C min^{-1} to cross-link silane groups and remove residual solvent. A final temperature of 200 °C gave hydrophobic films whilst further heating exceeding 400 °C gave hydrophilic films.[2]

2.14 References

1. T. Young T, "*Miscellaneous Works*," Peacock, G. (editor), London: Murray, **1855**, 1, 418
2. N.J. Shirtcliffe; G. McHale; M.I. Newton; C.C. Perry; P. Roach, "Porous Materials Show Superhydrophobic to Superhydrophilic Switching," *Chem. Commun.*, **2005**, 25, 3135-3137
3. N.J. Shirtcliffe; G. McHale; M.I. Newton; G. Chabrol; C.C. Perry, "Dual-Scale Roughness Produces Unusually Water-Repellent Surfaces," *Adv. Mater.*, **2004**, 16(21) 1929-1932
4. R.N. Wenzel, "Resistance of Solid Surfaces to Wetting by Water," *Indust. Eng. Chem.*, **1936**, 28, 988-994
5. A.B.D. Cassie ; S. Baxter, "Wettability of Porous Surfaces," *Trans. Faraday Soc.*, **1944**, 40, 546-551
6. D. Quéré, "Rough Ideas on Wetting," *Physica A*, **2002**, 313, 1-2, 32-46
7. D.A. Buttry; M.D. Ward, "Measurement of Interfacial Processes at Electrode Surfaces With the Electrochemical Quartz Crystal Microbalance," *Chemical Reviews*, **1992**, 92(6)1355–1379
8. C.S. Lu; O. Lewis, "Investigation of Film-Thickness Determination by Oscillating Quartz Resonators With Large Mass Load," *J. Appl. Phys.*, **1972**, 43(11) 4385–4390
9. G. Sauerbrey, "The Use of Quartz Oscillators for Weighing Thin Layers and for Microweighing," *Z. Phys.*, **1959**, 155, 206-222
10. K.K. Kanazawa; O.R. Melroy. "The Quartz Resonator: Electrochemical Applications," *IBM J. Res. Dev.*, **1993**, 37(2) 157–171
11. M.D. Ward; D.A. Buttry, "In Situ Interfacial Mass Detection With Piezoelectric Transducers," *Science*, **1990**, 249(4972) 1000–1007
12. A.P.M. Glassford, "Kinetics Data for Diffusion of Outgassing Species From RTV 560 Silicone Rubber," *J. Vac. Sci. Technol.*, **1978**, 15(6) 1836-1838
13. K.K. Kanazawa; J.Gordon, "Frequency of a Quartz Microbalance in Contact With Liquid," *Anal. Chem.*, **1985**, 57, 1770-1771
14. C.Galli Marxer; M. Collaud Coen; H. Bissig; U.F. Greber; L. Schlapbach, "Simultaneous Measurement of the Maximum Oscillation Amplitude and the Transient Decay Time Constant of the QCM Reveals Stiffness Changes of the Adlayer," *Anal. Bioanal. Chem.*, **2003**, 371(3) 570-577

15. C.G. Marxer; M.C. Coen; L. Schlapbach, "Study of Adsorption and Viscoelastic Properties of Proteins With a Quartz Crystal Microbalance by Measuring the Oscillation Amplitude," *J. Colloid and Int. Sci.*, **2003**, 261, 291-298
16. M.V. Voinova; M. Jonson; B. Kasemo, "'Missing Mass' Effect in Biosensor's QCM Applications," *Biosensors and Bioelectronics*, **2002**, 17, 835-841
17. E-L, Lyle; G.L. Hayward; M. Thompson, "Acoustic Coupling of Transverse Waves as a Mechanism for the Label-Free Detection of Protein-Small Molecule Interactions," *The Analyst*, **2002**, 127, 1596-1600
18. G. McHale; R. Lucklum; M.I. Newton; J.A. Cowen, "Influence of Viscoelasticity and Interfacial Slip on Acoustic Wave Sensors," *J. Appl. Phys.*, **2000**, 88(12) 7304-7312
19. G. McHale; M.I. Newton, "Surface Roughness and Interfacial Slip Boundary Condition for Quartz Crystal Microbalances," *J. Appl. Phys.*, **2004**, 95(1) 373-380
20. V.P. Tolstoy; L.V. Chernyshova; V.A. Skryshevsky, "*Handbook of Infrared Spectrocopy of Ultrathin Films*," John Wiley and Sons, Canada, **2003**
21. R.G. Greenler, "Infrared Study of Adsorbed Molecules on Metal Surfaces By Reflection Techniques," *J. Chem. Phys.*, **1966**, 44(1) 310-315
22. R.G. Greenler, "Reflection Method for Obtaining the Infrared Spectrum of a Thin Layer on a Metal Surface," *J. Chem. Phys.*, **1969**, 50(5) 1963
23. P.R. Griffiths; J.A. de Haseth, "*Fourier Transform Infrared Spectroscopy*," Vol 83 in "*Chemical Analysis*", John Wiley and Sons, Canada, P.J. Elving, J.D. Winefordner, (ed.) **1986**
24. M. Jackson; H. H. Mantsch, "The Use and Misuse of FTIR Spectroscopy in the Determination of Protein Structure," *Crit. Rev. Biochem. Mol. Biol.*, **1995**, 30(2) 95-120
25. T.J. Lenk; T.A. Horbett; B.D. Ratner; K.K. Chittur, "Infrared Spectroscopic Studies of Time-Dependent Changes in Fibrinogen Adsorbed to Polyurethanes," *Langmuir*, **1991**, 7(8) 1755-1764
26. B.J. Frushour; J.L. Koenig, "*Raman Spectroscopy of Proteins*," in, "*Advances in Infrared and Raman Spectroscopy*," R.J.H Clark; R.E. Hester (Eds.) Heyden, London, **1975**, 1, 35-97
27. M. Jackson; P.I. Haris; D. Chapman, "Fourier Transform Infrared Spectroscopic Studies of Calcium-Binding Proteins," *Biochemistry*, **1991**, 30(40) 9681-9686

28. A. Muga; H.H. Mantsch; W.K. Surewicz, "Membrane binding induces destabilization of cytochrome c structure," *Biochemistry*, **1991**, 30(29) 7219-7224
29. S. Kidoaki; T. Matsuda, "Adhesion Forces of the Blood Plasma Proteins on Self-Assembled Monolayer Surfaces of Alkanethiolates with Different Functional Groups Measured by an Atomic Force Microscope," *Langmuir*, **1999**, 15(22) 7639-7646
30. K.K. Chittur, "FTIR/ATR For Protein Adsorption to Biomaterial Surfaces," *Biomaterials*, **1998**, 19(4-5), 357-369
31. Y. Wu; K. Murayama; B. Czarnik-Matusewicz; Y. Ozaki, "Two-Dimensional Attenuated Total Reflection / Infrared Correlation Spectroscopy Studies on Concentration and Heat-Induced Structural Changes of Human Serum Albumin in Aqueous Solutions," *Appl. Spectrosc.*, **2002**, 56(9) 1186-1193
32. D.H. Williams; I. Flemming, "*Spectroscopic Methods in Organic Chemistry*," 5th Ed., McGraw Publishing Company, **1997**, 1-27
33. S. Brunauer; L.S. Deming; W. Deming; E. Teller, "A Theory of the van der Waals Adsorption of Gases," *J. Am. Chem. Soc.*, **1940**, 62, 1723
34. S. Brunauer; P. H. Emmett; E. Teller, "Adsorption of gases in multimolecular layers," *J. Am. Chem. Soc.*, **1938**, 60, 309
35. J. H. de Boer, "*The Structure and Properties of Porous Materials,*" Butterworths, London, **1958**
36. E.P. Barrett, L.G. Joyner, P.H. Halenda, "The Determination of Pore Volume and Area Distributions in Porous Substances. I. Computations From Nitrogen Isotherms," *J. Am. Chem. Soc.*, **1951**, 73, 373-380
37. I. Langmuir, "Constitution and Fundamental Properties of Solids and Liquids. I. Solids," *J. Am. Chem. Soc.*, **1916**, 38, 2221-2295
38. C.H. Giles, "History and Use of the Freundlich Adsorption Isotherm," *J. Soc. Dyers and Colourists*, **1973**, 287-291
39. J-H. Kim; J-Y. Loon; Encyclopedia of Surface and Colloid Sci., 2002, 4373-4381
40. J-Y. Loon; J-H. Kim; W-S. Kim, "Interpretation of Protein Adsorption Phenomena onto Functional Microspheres," *Colloids and Surfaces B: Biointerfaces*, **1998**, 12, 15-22

41. O.J.M. Bos; F.A.J. Labro; M.J.E. Fischer; J. Wilting; L.H.M. Janssen, "The Molecular Mechanism of the Neutral-to-Base Transition of Human Serum Albumin. Acid/Base Titration and Proton Nuclear Magnetic Resonance Studies on a Large Peptic and a Large Tryptic Fragment of Albumin," *J. Bio. Chem.*, **1989**, 264, 2, 953-959
42. D.C. Carter; X.M. He; S.H. Munson; P.D. Twigg; K.M. Gernert; M.B. Broom; T.Y. Miller, "Three-Dimensional Structure of Human Serum Albumin" *Science (Washington, DC, United States)*, **1989**, 244, 4909, 1195-8
43. I. Sjoholm; I. Ljungstedt, "Studies on the Tryptophan and Drug-Binding Properties of Human Serum Albumin Fragments by Affinity Chromatography and Circular Dichroism Measurements," *J. Bio. Chem.*, **1973**, 248(24) 8434-8441
44. R.G. Reed; R.C. Feldhoff; O.L. Clute; T. Peters Jr, "Fragments of Bovine Serum Albumin Produced by Limited Proteolysis. Conformation and Ligand Binding," *Biochemistry*, **1975**, 14(21) 4578-4583
45. J.F. Foster, "Some Aspects of the Structure and Conformational Properties of Serum Albumin," *Albumin Struct., Funct. Uses*, **1977**, 53-84
46. D.C. Carter; JX Ho, "Structure of Serum Albumin," *Adv. Protein Chem.*, **1994**, 45, 153-203
47. A.D. McLachlan; J.E. Walker, "Evolution of Serum Albumin," *J. Mol. Biol.*, **1977**, 112, 543-558
48. T. Peters Jr., "Serum Albumin," *Adv. Protein Chem.*, **1985**, 37, 161-245
49. Z.Yang; I. Mochalkin; L. Veerapandian; M. Riley; R.F. Doolittle, "Crystal Structure of N ative Chicken Fibrinogen at 5.5-Å Resolution," *Biochemistry* , **2000**, 97(8) 3907-3912
50. Y.L.Chen; X.F. Zhang; Y.D. Gong; N.M. Zhao; T.Y. Zeng; X.Q. Song, "Conformational Changes of Fibrinogen Adsorption onto Hydroxyapatite and Titanium Oxide Nanoparticles," *J. Colloid Int. Sci.*, **1999**, 214(1) 38-45
51. J.H. Brown; N. Volkmann; G. Jun; A.H. Henschen-Edman; C. Cohen, " The Crystal Structure of Modified Bovine Fibrinogen," *Proc Natl Acad Sci USA.* **2000**, 97(1) 85-90
52. B. Giordano; L. Jin; A.J. Couch; J.P. Ferrance; J.P. Landers, "Microchip Laser-Induced Fluorescence Detection of Proteins at Submicrogram Per Milliliter

Levels Mediated by Dynamic Labeling Under Pseudonative Conditions," *Anal. Chem.*, **2004**, 76(16) 4705-4714

53. M.D. Harvey; V. Bablekis; P.R. Banks; C.D. Skinner, "Utilization of the Non-Covalent Fluorescent Dye, NanoOrange, as a Potential Clinical Diagnostic Tool. Nanomolar Human Serum Albumin Quantitation," *J. Chromatography, B*, **2001**, 754, 345-356
54. L.J. Jones; R.P. Haugland; V.L. Singer, "Development and Characterization of the NanoOrange Protein Quantitation Assay: A Fluorescence-Based Assay of Proteins in Solution," *Biotechniques*, **2003**, 34, 850-861
55. S. Silberblatt; R.A. Felder; T.E. Mifflin, "Optimizing Reaction Conditions of the NanoOrange Protein Quantitation Method for use With Microplate-Based Automation," *JALA*, **2001**, 6(6) 83-88
56. M.I. Jones; I.R. McColl; D.M. Grant; T.L.Parker, "Protein Adsorption and Platelet Attachment and Activation, on TiN, TiC, and DLC Coatings on Titanium for Cardiovascular Applications," *J. Biomed. Mater. Res.*, **2000**, 52, 413-421
57. C. Tsopelas; R. Sutton, "Why Certain Dyes are Useful for Localizing the Sentinel Lymph Node," *J. Nuclear Medicine*, **2002**, 43, 1377-1382
58. D.S.Wilbur, "Formation of Sulfonamide Bonds Through Reaction of Dyes With Serum Proteins," *J. Nuclear Medicine*, **2003**, 44(9) Author Reply 1540-1541
59. A. Dieckmann-Schuppert; H-J. Schnittler, "A Simple Assay for Quantification of Protein in Tissue Sections, Cell Cultures, and Cell Homogenates, and of Protein Immobilized on Solid Surfaces," *Cell Tissue Res.*, **1997**, 288, 119-126
60. R.G. Nuzzo; D.L.J. Allara, "Adsorption of Bifunctional Organic Disulfides on Gold Surfaces," *Am. Chem. Soc.*, **1983**, 105, 4481-4483
61. S. Ferretti; S. Paynter; D.A. Russell; K.E. Sapsford; D.J. Richardson, "Self-Assembled Monolayers: a Versatile Tool for the Formulation of Bio-Surfaces," *Trends Anal. Chem.*, **2000**, 19(9) 530-540
62. C.D. Bain; E.B. Troughton; Y.-T. Tao; J. Evall; G.M. Whitesides; R.G. Nuzzo, "Formation of Monolayer Films by the Spontaneous Assembly of Organic Thiols From Solution onto Gold," *J. Am. Chem. Soc.*, **1989**, 111, 321-335
63. M.D. Porter; T.B. Bright; D.L. Allara; C.E.D. Chidsey, "Spontaneously Organized Molecular Assemblies. 4. Structural Characterization of n-Alkyl

Thiol Monolayers on Gold by Optical Ellipsometry, Infrared Spectroscopy, and Electrochemistry," *J. Am. Chem. Soc.*, **1987**, 109, 3559-3568

64. C.A. Widrig; C.A. Alves; M.D. Porter, "Scanning Tunneling Microscopy of Ethanethiolate and n-Octadecanethiolate Monolayers Spontaneously Absorbed at Gold Surfaces," *J. Am. Chem. Soc.*, **1991**, 113, 2805-2810
65. H. Sellers; A. Ulman; Y. Shnidman; J.E. Eilers, "Structure and Binding of Alkanethiolates on Gold and Silver Surfaces: Implications for Self-Assembled Monolayers," *J. Am. Chem. Soc.*, **1993**, 115, 9389-9401
66. J. Lukkari; M. Meretoja; I. Kartio; K. Laajalehto; M. Rajamaki; M. Lindstrom; J. Kankare, "Organic Thiosulfates (Bunte Salts): Novel Surface-Active Sulfur Compounds for the Preparation of Self-Assembled Monolayers on Gold," *Langmuir*, **1999**, 15, 3529-3537
67. A. Ulman, "*An Introduction to Ultrathin Organic Films*," Academic Press, Boston, MA, **1991**
68. A. Ulman, "Formation and Structure of Self-Assembled Monolayers," *Chem. Rev.* **1996**, 96, 1533
69. J.L Tan; J. Tien; C.S. Chen, "Microcontact Printing of Proteins on Mixed Self-Assembled Monolayers," *Langmuir*, **2002**, 18, 519-523
70. C.D. Bain; J. Evall; G.M. Whitesides, "Formation of Monolayers by the Coadsorption of Thiols on Gold: Variation in the Head Group, Tail Group, and Solvent," *J. Am. Chem. Soc.*, **1989**, 111, 7155
71. J.L. Tan; W. Liu; C.M. Nelson; S. Raghavan; C.S. Chen, "Simple Approach to Micropattern Cells on Common Culture Substrates by Tuning Substrate Wettability," *Tissue Engineering*, **2004**, 10(5/6) 865-872
72. F. Caruso; D.N. Furlong; P. Kingshott, "Characterization of Ferritin Adsorption onto Gold," *J. Colloid Int. Sci.*, **1997**, 186, 129-140
73. W. Stöber; A. Fink; E. Bohn, "Controlled growth of monodisperse silica spheres in the micron size range," *J. Colloid Interface Sci.*, **1968**, 26(1) 62-69
74. K. Nakanishi; R. Takahashi; T, Nagakane; K, Kitayama; N. Koheya; H. Shikata; N. Soga; "Formation of Hierarchical Pore Structure in Silica Gel," *J. Sol-Gel Sci.*, **2000**, 17, 191-210
75. K. Kanamori; N. Ishizuka; K. Nakanishi; K. Hirao, "Phase Separation in Methylsiloxane Sol-Gel Systems in a Small Confined Space," *J. Sol-Gel Sci. Tech.*, **2003**, 26(1-3) 157-160

Chapter 3

Interpretation of Protein Adsorption: Surface-Induced Conformational Changes

3.1 Introduction

Biocompatibility is closely related to cell behaviour on contact with implant surfaces,[1,2] and is decided by two main factors; the response of the host to the implant and the response of the implant in the host. It has been suggested that biological tissues interact with only the outermost atomic layers of an implant[2-3] and consequently, much research has been devoted to methods that modify the surfaces of existing biomaterials in order to achieve more desirable biological integration. Changes in morphological, physicochemical and biochemical aspects of biomaterials have been investigated.[2]

Cell adhesion is mediated by interaction with pre-adsorbed proteins during implant integration. The adsorption of proteins from blood to biomaterial surfaces is a dynamic process during which proteins may bind, rearrange and detach, Figure 3.1.[1] Thus, the biomaterial surface can be coated with a range of proteins long before any interaction occurs with platelets or cells.

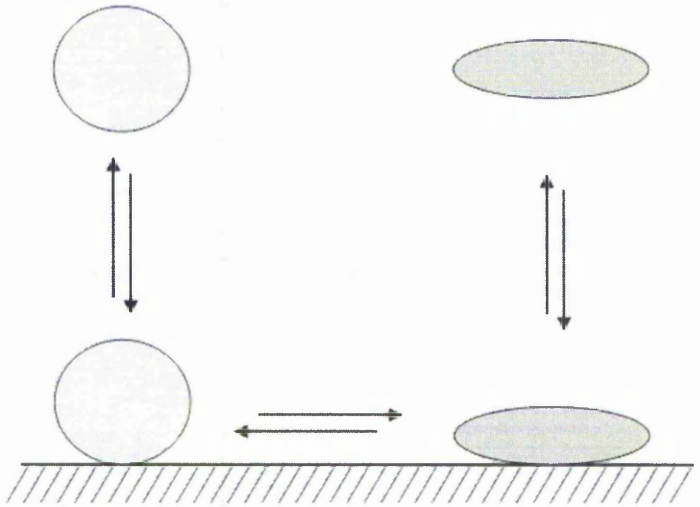

Figure 3.1. Schematic of possible protein adsorption processes.

Although it is now generally accepted that the initial stages of protein adsorption to biomaterials plays an important role in the incorporation of the implant,[1] earlier research in this field mainly focused on cell-surface interactions.[4-7] A number of factors including surface chemistry, charge, topography, and wetting behaviour have been shown to play a role in determining cell growth and proliferation, as discussed in Chapter 1.

Proteins adsorb in differing quantities, densities, conformations and orientations, depending on the chemical and physical characteristics of the surface.[8-12] Protein adsorption is a complex process involving Van der Waals, hydrophobic and electrostatic interactions and hydrogen bonding. Although surface-protein interactions are not well understood, surface chemistry has been shown to play a fundamental role in protein adsorption.[9,10,12] Moreover, the properties of protein over-layers can be altered by the underlying chemistry, which directly impinges on the control of surface-bound protein conformation and / or orientation.[9,10] Adsorbed proteins may act as pilots for cell adhesion if they have the correct geometry to mediate cell attachment. For example, integrin binding sites of cells interact with specific peptide regions within

proteins (e.g. the RGD tripeptide in fibronectin[13]). If these are exposed and available then attachment may occur.

Although cell-surface interactions are understood to be affected by underlying surface chemistry, structural information on surface bound protein conformations and geometries governing cell adhesion have not yet been elucidated. The ability of antibody binding assays to detect the availability of specific binding sites provides indirect evidence of protein conformational or orientational change upon adsorption, although no structural information can be obtained from such investigations.[14] Other analytical tools have been used to study protein adsorption.[14-18] These methods yield only generalized information on the adsorbed protein implying conformational changes; however, no quantitative data on the secondary structure of the adsorbed protein has been presented.

During the past decade substantial progress has been made in understanding the mechanism of protein adsorption. Researchers have developed a number of techniques, e.g. QCM,[15-17] surface plasmon resonance (SPR),[11,15,17] ellipsometry,[15] FTIR,[18] atomic force microscopy (AFM),[9,12,17,19] to tackle this problem although none alone are able to monitor the whole process of adsorption, rearrangement and possible desorption. Here we describe the use of a quartz crystal microbalalance (QCM) and grazing angle Fourier Transform infrared spectroscopy (GA-FTIR) to obtain information on protein adsorption characteristics. To our knowledge this is the first report illustrating the use of QCM together with GA-FTIR to assess protein-surface interactions. QCM allows an insight into the rate and amounts of protein adsorbed whilst FTIR allows the assessment of protein conformation that has previously been well documented,[10,18,20,21] although here surface-bound protein is assessed.

We describe the adsorption characteristics of two plasma proteins: bovine serum albumin (BSA), the most abundant plasma protein which transports fatty acids along with other small molecules throughout the circulatory system and bovine fibrinogen (Fg), the most abundant protein involved in the coagulation cascade.

It is important to understand the effects of different surface properties on protein adhesion, i.e. chemistry and topography. Here we focus on the influence of surface chemistry. The two surfaces examined exhibit differing wetting behavior due only to their contrasting chemically defined surfaces.

3.2 Results and Discussion

3.2.1 Hydrophilic and Hydrophobic Surfaces

The surfaces used in this study were prepared by self assembled monolayer formation of heptanethiol and mercaptoethanol, chosen for their contrasting chemistries as described in section 2.9. Surface wettability was investigated to assess hydrophobicity as discussed in section 2.1. Water contact angles of 94° and 48° were found for CH_3 and OH terminated surfaces respectively, Figure 3.2, which are in good agreement with previous reports.[22-24]

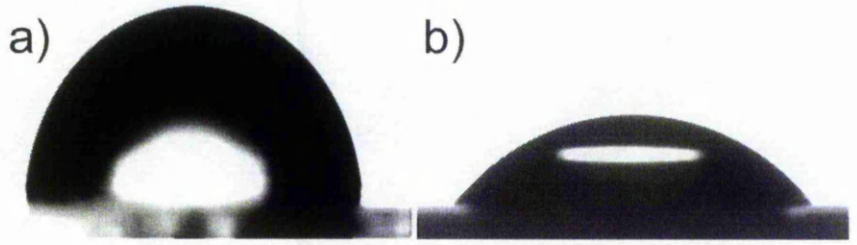

Figure 3.2. Water contact angles on a) hydrophobic and b) hydrophilic surfaces.

3.2.2 Quartz Crystal Microbalance (QCM) Measurements

A quartz crystal microbalance was used to compare the adsorption characteristics of albumin and fibrinogen onto model hydrophilic and hydrophobic surfaces. A steady frequency was obtained by flowing a buffer solution over the crystal before flow was diverted allowing a protein solution to flow at the same rate over the crystal face, as described in section 2.2

As an example of the data obtained Figure 3.3 shows the QCM adsorption profiles of fibrinogen onto a hydrophobic alkane terminated surface. With increasing protein concentration a greater frequency shift and higher rate of frequency change was observed for adsorption onto both CH_3 and OH terminated surfaces.

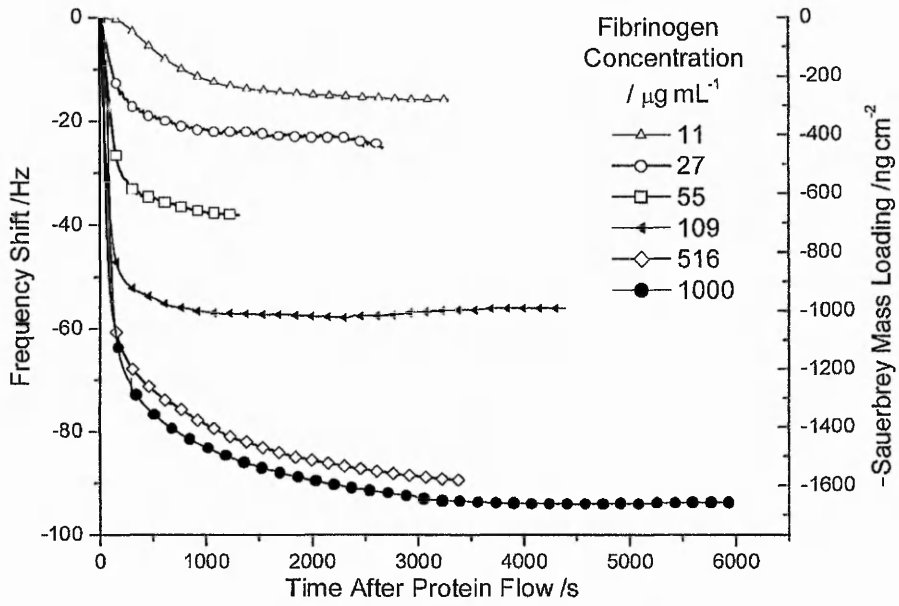

Figure 3.3. Fibrinogen adsorption profiles onto CH_3 terminated surfaces.

Although this trend is true for both fibrinogen and BSA, differing protein-surface interactions are apparent from the shapes of the adsorption profiles. At higher concentrations the equilibrium protein surface concentration increases to a limiting value due to surface saturation. At lower concentrations it is expected that protein molecules will adsorb until an equilibrium surface concentration is reached. At this point the amount of protein adsorbing is equal to that desorbing from the surface. The rate of adsorption of BSA onto the CH_3 terminated surface is greater than that onto the OH terminated surface tested, whereas Fg seems to undergo a similarly rapid adsorption process on both, Figure 3.4. The data shows that BSA has a weaker attraction towards the hydrophilic than the hydrophobic surface.

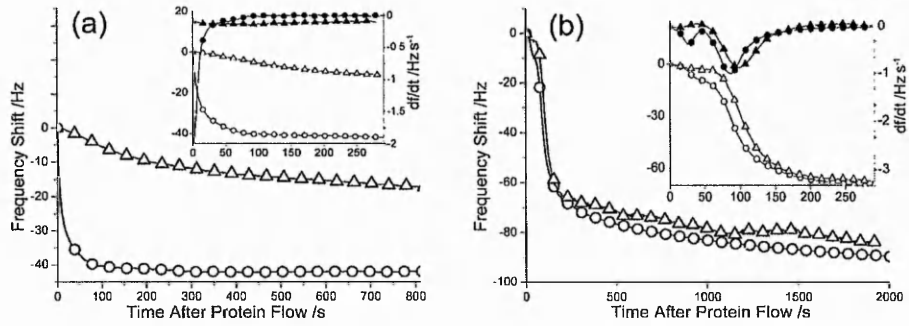

Figure 3.4. Initial adsorption profiles of a) BSA and b) fibrinogen onto CH_3 (O) and OH (Δ) terminated surfaces. Initial bulk protein concentration was 1 mg mL^{-1}. Inserts show derivative plots of early stages of adsorption with solid symbols corresponding to those of the main figure.

A convenient method to assess the protein-surface affinity is to deduce 'binding constants' that compare the rate of adsorption to desorption. When data is fitted to a Langmuir curve, the binding constant '*k*' and a saturation value for the amount adsorbed can be estimated. '*k*' relates to the affinity of the adsorbent to the adsorbate with a high value representing higher affinity, as discussed in Chapter 2. Langmuir isotherms for BSA and Fg onto CH_3 and OH terminated surfaces were fitted using Origin v6.1 software and are shown in Figure 3.5, and values (Table 3.1) of '*k*' were calculated as 5.3 and 5.4 for BSA onto OH and CH_3 terminated surfaces respectively.

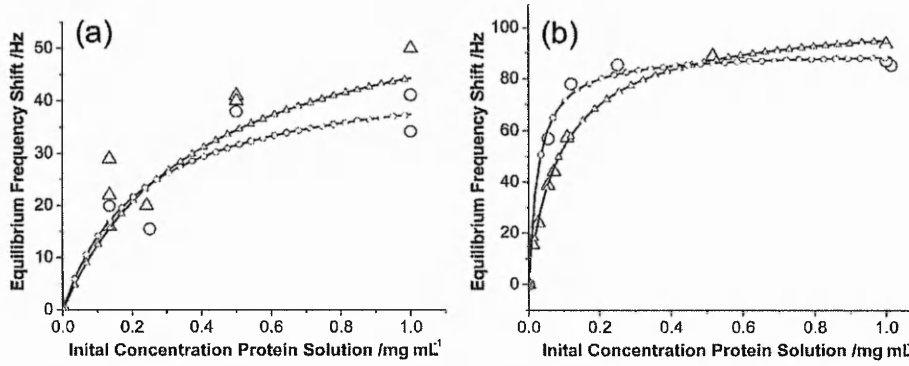

Figure 3.5. Langmuir adsorption isotherms of a) BSA and b) fibrinogen onto CH_3 (O) and OH (Δ) terminated surfaces.

Surface saturation frequency shift values of 47.2 and 40.9 Hz were also obtained for BSA adsorption onto the hydrophilic and hydrophobic surfaces respectively. Greater amounts of BSA can adsorb to a hydrophilic surface, although higher affinity towards the hydrophobic surface causes deformation of the protein (see

later) and this helps to explain the lower surface coverage at saturation. Similarly Fg has a greater affinity towards the CH_3 terminated surface ($k = 36.0$ versus 10.9 for the OH surface) and has lower saturation values (92.6 versus 102.0 Hz). The greater frequency shift due to greater mass loading was as expected for the higher molecular weight fibrinogen.

Table 3.1. Binding constants and saturation values for BSA and Fibrinogen

	Binding Constant	Saturation Values /Hz
BSA **OH**[a]	5.3	47.2
BSA **CH_3**[a]	5.4	40.9
Fg **OH**	10.9	102.0
Fg **CH_3**	36.0	92.6

[a]**OH** and **CH_3** represent hydrophilic and hydrophobic surfaces respectively

The adsorption profiles of both proteins on the surfaces tested, Figure 3.4, indicate that for albumin onto alkane terminated surfaces and fibrinogen onto both surfaces adsorption is rapid, slowing as surface coverage increases. Proteins adsorbing later in the process compete for free sites that become fewer as coverage increases.

The adsorption process for fibrinogen is complex and this is clearly visible in the derivatives of the adsorption profiles (Figure 3.4 inserts). Adsorption appears to occur in a stepwise fashion with initial rapid adsorption and sequential slowing (~50 sec), followed by a second rapid adsorption stage, again progressively slowing but over a longer time period (~60 min). The results may indicate that the protein initially adsorbs rapidly with its long axis parallel to the surface, thus covering the surface quickly. After this time, rearrangement of the protein to perhaps a perpendicular orientation may allow further protein molecules to adsorb on the uncovered, free sites, a process that is observed as a second rapid adsorption stage. A schematic of possible protein adsorption processes is shown in Figure 3.6. Such surface rearrangement may be driven by increased hydrophobic interaction of the fibrinogen molecules as their long axes become aligned parallel to each-other.

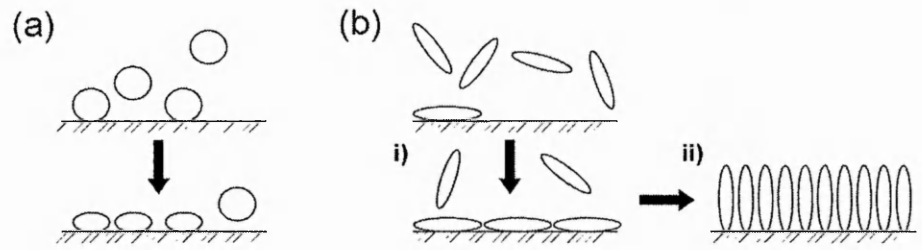

Figure 3.6. A schematic to show adsorption of a) a globular protein (e.g. BSA) whose conformation may become distorted on interaction with the surface and b) rod-like protein that undergoes a multistage adsorption process where (i) initially the protein adsorbs with its long axis parallel to the surface and then (ii) rearrangement occurs to increase protein-protein interaction and surface concentration of protein.

Multi-stage adsorption of fibrinogen was only observed at high concentrations, supporting the proposal for molecular rearrangement of the protein on the surface. At high protein concentrations adsorption is rapid as shown in Figure 3.4, wherein rearrangement occurs in a step-wise fashion giving rise to distinct adsorption as highlighted by derivative plots in Figure 3.4. At lower concentrations adsorption is slower, allowing rearrangement to take place over a long period of time. In this case there are no defined stages indicating rearrangement.

In contrast, albumin seems to undergo a single step adsorption process at the concentrations used. Albumin is approximately globular in shape compared to fibrinogen, so adsorption in any orientation would result in almost the same surface area coverage and packing, Figure 3.6.

It should be noted that the initial adsorption of fibrinogen appears to be affected by the underlying surface chemistry. Derivatives of adsorption profiles show that the first adsorption stage is faster and well defined onto a CH_3 terminated surface, but the second adsorption stage reaches a maximum rate of adsorption earlier in time compared with adsorption onto an OH terminated surface. This data suggests that there is a greater attractive force between a fibrinogen molecule and a hydrophobic compared to a hydrophilic surface. Albumin adsorbs more rapidly to the CH_3 surface than onto the OH terminated surface, which may be due to hydrophobic interactions between the protein and the surface.

3.2.3 Grazing Angle Infrared Analysis

Infrared spectroscopy has been used in this study to assess the conformational state of proteins adsorbed on surfaces modified with CH_3 groups (hydrophobic) and OH groups (hydrophilic). Grazing angle infrared spectroscopy allows the analysis of ultrathin films such as an adsorbed layer of protein by directing the infrared beam to the sample surface at a high incident angle, as discussed in section 2.3. A surface enhancement effect observed when using a conductive substrate also increases the quality spectra. Infrared spectra of proteins consist mainly of amide band vibrations, Figure 3.7. The amide I region (~1700-1600 cm^{-1}), largely due to a C=O stretching vibration, has been widely used for conformational studies, as discussed in Chapter 2.[10,18,20,21] However, few studies have examined surface-bound proteins on well defined chemical surfaces.

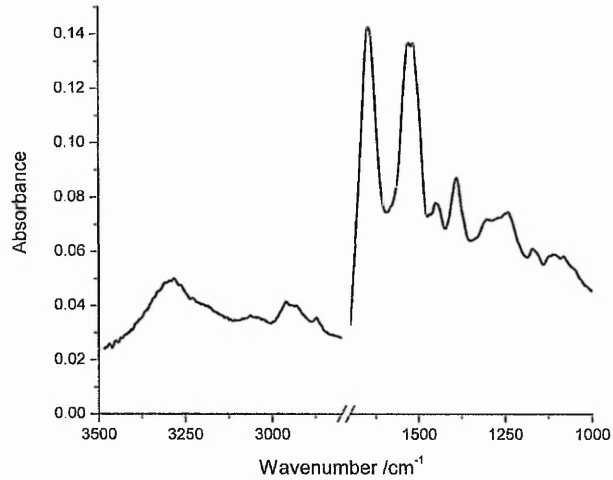

Figure 3.7. Example infrared spectrum of BSA.

Differences in the amide bond orientations within a protein backbone due to varying secondary structures; α-helices, β-sheet, β-turn and unordered, give rise to different vibrational frequencies, observed as component peaks which contribute to the characteristic amide I band. The overall shape and maxima of this band are determined by the secondary structure of the protein analysed.[10,18,20,21] Component amide I bands can be curve fitted to assess protein conformations.

The amide II region (1500-1600 cm^{-1}) contains information from the in-plane N-H bend and C-N stretch of the amide bond. This band is less sensitive to conformational changes compared to the amide I region, although the amide I/II intensity ratio has been identified as a useful tool to qualitatively assess orientation

changes.[10,25] The selection rules for vibrational transitions observed at a grazing angle allow only those dipole moments normal to the surface to absorb. Because the dipole moments of the amide I and II are approximately perpendicular to each other[26] the ratio of these two bands changes if the adsorbed protein changes conformation or orientation. Therefore, time dependent conformational / orientational investigations of surface-bound proteins can be performed. As an illustration of the data obtained within this study Figure 3.8 shows example infrared spectra of fibrinogen and albumin attached to CH_3 and OH terminated surfaces.

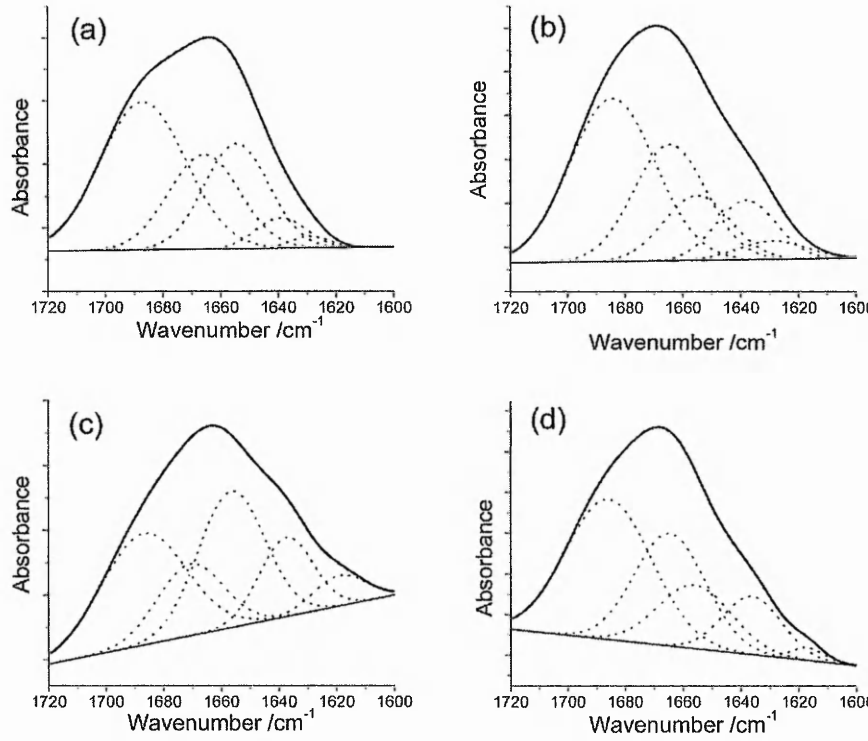

Figure 3.8. Amide I bands with fitted component peaks: a) and b) fibrinogen, c) and d) BSA; a) and c) OH terminated surface, b) and d) CH_3 terminated surface.

Amide I and II maxima and intensity ratios for the proteins adsorbed onto both OH and CH_3 terminated surfaces are presented in Table 3.2. No significant changes in either peak position or their relative intensities were observed with time, suggesting that after an initial one hour adsorption period no further conformational or orientational changes are observed for either protein on either surface.

Table 3.2. Infrared data obtained for adsorbed proteins. Errors are standard deviations obtained from data collection in triplicate.

	Incubation Time /hrs	Amide I Maxima /cm^{-1}	Amide II Maxima /cm^{-1}	Amide I / II Intensity Ratio
BSA **OH**[a]	1	1662.7 ± 0.3	1541.2 ± 3.2	1.05 ± 0.020
	4.5	1661.2 ± 0.9	1538.2 ± 0.7	1.00 ± 0.005
BSA **CH_3**[a]	1	1667.8 ± 2.5	1545.7 ± 1.9	1.01 ± 0.001
	4.5	1666.5 ± 3.2	1545.4 ± 0.6	1.02 ± 0.001
Fg **OH**	1	1666.3 ± 2.0	1541.2 ± 5.6	1.02 ± 0.016
	4.5	1667.0 ± 0.9	1540.8 ± 2.5	1.03 ± 0.016
Fg **CH_3**	1	1668.2 ± 1.0	1547.3 ± 0.7	1.04 ± 0.002
	4.5	1666.4 ± 1.1	1544.7 ± 1.9	1.05 ± 0.003

[a]**OH** and **CH_3** represent hydrophilic and hydrophobic surfaces respectively

Results of the amide I band analysis show that protein secondary structure is affected by protein-surface interactions. Both proteins exhibit different conformations on the two underlying surface chemistries, with albumin in particular showing the strongest apparent change with respect to surface chemistry. Figure 3.8 shows the amide I regions of albumin and fibrinogen attached to CH_3 and OH terminated surfaces respectively, whilst conformational data are summarised in Table 3.3. It is clear from the markedly differing band shapes and the shift of the peak maxima to higher wavenumber on the hydrophobic compared to hydrophilic surfaces that the proteins are held in differing conformations due to their interaction with the surface.

Table 3.3. Conformational analyses of adsorbed proteins on OH (hydrophilic) and CH_3 (hydrophobic) surfaces. Structure percentage values are given. Errors are standard deviations obtained from data collection in triplicate.

Incubation Time (% Structure)	BSA **OH**[a]		BSA **CH_3**[a]		Fibrinogen **OH**		Fibrinogen **CH_3**	
	1 Hour	4.5 Hours	1 Hour	4.5 Hours	1 Hour	4.5 Hours	1 Hour	4.5 Hours
β-sheet / Random	53 ± 4.7	52 ± 2.5	70 ± 1.7	69 ± 1.2	64 ± 2.8	62 ±6.9	68 ± 2.4	73 ±1.8
α-Helix	32 ± 1.9	34 ± 0.4	17 ± 0.9	17 ± 0.6	25 ± 2.7	23 ± 3.0	16 ± 2.4	15 ± 1.2
β-Turn / Sheet	15 ± 1.5	14 ± 1.6	13 ±1.7	14 ± 0.6	10 ± 3.7	13 ± 2.2	15 ± 2.7	12 ± 0.4

[a]**OH** and **CH_3** represent hydrophilic and hydrophobic surfaces respectively

Curve fitting analysis of component bands demonstrates that on the alkane terminated surface, proteins lose a large percentage of their α-helical character; shown by a decrease in the percent area of the component band centred at ~1655 cm^{-1} with a concurrent increase in the β-sheet or random structure component. This behaviour was observed to a greater extent for albumin than fibrinogen. The component band centred at 1638 cm^{-1} for fibrinogen was larger on the alkane surface, which can be related to the extended chain conformation of this protein. These findings suggest that both proteins are somewhat denatured on interaction with a hydrophobic surface, losing a large degree of their helical secondary structure. This change in conformation may arise from a stronger interaction with the surface due to hydrophobic bonding, a feature that has been previously reported for both BSA and fibrinogen along with other proteins, studied by SPR[11] and AFM.[19]

The exposure of a hydrophobic protein to water is energetically unfavourable. Whilst the enthalpy of this interaction is small and negative, the Gibbs free energy will increase as a result of the negative entropic contribution ($\Delta G=\Delta H-T\Delta S$), as discussed in Chapter 2. As a protein molecule interacts with a surface, the energy of the system is minimised. Here a large positive change in entropy occurs on the loss of water from the protein and from the surface. When the surface is hydrophobic, adsorption is even more energetically favourable, thus the affinity of a protein will be greater towards a hydrophobic compared to a hydrophilic surface unless the protein in question contains few hydrophobic regions on its surface. Exclusion of water also allows a greater proportion of the protein molecule to interact with the surface, which may help to explain the greater conformational change of albumin on the hydrophobic surface. Upon binding, hydrophobic surface interactions from the outer layer and possibly from the inner core of the protein may occur. The protein will be distorted as the structure deforms to maximise any such surface interactions, Figure 3.9. The degree of conformational change will therefore be dependent on the protein-surface interactions and the internal bonding strengths holding the protein in its particular conformation.

If a protein molecule were to deform, spreading over the surface, the amount of surface area required per molecule would increase. This would mean that less surface area is available for further protein molecules to adsorb, Figure 3.9. This would ultimately lead to a lower maximum surface saturation value, as was observed by QCM.

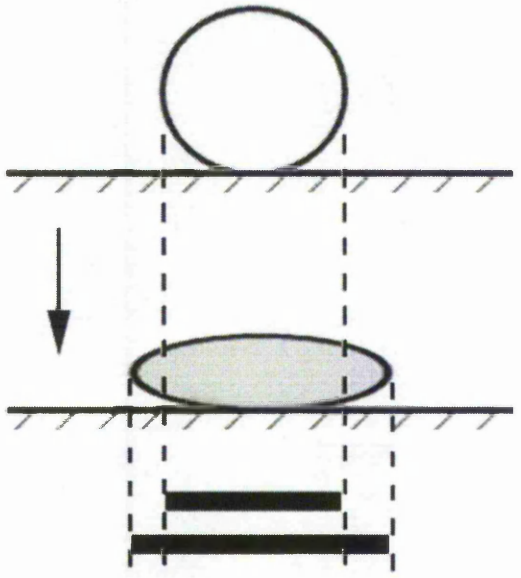

Figure 3.9. Schematic demonstrating protein spreading, the interaction area shown as a black line.

In a similar argument to that above, fibrinogen molecules may adsorb with their axis parallel to the surface, although a minimum energy could be achieved if the fibrinogen molecules stacked to reduce their interaction with water, Figure 3.6. Some supporting evidence for such a behaviour is provided by the multi-stage adsorption process measured by QCM.

3.3 Conclusions

In summary, this study demonstrates the use of QCM and grazing angle infrared spectroscopy for the study of protein-surface interactions. Serum albumin and fibrinogen readily adsorb onto hydrophilic (OH terminated) and hydrophobic (CH_3 terminated) surfaces. Albumin adsorbs more rapidly onto hydrophobic compared to hydrophilic surfaces possibly due to its higher affinity towards the former. When adsorbed onto hydrophobic surfaces albumin has a lower degree of ordered structure, with predominantly a loss of helical structure. A higher saturation value is apparent for albumin adsorbing onto hydrophilic surfaces which may also support the hypothesis that proteins denature to a greater extent on hydrophobic surfaces.

Fibrinogen adsorbs rapidly to both surfaces in contrast to albumin and is less deformed in its surface-bound state. Infrared conformational analysis suggested that adsorption induced deformation of fibrinogen occurs to a greater extent on the

hydrophobic compared to hydrophilic surface, which supports the QCM data showing a higher binding affinity towards the former. Again higher saturation values are observed for fibrinogen adsorbing on hydrophilic surfaces.

Both proteins show a rapid initial adsorption within the first few minutes which slows until an equilibrium adsorption level is reached within one hour. After this time few time-dependant conformational changes are apparent suggesting that protein deformation occurs either instantaneously upon adsorption or at a short time afterwards.

At high concentrations (>0.5 mg mL^{-1}) fibrinogen undergoes a multi-stage adsorption process, unlike albumin which was found to adsorb in a single stage process at all concentrations used. This suggests a rearrangement or orientational change for fibrinogen upon binding, possibly due to protein-protein interactions. Adsorbed fibrinogen molecules may reorient moving their long axis perpendicular to the surface, a rearrangement driven by increased hydrophobic interaction between adsorbed molecules, Figure 3.6.

This study highlights the ability to control protein conformation and orientation upon adsorption through surface-protein interactions. By further understanding the interface between biomaterial and biomatter, protein adhesion and subsequent cell mediation can be controlled to either promote or hinder integration.

3.4 References

1. B. Kasemo; J. Gold, "Implant Surfaces and Interface Processes," *Adv. Dental Res.*, **1999**, 13, 8-20
2. D.A. Puleo; A. Nanci, "Understanding and Controlling the Bone-Implant Interface," *Biomaterials*, **1999**, 20, 2311, 2321
3. B. Kasemo, "Biological surface science," *Surface Science*, **2002**, 500(1-3) 656-677
4. K. Anselme, "Osteoblast Adhesion on Biomaterials," *Biomaterials*, **2000**, 21(7) 667-681
5. K.D. Chesmel; C.C. Clark; C.T. Brighton; J. Black, " Cellular Responses to Chemical and Morphologic Aspects of Biomaterial Surfaces. II. The Biosynthetic and Migratory Response of Bone Cell Populations," *J. Biomed. Mater. Res.*, **1995**, 29(9) 1101-1110
6. C. Fredriksson; S. Khilman; B. Kasemo; D.M. Steel, "In Vitro Real-Time Characterization of Cell Attachment and Spreading,"*J. Mater. Res.:Mat. Res.*, **1998**, 9(12) 785-788
7. M. Lampin; R. Warocquier-Clerout; C. Legris; M. Degrange; M.F. Sigot-Luizard, "Correlation Between Substratum Roughness and Wettability, Cell Adhesion, and Cell Migration," *J. Biomed. Mater. Res.*, **1997**, 36(1) 99-108
8. W.G. Pitt; S.L. Cooper, "Albumin Adsorption on Alkyl Chain Derivatized Polyurethanes: I. The Effect of C-18 Alkylation," *J. Biomed. Mater. Res.*, **1988**, 22(5) 359-382
9. M. Taborelli; L. Eng; P. Descouts; J.P. Ranieri; R. Bellamkonda; P. Aebischer, "Bovine Serum Albumin Conformation on Methyl and Amine Functionalized Surfaces Compared by Scanning Force Microscopy," *J. Biomed. Mater. Res.*, **1995**, 29(6) 707-714
10. T.J. Lenk; T.A. Horbett; B.D. Ratner; K.K. Chittur, "Infrared Spectroscopic Studies of Time-Dependent Changes in Fibrinogen Adsorbed to Polyurethanes," *Langmuir*, **1991**, 7(8) 1755-1764
11. G.B. Sigal; M. Mrksich; G.M. Whitesides, "Effect of Surface Wettability on the Adsorption of Proteins and Detergents," *J. Am. Chem. Soc.*, **1998**, 120(14) 3464-3473

12. T.C. Ta; M.T. McDermott, "Mapping Interfacial Chemistry Induced Variations in Protein Adsorption with Scanning Force Microscopy," *Anal. Chem.*, **2000**, 72, 2627-2634
13. S. Johansson; G. Svineng; K. Wennerberg; A. Armulik; L. Lohikangas, "Fibronectin-Integrin Interactions," *Front. Biosci. 2.*, **1997**, 126-146
14. D. Kiaei; A.S. Hoffman; T.A. Horbett; K.R. Lew, "Platelet and Monoclonal Antibody Binding to Fibrinogen Adsorbed on Glow-Discharge-Deposited Polymers," *J. Biomed. Mater. Res.* **1995**, 29(6) 729-39
15. F. Höök; B. Kasemo, "Variations in Coupled Water, Viscoelastic Properties, and Film Thickness of a Mefp-1 Protein Film During Adsorption and Cross-Linking: a Quartz Crystal Microbalance With Dissipation Monitoring, Ellipsometry, and Surface Plasmon Resonance Study," *Anal. Chem.*, **2001**, 73(24) 5796-5804
16. F. Höök; M. Rodahl; P. Brzezinski; B. Kasemo, "Energy Dissipation Kinetics for Protein and Antibody-Antigen Adsorption under Shear Oscillation on a Quartz Crystal Microbalance," *Langmuir*, **1998**, 14(4) 729-734
17. F. Caruso; D.N. Furlong; P. Kingshott, *"Characterization of Ferritin Adsorption onto Gold," J. Colloid Int. Sci.*, **1997**, 186, 129-140
18. K.K. Chittur, "FTIR/ATR For Protein Adsorption to Biomaterial Surfaces," *Biomaterials*, **1998**, 19(4-5) 357-369
19. S. Kidoaki; T. Matsuda, "Adhesion Forces of the Blood Plasma Proteins on Self-Assembled Monolayer Surfaces of Alkanethiolates with Different Functional Groups Measured by an Atomic Force Microscope," *Langmuir*, **1999**, 15(22) 7639-7646
20. Y. Wu; K. Murayama; B. Czarnik-Matusewicz; Y. Ozaki, "Two-Dimensional Attenuated Total Reflection / Infrared Correlation Spectroscopy Studies on Concentration and Heat-Induced Structural Changes of Human Serum Albumin in Aqueous Solutions," *Appl. Spectrosc.*, **2002**, 56(9) 1186-1193
21. F-N. Fu; D.B. DeOliveira; W.R. Trumble; H.K. Sarkar," Secondary Structure Estimation of Proteins Using the Amide III Region of Fourier Transform Infrared Spectroscopy: Application to Analyze Calcium-Binding-Induced Structural Changes in Calsequestrin," *Appl. Spectrosc.*, **1994**, 48(11) 1432-1441
22. J.L. Tan; J. Tien; C.S. Chen, " Microcontact Printing of Proteins on Mixed Self-Assembled Monolayers," *Langmuir*, **2002**, 18, 519

23. C.D. Bain; J. Evall; G.M. Whitesides, "Formation of Monolayers by the Coadsorption of Thiols on Gold: Variation in the Head Group, Tail Group, and Solvent," *J. Am. Chem. Soc.*, **1989**, 111(18) 7155
24. J.L. Tan; W. Liu; C.M. Nelson; S. Raghavan; C.S. Chen, "Simple Approach to Micropattern Cells on Common Culture Substrates by Tuning Substrate Wettability," *Tissue Engineering*, **2004**, 10(5/6) 865-872
25. H.S. Kim; J.D. Hartgerink; M.R. Ghadiri, "Oriented Self-Assembly of Cyclic Peptide Nanotubes in Lipid Membranes, " *J. Am. Chem. Soc.*, **1998**, 120(18) 4417-4424
26. T. Miyazawa; E.R. Blout, "The Infrared Spectra of Polypeptides in Various Conformations: Amide I and II Bands," *J. Am. Chem. Soc.*, **1961**, 83, 712-719

Chapter 4

Surface Tailoring for Controlled Protein Adsorption: Effect of Topography and Chemistry

4.1 Introduction

Protein adsorption is of relevance to a wide audience due to many possible applications, especially with the increasing interest in nanotechnology. The interaction of proteins on surfaces is of crucial importance, particularly in biochip developments,[1-3] biosensors,[4] medical device coatings,[5] drug delivery[6] and even in the fabrication of a new class of hybrid materials[7]. Immobilisation of proteins / enzymes and conservation of their activity may give rise to functional surfaces suitable for use in many fields such as biosensors and biocompatible materials development. However, the protein-surface interactions that underpin the behaviour of immobilised protein molecules are not well established.

It has been shown than protein adsorption characteristics can be controlled by changing substrate surface parameters.[7-10] The previous chapter has demonstrated that surface chemistry, plays an important role in determining adsorbed protein conformation as well as rates of adsorption and amounts of protein adsorbed, through the interaction between the functional groups of the substratum and those of the protein backbone, Figure 4.1. Topography has also been shown, to some extent, to impact on the conformation of bound proteins, wherein varying sized colloidal substrates have been employed, using surface curvature as a means to model topography on the nanoscale.[11,12] Such topographical changes can alter the activity of adsorbed protein molecules,[11,13] a finding which supports a change in protein conformation having occurred. The investigation of topographical effects is somewhat sparse at present, with only a small number of reports covering a narrow size range.

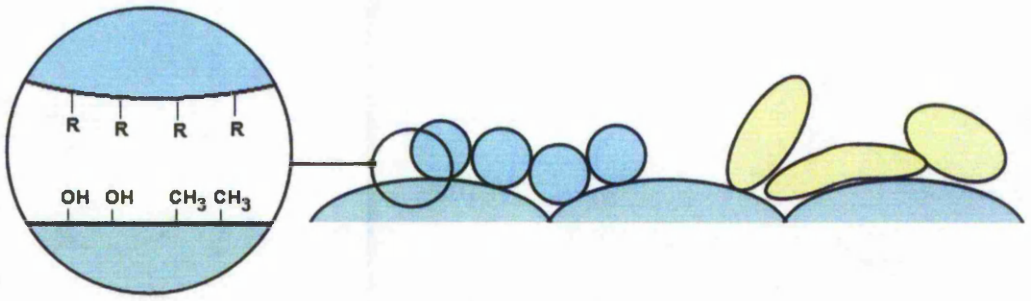

Figure 4.1. Surface characteristics which may control protein adhesion parameters.

Although both surface chemistry and topography are known to be important parameters that control protein conformation and thus the activity of surface-bound proteins once adsorbed, the extent to which each factor contributes is not fully understood. Furthermore, studies examining the effect of surface topography (through surface curvature) have focussed on small globular proteins such as lysosyme (4.5 by 3.5 by 3.5 nm)[11,14] and cytochrome C[10,15].

Here we broaden the knowledge base by investigating the effects of surface chemistry with and without surface curvature, using two model proteins: bovine serum albumin (BSA) - a small globular protein and bovine fibrinogen (Fg) - a rod-like protein. Both are of significant relevance not only as model systems, but also to biocompatibility and drug delivery applications due to the high abundance of these proteins at implant sites.

In shown in Chapter 3, both albumin and fibrinogen undergo conformational changes when adsorbing onto solid surfaces, becoming more denatured (having less ordered secondary structure) on hydrophobic surfaces.[16] A large number of other investigations examining bound proteins have used techniques that give limited information. Circular dichroism (CD) for instance is one of the more common methods used to study protein adsorption onto colloidal particles, although changes in secondary structure can be followed this technique has inherent inconsistency problems in absolute secondary structure determination.[17] Colloidal scattering also restricts the size of substrates that can be used which obviously limits the range of investigations using this technique.[11] Infrared spectroscopy (IR) has been used in this study, allowing a more thorough examination of the bound protein secondary structure[18] as it is a method not constrained by substrate size or material. Previous studies examining how surface chemistry affects protein adsorption have focused on the effects of surface chemistry alone, most taking little account of surface roughness on the nano-scale that can be experienced by adsorbing proteins. The study presented in this chapter is the first report examining how proteins of differing size and shape (albumin and fibrinogen) interact with surfaces having defined chemistry and topography.

Substrates having diameters in the range ca. 15-165 nm have been synthesised and chemically modified to give model hydrophilic (hydroxy terminated) and hydrophobic (alkane terminated) surfaces. It was the intention that the particles would coincide with protein dimensions. The smaller substrates present high surface curvature whilst the larger substrates are perceived as pseudo-flat surfaces, in relation to the sizes of the protein molecules used. Infrared spectroscopy has been employed to assess, in detail, conformational and also orientational differences of proteins bound to a range of surfaces presenting contrasting surface chemistry and curvature. Due to the high substrate surface area used, it was possible to measure protein loss from solution directly via ultraviolet (UV) spectroscopy. Together, these complimentary techniques have been used to elucidate the adsorption characteristics of two serum proteins.

By understanding protein-surface interactions, it is hoped that functionalisation of surfaces will give rise to new materials with preserved or even enhanced protein / enzyme activity for use in a range of biotechnology applications.

4.2 Results and Discussion

4.2.1 Surface Characterisation

Silica particles were formed via the Stöber process[19] to afford batches of monodisperse spheres. Each sample batch was analysed by transmission electron microscopy (TEM) to assess the average particle size. Substrates were required to present a range of surface curvature, from those coinciding with protein dimensions with high surface curvature, to those substrates being much larger presenting a pseudo-flat surface. Particles having diameters in the range 15-165 nm were used. Samples were freeze dried to minimise aggregation although when applied as a powder to transmission electron micrograph (TEM) grids loose clusters of particles were apparent, Figure 4.2.

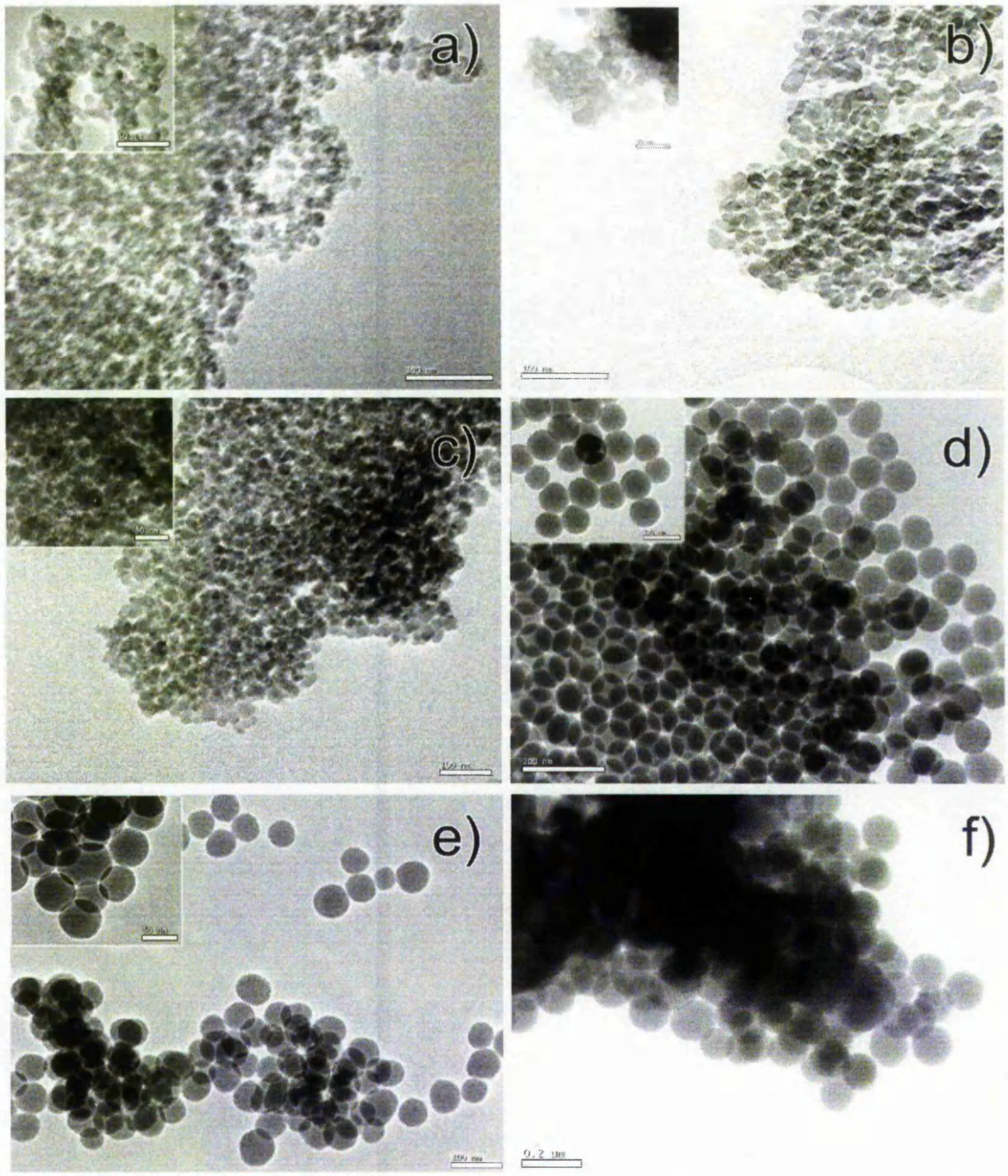

Figure 4.2. Transmission electron micrographs of sample silica spheres of average radii, a) 7.5 nm, b) 9.6 nm, c) 14.4 nm, d) 30.6 nm, e) 41.0 nm and f) 82.5 nm, inserts show enlarged regions.

Analysis by IR showed that after work-up, terminal ethoxy groups were still present on the silica spheres, so acid treatment was necessary, Equation 4.1.

$$R_3Si - OEt + H_3O^+ \Rightarrow R_3Si - O - H + EtOH + H^+ \qquad \text{Equation (4.1)}$$

The enlarged aliphatic stretching region of infrared spectra taken of samples before and after acid treatment are shown in Figure 4.3, wherein unwanted terminal ethoxy groups were removed to give hydroxyl terminated substrates.

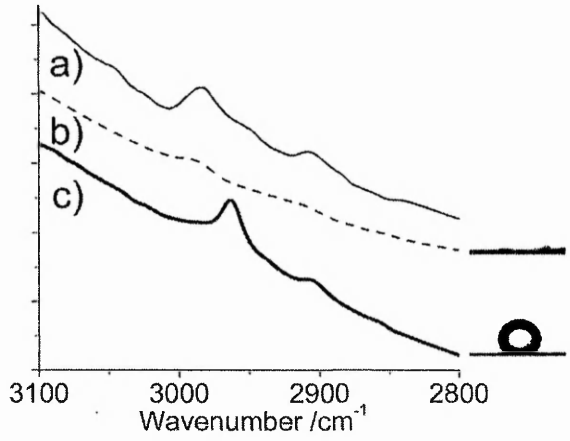

Figure 4.3. Infrared spectra of C-H stretching region of silica particles, a) pre-acid, b) post-acid treatment and c) after further methyl termination. Inserts adjacent to corresponding spectra show water droplets placed on hydrophilic and hydrophobic spheres.

Nitrogen adsorption analysis was used to determine the surface area for each batch of spheres, using BET analysis as described in Chapter 2. Data obtained from TEM and surface area measurements are summarised in Table 4.1.

Table 4.1. Spheres prepared for protein adsorption experiments.

*Sphere Radius / nm	Surface Area / $m^2 g^{-1}$
7.5 ± 0.2	373
9.6 ± 0.4	350
14.4 ± 2.1	327
30.6 ± 1.6	174
41.0 ± 1.8	81
81.8 ± 3.9	65

* From TEM measurements.

Further treatment with chlorotrimethylsilane allowed both hydrophilic and hydrophobic spheres of the same size to be available for further experimentation, Equation 4.2.

$$R_3Si-OH+Cl-Si(CH)_3 \Rightarrow R_3Si-O-Si(CH)_3+HCl \qquad \text{Equation (4.2)}$$

Surface chemistry was checked by ATR-IR, Figure 4.3c. The ability of a water droplet to spread over a surface was used to assess the wettability of the spheres.[20] The contact angle between the solid-liquid and the liquid-air interface depends on the relative interfacial energies of the surface and the liquid. Water contact angles shown in Figure 4.3 inserts demonstrate the difference in wettability observed for the treated substrates. Here the substrates could be considered as randomly stacked spheres. The water droplet rested on the silylated spheres showing that they were hydrophobic, in contrast to the hydrophilic samples onto which the water droplet rapidly spread over the surface and entered the space between the spheres.

4.2.2 Protein-Surface Affinity and Saturation Levels

All analyses conducted were experimentally normalised to surface area to eliminate problems associated with available protein adsorption sites. Due to the high surface area of the substrate the difference in free protein before and after incubation was easily observed by a reduction in absorbance at 280 nm. A range of protein concentrations were used well within detection limits.

The shape of an adsorption isotherm can yield information about the affinity of an adsorbing species towards the surface as well as the maximum equilibrium surface concentration of adsorbed protein. As shown in Chapter 3, surface protein concentrations reach an equilibrium value in approximately one hour of incubation, which is consistent with other studies.[21-23] The substrates in this study were silica spheres and hence sonication of the silica particles was performed in order to break any aggregates. Protein solutions diluted from a stock were added into homogenous silica particle dispersions to achieve desired final protein concentrations, each solution having the same total volume. The solutions were stirred for one hour to ensure protein and silica sphere mixing and to avoid any aggregation of silica particles in the presence of proteins. The solutions were then left standing for a further two hours to minimise any shearing effect due to stirring.

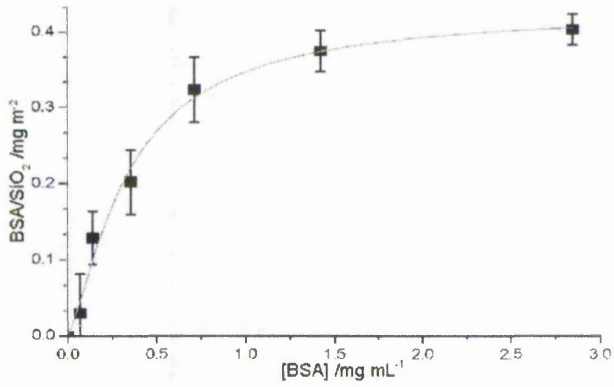

Figure 4.4. Example saturation curve for BSA adsorbing onto ca. 80 nm hydrophobic substrates.

Vials were then centrifuged and the amount of free protein remaining in each solution was assessed by UV spectroscopy, quantifying by means of a calibration curve (Chapter 2). As an example of the data obtained the saturation curve of BSA onto ca. 80 nm hydrophobic substrates is shown in Figure 4. 4. By fitting the data to a Langmuir model, estimates of affinity and maximum amount of protein adsorbed can be found (section 2.6). The binding constant is related to the equilibrium between adsorbing and desorbing species and directly correlates with the affinity of the adsorbate to the adsorbent, a higher value indicative of a stronger attraction.

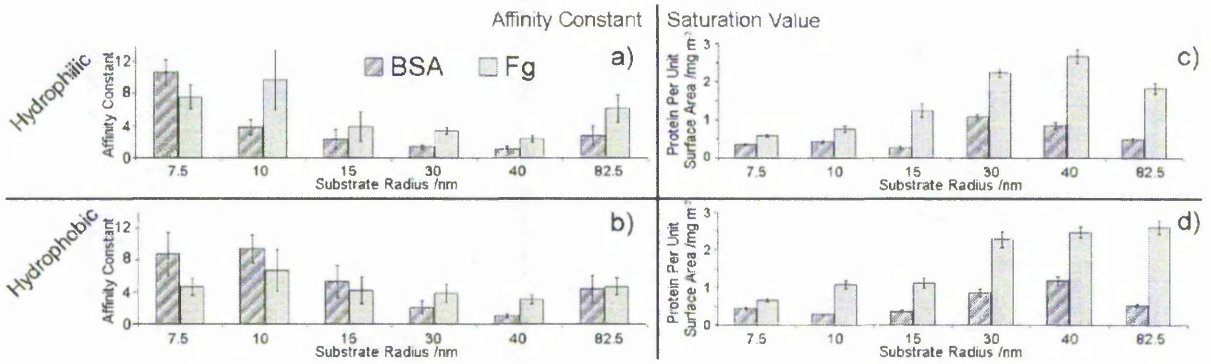

Figure 4.5. Plots showing variation in a) and b) affinity constant and c) and d) saturation amounts of BSA and Fg with a range of sized hydrophilic and hydrophobic spheres. Error bars show 95% confidence limits.

Figure 4.5 shows changes in affinity constants and saturation values for BSA and Fg adsorbing onto hydrophilic and hydrophobic substrates of varying sizes.

In general, with decreasing substrate size, i.e. higher surface curvature, the binding affinity of BSA increased with the saturation values following an opposite trend. Similar to the results discussed in Chapter 3 which compared protein adsorption onto 'flat' surfaces of different wettabilities, albumin typically adsorbed in lower quantities onto hydrophobic compared to hydrophilic curved surfaces tested.

A plot of the maximum amount of protein molecules adsorbing over a range of particle sizes can be constructed from the saturation value data. Figure 4.6 compares protein saturation values obtained experimentally with those predicted for a close packed mono-layer of each protein. Schematics of monolayer protein adsorption are shown as inserts in Figure 4.6.

Values of molecules per particle were estimated, taking surface area of a sphere to be equal to πd^2, where 'd' is the sphere diameter. It is acknowledged that these vales are slight over-estimates of the actual surface area available for protein adsorption due to the porous nature of the particles. Protein molecular dimensions (given in section 2.8) allowed estimates of surface area per adsorbed protein molecule. The packing density of close packing circles is $\left(\frac{\pi\sqrt{3}}{6}\right) = 0.9069$ that of square packing circles, although it should be noted that care should be taken when using this packing factor to estimate close packing protein molecules as these are non-rigid masses, and may spread as they interact with a surface. For this reason the area per protein molecule was taken as the square dimensions of the molecule, i.e. for fibrinogen end-on adsorption an area of 4×4 nm was assumed.

Experiments were conducted keeping total substrate surface area constant, and as all size and concentration parameters are known (of both substrate and protein molecules), the number of protein molecules adsorbing per substrate sphere can be calculated. Albumin adsorbs in lower amounts to all hydrophobic surfaces in the range tested, but increases with an increase in particle size due to the greater surface area available. It should be noted that a close-packed monolayer was not reached during this investigation, possibly suggesting that albumin denaturation hinders such a packing arrangement (see below).

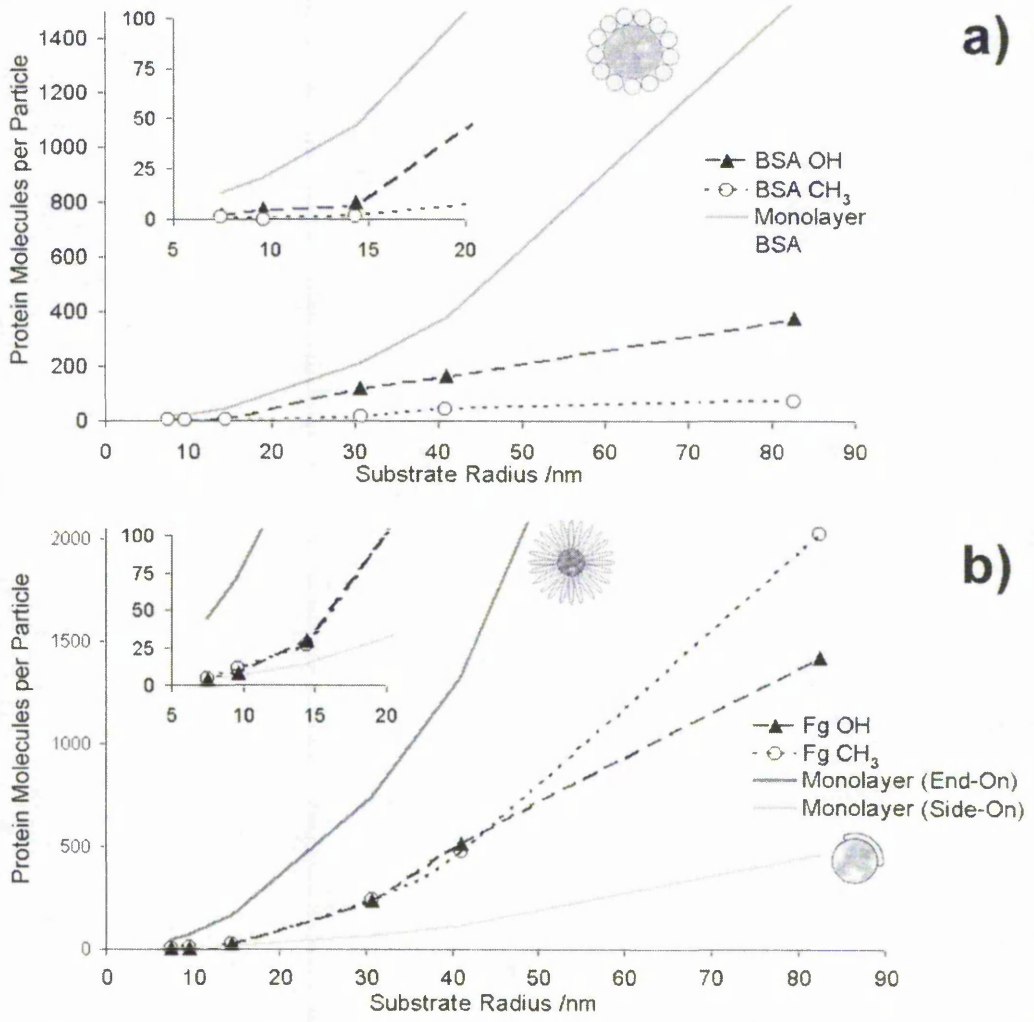

Figure 4.6. Saturation values obtained for a) BSA and b) fibrinogen onto –▲– hydrophilic and –O– hydrophobic surfaces tested. Inserts show schematic of surface-bound proteins adjacent to corresponding monolayer lines.

Fibrinogen follows similar trends observed for albumin, with high affinity constants and low saturation values when adsorbing onto smaller particles. Due to fibrinogen shape, two possible adsorption orientations can be achieved as discussed in the previous chapter: side-on – with its long axis perpendicular to the radius or end-on – with it axis perpendicular to the radius. Interestingly for particles smaller than ~30 nm radii, the amount of protein adsorbed corresponds well to a side-on monolayer, Figure 4.6b insert. Above this particle size a side-on monolayer is exceeded although an end-on monolayer is not reached, possibly due to the constraints of close packing. Generally fibrinogen adsorbs in similar amounts to both hydrophilic and hydrophobic surfaces.

4.2.3 Conformational Assessment

Infrared spectroscopy using an attenuated total reflectance (ATR) accessory has allowed adsorbed protein conformation to be analysed. The powdered samples could have been investigated using transmission infrared spectroscopy but the atmospheric water bands between 1850-1500 cm^{-1} caused problems as they obscured the amide I band of interest, making protein conformational assessment difficult. The ATR accessory permitted complete purging of the infrared spectrometer, removing moisture. Another advantage of using ATR is that the sample can be completely recovered avoiding unnecessary complications (such as dialysis) that would be present if transmission spectroscopy was used. The sample can then be re-run at a later date, or analysed further by different techniques such as thermogravimetry (TGA), differential scanning calorimetry (DSC) or dynamic light scattering (DLS), each of which could give further insight into protein adsorption characteristics.

Protein infrared spectra consist mainly of amide band vibrations as discussed in Chapter 2. Briefly, the amide I band centered ~1700-1600 cm^{-1} is largely due to C=O stretching vibrations arising from amide bonds within the protein structure. Each secondary structure gives rise to specific vibrational bands making the amide I band sensitive to changes in secondary structure. From previous studies, peaks with maxima at 1685-1663 cm^{-1} have been assigned to β-sheet structures, 1655-1650 cm^{-1} to α-helices, 1648-1644 cm^{-1} to random chains, 1639-1635 cm^{-1} to extended chains and 1632-1621 cm^{-1} to extended chains or β-sheets / turns. Bands observed at lower wavenumbers ~1616 cm^{-1} are often considered to arise from intermolecular bonding.[24-26]

The secondary structure variation of albumin and fibrinogen when adsorbed onto varying sized particles is shown in Figure 4.7. Albumin has a less organised secondary structure when adsorbed onto larger particles, predominantly losing helical structure with a corresponding increase in random coil / extended chain. Such trends are observed for both hydrophilic and hydrophobic surfaces although a greater loss of structure is observed on the latter. This data supports earlier findings that proteins become more denatured when adsorbed onto hydrophobic compared to hydrophilic surfaces, Chapter 3.

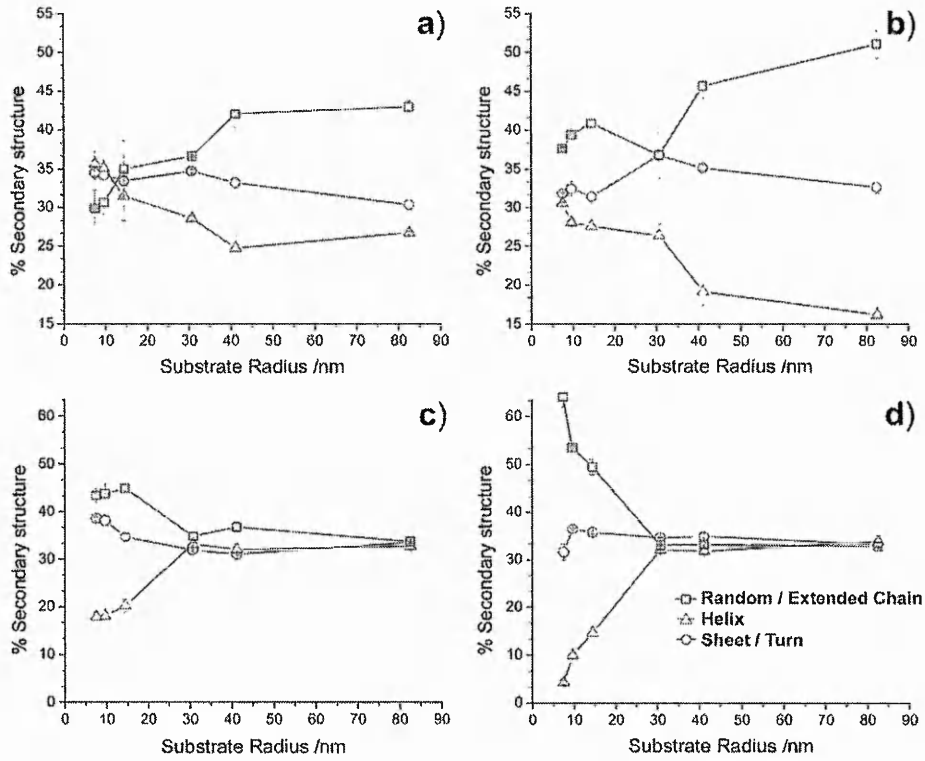

Figure 4.7. Conformational assessment of surface bound BSA a) and b); fibrinogen c) and d) onto hydrophilic a) and c); hydrophobic b) and d) spheres of varying radii.

In contrast, fibrinogen becomes more disordered on smaller particles, losing helical structure at the expense of an increasing random component. Onto particles above 30 nm, little variation in fibrinogen conformation is observed. This trend is apparent for both hydrophilic and hydrophobic surfaces, again being more pronounced on the latter.

Similar to the amide I band, the amide II band centred at around 1500-1600 cm^{-1} is composed of component in-plane N-H bending and C-N stretching bands of the amide bond. Due to the lower intensity and different vibrational modes contained, this band is less sensitive to conformational changes compared to the amide I region. The amide I/II ratio has, however, been used to qualitatively assess conformation /orientation changes.[18] Our data suggests subtle differences in the orientation of albumin and fibrinogen when adsorbed onto differently sized spheres. Although such a ratio can give little quantitative information it is interesting to observe variation in bound protein structure and one can use this as a secondary measure of conformation / orientation change.

Generally higher amide I/II ratios are observed for albumin and fibrinogen with increasing substrate size, Figure 4.8. This indicates that both proteins bind having different geometries onto substrates with differing surface curvature. These data show significantly different amide I/II ratios (both height and area ratios) for proteins adsorbed onto particles above ~30 nm radius compared to proteins adsorbed on smaller particles. This corresponds well with the amide I curve fitting analysis, again suggesting that both albumin and fibrinogen have differing conformations and/or orientations when adsorbing onto small particles with radii <30 nm than when adsorbed onto larger particles. Band ratios for albumin are greater than those observed for fibrinogen which may indicate a greater degree of structural change.

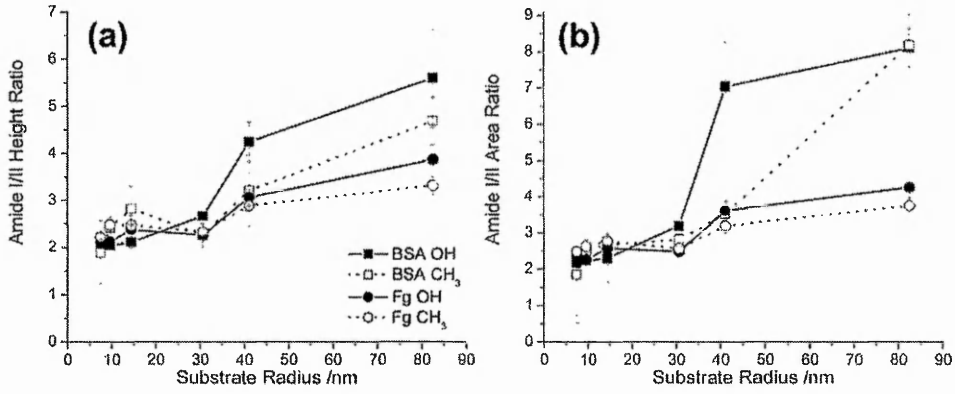

Figure 4.8. Variation in amide I/II, a) height and b) area ratio. Error bars show standard deviation of samples measured in triplicate.

4.2.4 Protein-Protein Interactions

The extent of intermolecular bonding can be used as an indication of lateral protein-protein interactions experienced by neighbouring bound proteins. It has been suggested by others that amide I component bands centred at ~1610 cm^{-1} are sensitive to hydrogen bonding and can be used as a measure of intermolecular protein-protein interaction.[24-26] Analysis of the contribution of this peak to the total amide I area, suggests that the interaction between bound proteins (both BSA and Fg) is generally greater on hydrophilic compared to hydrophobic surfaces, Figure 4.9. This is probably an effect of surface induced deformation as spreading of the protein would reduce the interaction area between neighbouring adsorbed proteins. Fibrinogen, however, again shows differing characteristics on spheres with radii <30 nm, where intermolecular bonding becomes higher for hydrophobic substrates. A trend towards higher intermolecular interaction with increasing sphere size suggests greater lateral interaction

between bound proteins, which is expected from the geometry of adjacent protein molecules.

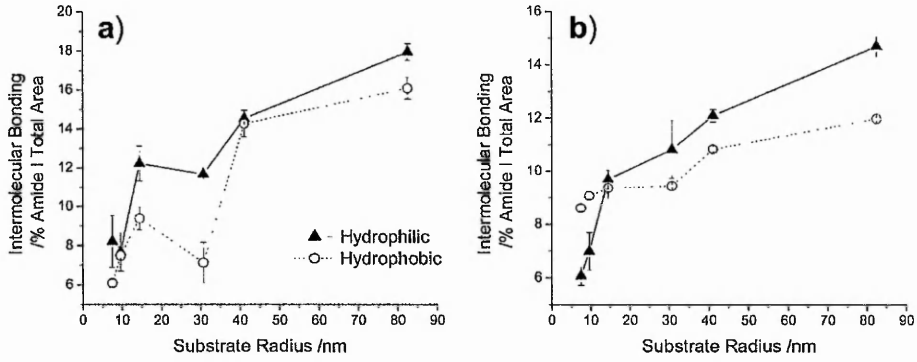

Figure 4.9. Bound protein-protein interactions of a) BSA and b) Fg on –▲– hydrophilic and –O– hydrophobic spheres of varying radii.

4.3 Discussion

Protein surface interactions can induce conformational changes in the adsorbing protein molecules. It has been reported previously that both BSA and Fg undergo greater conformational disordering when adsorbing onto hydrophobic rather than hydrophilic surfaces, a finding supported by this study. However, few studies have been conducted that examine the effects of topography on protein adhesion. Here we describe protein surface interactions of albumin and fibrinogen using surface curvature as a measure of topography.

Albumin and fibrinogen interact very differently in relation to changes in surface curvature. Although research into the effects of surface topography on protein adsorption is in its infancy, an investigation examining lysosyme adsorption, a small globular protein comparable in size to albumin, strongly suggests that substrate curvature modifies protein conformation upon binding.[11] Few differing particle sizes were analysed and structural detail of the adsorbed species was limited such that only protein molecules adsorbed onto the smaller particles were able to be investigated. Furthermore, previous investigations have concentrated on small globular proteins.[10-12,14,27] To our knowledge there has been no systematic evaluation of protein responses to surfaces, taking into account protein size and shape as well as surface curvature and chemistry. Here we extend the knowledge-base of protein-surface interactions by examining the above effects on binding and structural characteristics of two geometrically very different proteins. In addition a number of particle sizes were

investigated, ranging from those presenting high surface curvature to those for which the protein molecules would observe a pseudo-flat surface.

4.3.1 Albumin

Particles with high surface curvature were found to stabilise the native-like conformation of albumin, Figure 4.10, thus supporting the earlier results on lysosyme adsorption[11]. The same effect for variants of human carbonic anhydrase, other globular proteins of comparable size to albumin, have also been reported.[12,27]

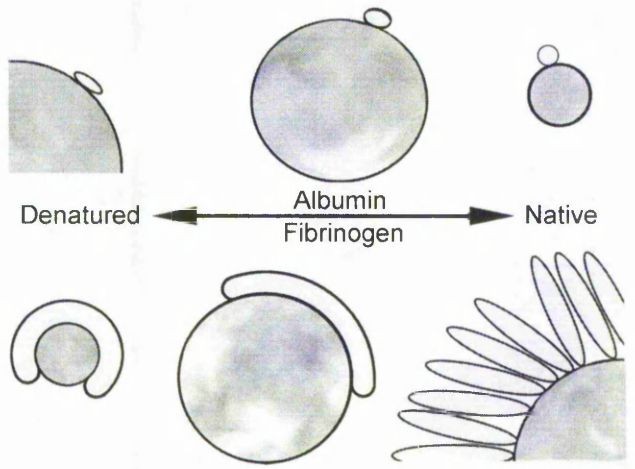

Figure 4.10. Schematic demonstrating control of conformation and orientation by surface curvature.

By modeling a globular protein as a non-rigid mass it can be seen that with an increase in particle size, the interaction area, i.e. the surface area in close proximity to the protein, is increased, Figure 4.11. This value tends to a limiting value as surface curvature (convex) decreases until a flat surface is reached, although it could again increase if concave surface curvature is also considered.

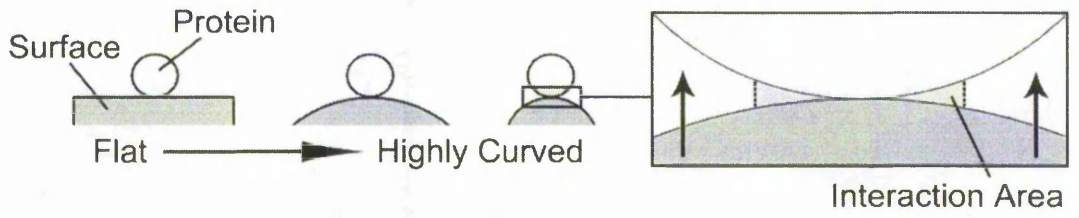

Figure 4.11. Schematic showing increase of interactions area as surface becomes flat.

We have also shown that the effects of surface curvature are also compounded by variation in surface chemistry. Albumin becomes more disordered upon binding to both flat (Chapter 3: Figure 3.8 and Tables 3.2 and 3.3) and curved hydrophobic surfaces compared with hydrophilic surfaces of the same geometry, Figure 4.7. Such disorder is more pronounced on particles with radius larger than ~30 nm. Albumin amide I/II ratios are fairly constant below 30 nm but also show a change above this size, Figure 4.8, demonstrating a difference in orientation / conformation of albumin bound on particles above and below this size.

4.3.2 Fibrinogen

Fibrinogen, in sharp contrast to albumin, becomes more denatured upon binding to smaller particles, i.e. those having higher surface curvature. In Chapter 3 it was proposed that fibrinogen, having a rod-like shape, can adsorb in two possible orientations: side-on – with its long axis parallel to the particle radius, or end-on – with its long axis perpendicular to the radius. The study in this chapter demonstrates that side-on orientation is favoured on smaller particles, Figure 4.6. A large change in fibrinogen conformation was observed on adsorption to particles with radii less than 30 nm ($3/5^{th}$ of the length of fibrinogen). Upon adsorption the molecule possibly wraps around the surface. Protein structural perturbation would therefore be expected to be greater on small particles with higher curvature, as was observed with the loss of the helical component. Such conformational change would be encouraged by an increase in protein-surface interaction that would probably also hinder surface rearrangement of the protein to the end-on orientation (discussion in Chapter 3). When adsorbing onto larger particles, surface curvature may be too small to induce such structural alteration. An end-on orientation could then be reached, the adsorption process being driven by increased protein-protein interactions. This hypothesis is supported by the increased amide I/II ratios and observed intermolecular bonding on particles with radii ≥30 nm, Figures 4.8 and 4.9 respectively. Furthermore, if rod-like proteins were to adsorb onto highly curved surfaces in an end-on orientation their backbones would be separated and neighbouring proteins would interact with each other to minimise solvation by water around their hydrophobic domains, Figure 4.12.

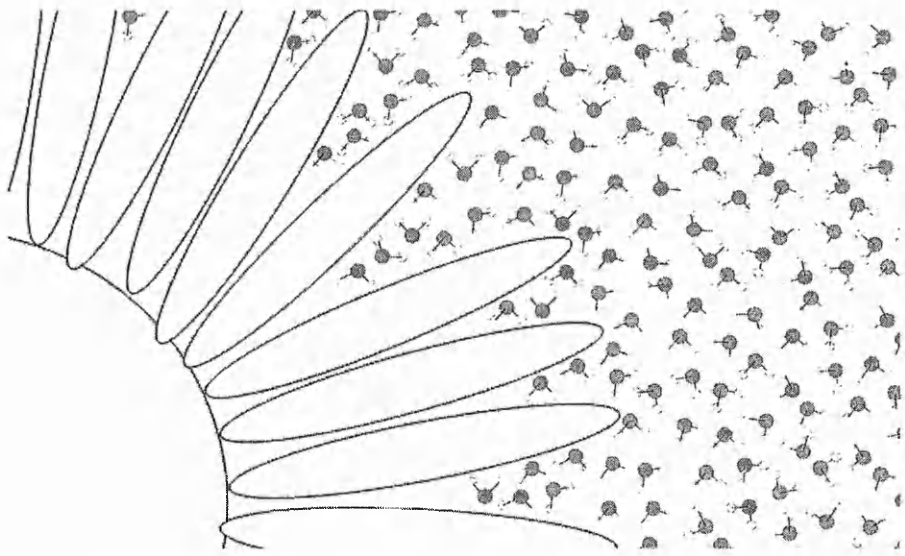

Figure 4.12. Schematic demonstrating the importance of close packing to reduce solvation of hydrophobic fibrinogen molecules adsorbed in an end-on orientation.

Therefore onto highly curved surfaces an end-on orientation of fibrinogen is not feasible. The effects of surface curvature on fibrinogen conformation are emphasised by surface chemistry – a finding also observed for albumin. Fibrinogen has a greater degree of random coil / extended chain structure on hydrophobic surfaces, as does albumin, suggesting that hydrophobic protein-surface interactions govern the structure of surface-bound protein.

4.4 Conclusions

Protein-surface interactions play an important role in determining the adsorbed conformation and, therefore, activity of surface bound proteins / enzymes. Here we describe the effects of surface curvature, with and without surface chemistry. Albumin and fibrinogen have dramatically differing interactions largely due to their differing shapes. Trends in binding affinity and surface saturation amounts correspond well with the extent of conformational change of the bound proteins as assessed by infrared spectroscopic methods. Together these data describe how the structure of albumin, a globular protein, is stabilised by high surface curvature. On the other hand, fibrinogen, a rod-like protein, is distorted by wrapping around surface curvature, inducing secondary structure loss.

By first understanding how biomolecules are affected by the nature of surfaces, control of their bound states can be achieved. This may give rise to an array of new

tailor-made materials / surface coating technologies for applications such as biosensors, hybrid materials, nanotechnology and biocompatible surfaces. Of particular current interest is the control over enzymatic activity or cell adhesion that can be harnessed by fine tuning surface coatings.

4.5 References

1. Y.-S. Lee; M. Mrksich, "Protein Chips: From Concept to Practice," *Trends Biotechnol.* **2002**, 20(12) S14-S18
2. H. Zhu; M. Snyder, "Protein Chip Technology," *Current. Opin. Chem. Biol.*, **2003**, 7, 55-63
3. T.G. Drummond; M.G. Hill; J.K. Barton, "Electrochemical DNA Sensors," *Nat. Biotechnol.* **2003**, 21, 1192-1199
4. J.M Nam; C.S. Thaxton; C.A. Mirkin, "Nanoparticle-Based Bio-Bar Codes for the Ultrasensitive Detection of Proteins," *Science*, **2003**, 301(5641) 1884-1886
5. T.J. Webster; L.S. Schadler; R.W. Siegel; R. Bizios, "Mechanisms of Enhanced Osteoblast Adhesion on Nanophase Alumina Involve Vitronectin," *Tissue Eng.*, **2001**, 7(3) 291-301
6. I. Brigger; C. Dubernet; P. Couvreur, "Nanoparticles in Cancer Therapy and Diagnosis," *Adv. Drug Delivery Rev.*, **2002**, 54(5) 631-651
7. S. Srivastava; A. Verma; B.L. Frankamp; V.M. Rotello; "Controlled Assembly of Protein-Nanoparticle Composites Through Protein Surface Recognition," *Adv. Mater.*, **2005**, 17(5) 617-621
8. G.B. Sigal; M. Mrksich; G.M. Whitesides, "Effect of Surface Wettability on the Adsorption of Proteins and Detergents," *J. Am. Chem. Soc.*, **1998**, 120(14) 3464-3473
9. T.C. Ta; M.T. McDermott, "Mapping Interfacial Chemistry Induced Variations in Protein Adsorption with Scanning Force Microscopy," *Anal. Chem.*, **2000**, 72, 2627-2634
10. L.-C. Huang; H.-C. Chang, "Adsorption and Immobilization of Cytochrome c on Nanodiamonds," *Langmuir*, **2004**, 20(14) 5879-5884
11. A.A. Vertegal; R.W. Siegel; J.S. Dordick, "Silica Nanoparticle Size Influences the Structure and Enzymatic Activity of Adsorbed Lysozyme," *Langmuir*, **2004**, 20(16) 6800-6807
12. M. Lundqvist; I. Sethson; B.-H. Jonsson, "Protein Adsorption onto Silica Nanoparticles: Conformational Changes Depend on the Particles' Curvature and the Protein Stability," *Langmuir*, **2004**, 20(24) 10639-10647
13. A. Kondo; F. Murakami; M. Kawagoe; K. Higashitani, "Kinetic and Circular Dichroism Studies of Enzymes Adsorbed on Ultrafine Silica Particles," *Appl. Microbiol. Biotechnol.*, **1993**, 39(6) 726-731

14. M. Tian; W.-K. Lee; M.K. Bothwell; J. McGuire, "Structural Stability Effects on Adsorption of Bacteriophage T4 Lysozyme to Colloidal Silica," *J. Colloid Int. Sci.*, **1998**, 200, 1, 146-154
15. X. Jiang; J. Jiang; Y. Jin; E. Wang; S. Dong, "Effect of Colloidal Gold Size on the Conformational Changes of Adsorbed Cytochrome C: Probing by Circular Dichroism, UV-Visible, and Infrared Spectroscopy," *Biomacromolecules*, **2005**, 6(1) 46-53
16. P. Roach; D. Farrar; C.C. Perry, "Interpretation of Protein Adsorption: Surface-Induced Conformational Changes," *J. Am. Chem. Soc.*, **2005**, 127(22) 8168-8173
17. B. Dalmas; W.H. Bannister, "Prediction of Protein Secondary Structure From Circular Dichroism Spectra: An Attempt to Solve the Problem of the Best-Fitting," *Anal. Biochem.*, **1995**, 225, 39-48
18. T.J. Lenk; T.A. Horbett; B.D. Ratner, "Infrared Spectroscopic Studies of Time-Dependent Changes in Fibrinogen Adsorbed to Polyurethanes," *Langmuir*, **1991**, 7(8) 1755-1764
19. W. Stöber; A. Fink; E. Bohn, "Controlled Growth of Monodisperse Silica Spheres in the Micron Size Range," *J. Colloid Interface Sci.*, **1968**, 26(1) 62-69
20. N.J. Shirtcliffe; S. Aqil; C. Evans; G. McHale; M.I. Newton; C.C. Perry; P. Roach, "The Use of High Aspect Ratio Photoresist (SU-8) for Super-Hydrophobic Pattern Prototyping," *J. Micromech. Microeng.*, **2004**, 14, 1384–1389
21. D.S. Salloum; J.B. Schlenoff, "Protein Adsorption Modalities on Polyelectrolyte Multilayers," *Biomacromolecules*, **2004**, 5(3) 1089-1096
22. F. Höök; M. Rodahl; P. Brzezinski; B. Kasemo, "Energy Dissipation Kinetics for Protein and Antibody-Antigen Adsorption under Shear Oscillation on a Quartz Crystal Microbalance," *Langmuir*, **1998**, 14(4) 729-734
23. F. Höök; B. Kasemo, "Variations in Coupled Water, Viscoelastic Properties, and Film Thickness of a Mefp-1 Protein Film During Adsorption and Cross-Linking: a Quartz Crystal Microbalance With Dissipation Monitoring, Ellipsometry, and Surface Plasmon Resonance Study," *Anal. Chem.*, **2001**, 73(24) 5796-5804
24. B.J. Frushour; J.L. Koenig, "*Raman Spectroscopy of Proteins*," in, "*Advances in Infrared and Raman Spectroscopy*," R.J.H Clark; R.E. Hester, (Eds.) Heyden, London, **1975**, 1, 35-97

25. M. Jackson; P.I. Haris; D. Chapman, "Fourier Transform Infrared Spectroscopic Studies of Calcium-Binding Proteins," *Biochemistry*, **1991**, 30(40) 9681-9686
26. A. Muga; H.H. Mantsch; W.K. Surewicz, "Membrane binding induces destabilization of cytochrome c structure," *Biochemistry*, **1991**, 30(29) 7219-7224
27. M. Lundqvist; I. Sethson; B.-H. Jonsson, "High-Resolution 2D ^{1}H-^{15}N NMR Characterization of Persistent Structural Alterations of Proteins Induced by Interactions with Silica Nanoparticles," *Langmuir*, **2005**, 21(13) 5974-5979

Chapter 5

Rapid Quantification of Surface-Bound Proteins by Fluorometric Assay – Comparison with QCM and Amido Black Assay

5.1 Introduction

Protein adsorption has become a research area of great interest due to its importance in biomedical[1] and biosensor applications[2]. The adsorption process depends largely on the specific protein-surface interactions that govern binding, possible orientational control and protein conformational change occurring as the protein molecules adhere.[3-4] Water molecules and solvated ions are also incorporated into an adsorbed protein layer, supporting electrostatic requirements.

Advances in staining methodologies have allowed specific identification and quantification of much smaller amounts of proteins in solution. Fluorescent dyes extend detection limits down to the ng mL^{-1} range compared to the more traditional methods such as the Bradford assay or ultraviolet (UV) spectroscopy which only extend to the

$\mu g\ mL^{-1}$ range. These fluorescent assays are a powerful tool for the accurate quantification of low protein concentrations in solution, although the quantification of surface-bound proteins still poses a problem. Investigations of surface-protein interactions commonly use a colloidal solid phase with a large surface area, measuring the remaining protein in solution after incubation and calculating the adsorbed amount by mass balance, as discussed in chapter 4.[5,6] Proteins labelled with a radioactive or fluorescent tag have been used,[1,7] although one must be wary that the inclusion of such a label may change the specific protein-surface interactions under investigation, causing unwanted conformational and / or orientational changes thereby affecting protein adsorption characteristics.

Other techniques used to study protein adsorption processes are dependant upon theoretical assumptions which may not be strictly true for such systems. The quartz crystal microbalance (QCM) is a very sensitive technique ($ng\ cm^{-2}$) relating the mass of an adsorbing layer to an observed oscillatory frequency shift of a quartz crystal. The problem here is that the frequency changes are connected with the total mass loading (including water and ions)[8] as well as viscoelastic contributions from the adsorbing protein.[8-10] Ellipsometric techniques measure small changes in the refractive index at an interface, which can be related to adsorbing layer thickness using an average density estimate.[11] Such assumptions however may lead to mis-interpretation of data. Other methods commonly used to study protein adsorption such as atomic force microscopy (AFM),[12-14] infrared (IR) spectroscopy,[4,11] circular dichroism[5,15] and X-ray photoelectron spectroscopy (XPS),[12,16] give information on conformation and relative amounts adsorbed but do not readily give an absolute quantification of surface-bound protein. Direct assessment of surface bound proteins using specific antibody binding assays are strongly affected by the conformational and orientational geometry of the adsorbed species.[17] If the antibody binding site within the protein is blocked then attachment may not be possible, leading to inaccurate results.

The nature of QCM and ellipsometric techniques, along with other methods used to study protein adsorption processes, limits the types of surfaces that can be analysed, restricting their ability to assess rough or porous surfaces.[11] However, it has been shown that protein-surface interactions are strongly directed by the topography of the surface.[3,5] A label-free technique for the accurate quantification of adsorbed protein in

the nanogram range, applicable over a wide range of surface textures would allow investigation of protein adsorption to be followed across a broad range of surfaces.

This chapter describes the development of a rapid assay for the quantification of surface-bound protein using a fluorescent dye, Nano Orange (Molecular Probes) that can be used as a stand-alone method or serve as an external calibration in conjunction with other methods. The adsorption of two serum proteins: fibrinogen and albumin, onto model hydrophobic and hydrophilic flat surfaces was investigated and the results obtained by fluorescence assay were compared to those obtained using QCM and amido black staining. Furthermore adsorption onto porous surfaces using superhydrophobic and superhydrophilic coatings as models was also examined to show the feasibility of the technique.

5.2 Results and Discussion

5.2.1 Surface Characterisation

A water droplet will rest on a solid surface with an equilibrium contact angle, the angle that the tangent to the liquid surface makes with the solid at the three phase boundary measured through the liquid, dependent on the nature of the surface, as discussed in chapter 2. The energetics of the system therefore govern the droplet shape allowing characteristic surface wettability to be analysed via the angle at which the droplet rests on the surface.[18] A small angle ($<90^{o}$), attained when water spreads over a surface, shows that the system is stabilised when having a high solid-water interface, i.e. the surface is hydrophilic. Conversely, high water contact angles ($\geq 90^{o}$) are observed on hydrophobic surfaces

The surfaces used within this study were chosen for their contrasting chemistries. Flat surfaces treated with heptanethiol and mercaptoethanol to produce thiolated self assembled monolayer gave water contact angles of 94° and 48° respectively.

5.2.2 Protein Adsorption

The main limitation of standard staining methods for protein adsorption analysis is that they are not directly quantitative. After incubation of protein solution the dye is added which binds to the surface-bound protein. After rinsing to remove any unbound stain the remaining dye is then analysed, Figure 5.1. Unlike solution phase assays a

calibration curve is not easily constructed because the quantity of protein bound to the surface, and hence the corresponding amount of dye is not known. Only a relative assessment of adsorbed proteins can be found.[19,20] Calibration methods for the amide black assay have been suggested that require samples containing proteins to be suspended on cellulose sheets which are then air dried and subsequently stained.[21] Such methods are labour intensive and time consuming and because the actual surface of investigation is not used during calibration, accurate quantification is difficult. If the dye binds specifically to certain domains or functional groups within the protein, changes in conformation and / or rearrangement may also cause a change in the amount of dye that can bind. A calibration method which can examine the specific protein-surface system of interest would be expected to give greater precision.

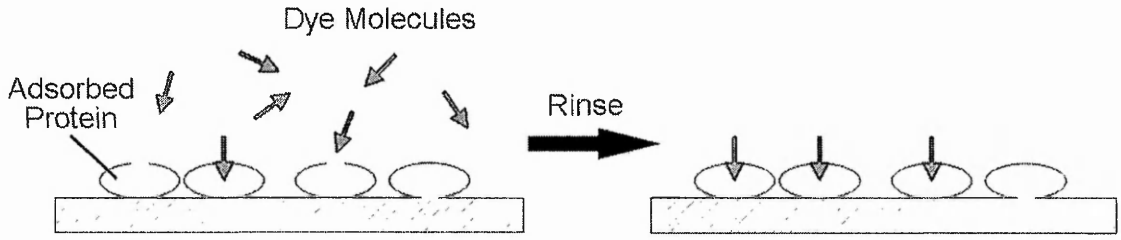

Figure 5.1. Schematic of staining of surface bound proteins using specific binding dyes.

Because it has recently been highlighted that surface topography plays an important role in controlling protein adsorption characteristics (chapter 4),[3,4] porous surfaces have also been analysed using the fluorometric assay. The use of porous materials also acts to highlight the limitations of common methods used to investigate protein adsorption such as QCM and ellipsometry.

5.2.3 Techniques Compared

A Nano Orange fluorescent assay has been used to quantitatively assess the amount of protein adsorbed onto a surface. This is an absolute method which can therefore be used as an external calibration for other methods that give only relative data. Results obtained from the Nano Orange assay were compared to QCM measurements and an amido black assay of the same protein-surface systems. The flexibility of this fluorescent assay will allow many other surface analysis techniques to be calibrated.

5.2.3.1 Quartz Crystal Microbalance (QCM) Measurements

Quartz crystal microbalance (QCM) technology measures frequency changes of an oscillating quartz crystal that arise due to the addition of an overlayer on the surface of the crystal. If the overlayer is rigid, the frequency change can easily be related to the adsorbed mass by means of the Sauerbrey equation:[22]

$$\Delta f = -\frac{2f^2}{\sqrt{\rho_q \mu_q}} \Delta m \qquad \text{Equation (5.1)}$$

where 'Δf' is the change in frequency observed in Hz, 'm' is the change in mass (g cm^{-2}), and 'ρ_q' and 'μ_q' are the density and shear modulus of quartz respectively. When using QCM for liquid studies one must be aware of deviations from the Sauerbrey equation, due to liquid density and viscosity factors as well as viscoelastic contributions of the overlayer, as detailed in chapter 2.[14] The energy of the crystal oscillation is dissipated through a non-rigid overlayer such as adhering protein molecules, making accurate determination of the actual adsorbed protein mass difficult, especially because the mass loading in such a system includes water molecules and ions entrapped within the protein layer.

5.2.3.2 Amide Black

Amido black staining is commonly used for electrophoresis to highlight protein bands in gels, although it has been used to assess relative amounts of adsorbed protein.[19] The dye molecule, naphthol blue black strongly interacts with proteins possibly forming a complex between an amine side chain and the sulphonic acid groups of the dye molecule.[23,24] Because of the strong absorption band of the dye at 620 nm, this method is very sensitive to small amounts of proteins, but does require external calibration. After protein incubation the solution is removed and the surface is rinsed to remove any unbound protein. The addition of the stain allows only the bound protein to be analysed, although the specific attachment between the dye and protein molecules means that the geometry of the bound protein affects the amount of dye captured at the surface.

5.2.3.3 Nano Orange

The Nano Orange protein quantification kit (Molecular probes, N6666) allows accurate determination of protein concentration in the range 10-0.001 $\mu g\ mL^{-1}$. The Nano Orange reagent is virtually non-fluorescent in aqueous solution, but upon binding to proteins the surfactant dye molecule undergoes a dramatic fluorescence enhancement,[25] having a broad excitation peak centered at 470 nm and a broad emission peak centered at 570 nm. A number of studies have examined pH,[26] contaminent,[27] and temperature effects[28] of the assay, reporting use of the fluorescent dye for up to 6 hours after addition of protein with no loss in sensitivity. The use of Nano Orange to follow protein adsorption processes allows detection and quantification of the total amount of protein present. The major disadvantage of this method is that this dye is non-protein specific preventing investigation of mixtures of protein.

5.2.4 Calibration Using Nano Orange and Comparison with Data Obtained Using QCM and Amido Black Assay

Saturation curves can be constructed over a range of concentrations which give information on protein-surface interactions. By fitting the data to a Langmuir curve, Equation 5.2, relative protein surface saturation amounts 'Q_m' and binding affinities 'K' can be found from the shape of the curve, as discussed in previous chapters.

$$\frac{Q}{Q_m} = \frac{KC}{1+KC} \qquad \text{Equation (5.2)}$$

where 'Q' and 'C' are the adsorbate surface concentration and the concentration in the phase adjacent to the surface respectively.

Fibrinogen and albumin were used as model proteins due to their relatively high abundance in plasma making their investigation applicable to biomaterial evaluation. Here we show fibrinogen adsorbing onto a chemically defined hydrophilic surface as example data to demonstrate calibration of QCM and amido black protein assay. Saturation curves constructed using the three techniques are shown in Figure 5.2.

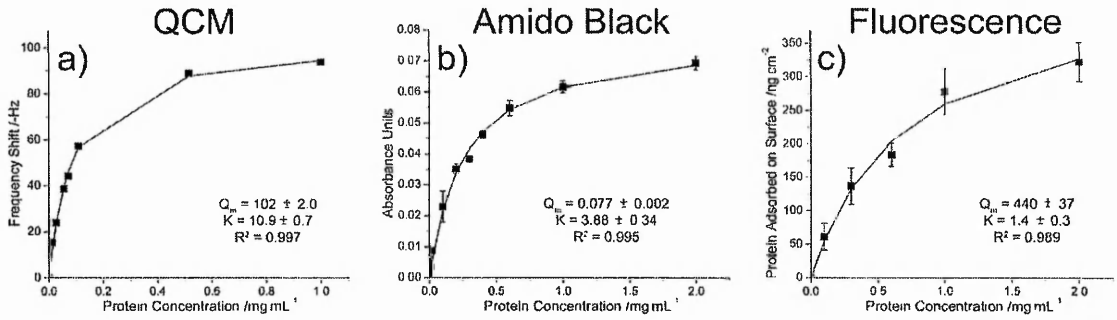

Figure 5.2. Saturation curves of fibrinogen adsorbing onto a model hydrophilic surface.

Each of the saturation curves differ slightly due to the limitations of the three techniques. Obviously the 'Q_m' values will differ because each of the methods gives a number relating to the quantity of protein assessed, i.e. a frequency is given in Hz for QCM. The fluorescence assay is the only method giving an absolute determination of the amount of adsorbed protein.

Binding affinity values should be the same for all techniques used to assess protein adsorption because this value relates to the equilibrium linking adsorbing and desorbing species, however, differences can be seen which demonstrates variability between the methods. The detection method in each case could be affected by varying parameters having an impact on the binding constant. It might be expected that a higher value is found using QCM because the frequency shift includes viscoelastic factors of the adsorbing layer. As protein is adsorbed the mass of water trapped between neighbouring bound proteins will also contribute to the observed frequency change, which will make adsorption appear to be more rapid initially, slowing earlier than it actually does. Amido black staining could be affected by the orientation or conformation of the bound protein, wherein geometric rearrangement of the protein may cause different amounts of amine groups to be presented at the surface of the protein, therefore having an impact on the number of dye molecules interacting with the protein. Such differences may be useful if structural changes are investigated but the specific binding nature of the naphthol blue black stain may influence quantitative analysis. Nano Orange, however, uses a surfactant-type molecule which binds to the hydrophobic regions of proteins. The fluorescent assay protocol described in this paper removes the protein molecules attached to the surface after incubation allowing the fluorescent dye to bind around the whole outer protein surface. Unlike the amido black assay the

fluorescent assay is less affected by surface induced conformational changes of the protein.

The Lineweaver-Burke linear form of each saturation curve can be obtained by plotting '*1/Q*' vs '*1/C*' over a range of concentrations. Any deviation from an ideal Langmuir curve can then be assessed. Such discrepancies may occur when investigating protein adsorption due to the nature of the protein-surface interactions including multiple-site binding and lateral interactions between binding proteins. The main assumptions within this model are that the surface is completely homogenous with each vacant surface site filled by one adsorbing species, and also that there are no lateral interactions between bound species. Although the Langmuir model is generally a good fit for most protein adsorption systems, proteins that spread or denature as they bind to the surface are not accounted for and lateral interactions are likely. Deviations from the Langmuir curve may also occur due to inaccuracies in measurement at the lower limits of detection. For this reason only those points lying on a linear region have been used, as shown in Figure 5.3.

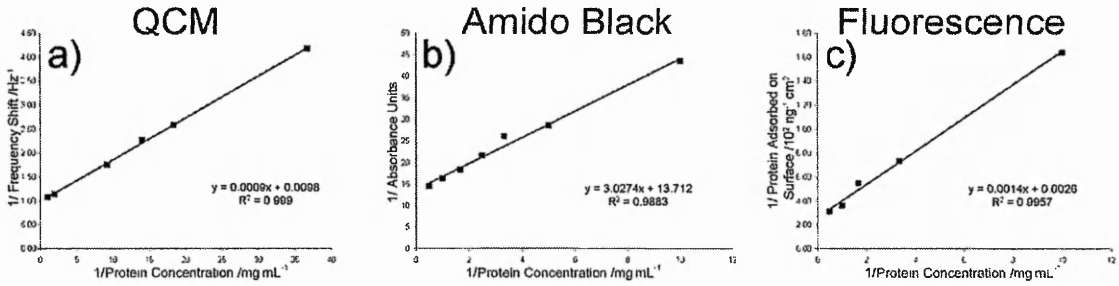

Figure 5.3. Linear form of saturation curves for QCM, Amido black and fluorescence assays.

The amount of fibrinogen adsorbed onto the hydrophilic surface is directly related to the concentration of the incubated protein solution by the line equation from the Nano Orange linear Langmuir plot, Figure 5.3c. Using this as a calibration method for the other methods a plot can be constructed relating the QCM frequency shift and amido black absorbance units to the mass of fibrinogen adsorbed, Figure 5.4.

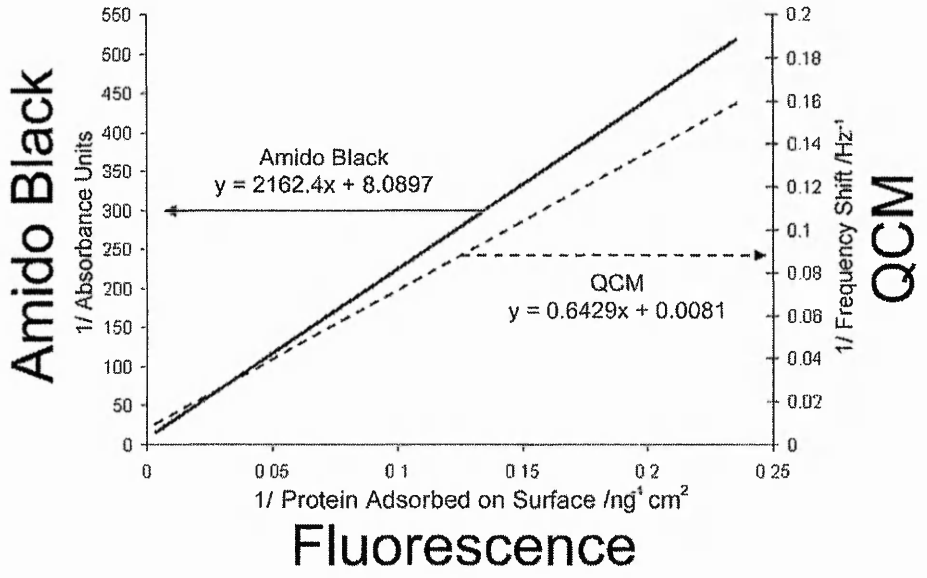

Figure 5.4. Calibration plot for QCM and Amido Black using a fluorescence assay as an absolute measure of surface bound protein.

If calibration is conducted on the same protein-surface system then it may be useful to convert data by means of calculation rather than graphically. This can be done by constructing the linear Langmuir plots for each method as shown in Figure 5.3, and relating the y-axis of the non-calibrated method to adsorbed protein mass from the Nano Orange assay (plotted in ng mL^{-1}) using the following equation:

$$\frac{1}{y} = \frac{1}{\underset{Mass\ /ng\ cm^{-1}}{Adsorbed\ \ Protein}} + \frac{(Gradient_a - Gradient_b)}{\underset{Concentration\ /mg\ mL^{-1}}{Incubated\ \ Protein}} + (y\text{-}Intercept_a - y\text{-}Intercept_b)$$

Equation (5.3)

where subscripts 'a' and 'b' denote values obtained for fluorescence and the non-quantitative technique respectively.

Due to small changes which may arise between proteins adsorbing onto different surfaces (see below) it may be best to calibrate each protein-surface system separately.

5.2.5 'Flat' Hydrophilic vs Hydrophobic Surfaces

To further establish the use of the fluorescent assay method for the quantification of surface bound protein the adsorption characteristics of fibrinogen were investigated further, comparing hydrophilic and hydrophobic surfaces. Albumin adsorption onto the model surfaces was also studied. It should be noted that

protein-protein variability may cause differences in detection; therefore calibration should be conducted for each protein used.

The adsorption profiles and saturation curves for albumin and fibrinogen onto heptanethiol and mercaptoethanol surfaces obtained using QCM have been previously reported and described in chapter 3. It was found that proteins binding strongly to surfaces become deformed, spreading over the surface giving rise to lower total amounts adsorbed.[3]

5.2.5.1 Quartz Crystal Microbalance (QCM)

QCM results showed that both albumin and fibrinogen adsorbed more rapidly onto hydrophobic surfaces although this effect was much more pronounced for albumin, as detailed in chapter 3. A lower saturation level was observed for both proteins adsorbing onto hydrophobic substrates, suggesting surface induced deformation due to hydrophobic binding. Mass loading calculated using the Sauerbrey equation gave values in the region of 1720 and 780 ng cm^{-2} for fibrinogen and albumin respectively, Table 5.1. The fraction of this mass contribution arising from entrapped water and viscoelastic effects cannot be calculated from QCM data alone. Other researchers often use a combination of techniques to gain a more complete picture about the adsorbing species. For instance, ellipsometry can give information on adsorbed layer thickness which can be used in conjunction with QCM to better estimate the mass of adsorbed layer.

Table 5.1. Data obtained from QCM measurements (chapter 3).[3]

	Saturation Frequency Value /Hz	Sauerbrey Mass Loading /ng cm^{-2}	Mass of adsorbed Protein from Nano Orange Assay /ng cm^{-2}	
			Using OH Calibration	Using CH_3 Calibration
Fg **OH**[a]	102.0	1805.4	377	341
Fg **CH_3**[a]	96.2	1702.7	280	289
BSA **OH**	47.2	835.4	240	337
BSA **CH_3**	40.9	723.9	218	289

[a]**OH** and **CH_3** represent hydrophilic and hydrophobic surfaces respectively.

Here we used the Nano Orange calibration of the QCM to assess the actual protein mass absorbed, finding values similar to those reported by others using surface plasmon resonance[29] and radiolabelling[30] Small differences were observed when cross calibration

was checked, i.e. using the calibration plot for fibrinogen onto hydrophilic surfaces to assess the amount of fibrinogen adsorbed onto a hydrophobic surface and vice versa. Results show that fibrinogen calibrations were consistent although much larger variation was observed for albumin, Table 5.1. This is possibly because albumin deforms to a greater extent than fibrinogen, supporting data reported in chapters 3 and 4.[3] Because proteins can denature and spread as they adsorb onto a surface, having differing conformations and orientations on different surfaces, each protein-surface system tested was calibrated separately.

5.2.5.2 Amido Black Assay

As with QCM results the amide black assay showed an increase in the amount of protein adsorbed with increasing protein concentration, Figure 5.5. On all surfaces tested fibrinogen gave rise to a higher absorbance in the amido black assay when compared to albumin, most probably due to fibrinogen having a higher number of amino acids with amine side chains that bind to the dye molecule.

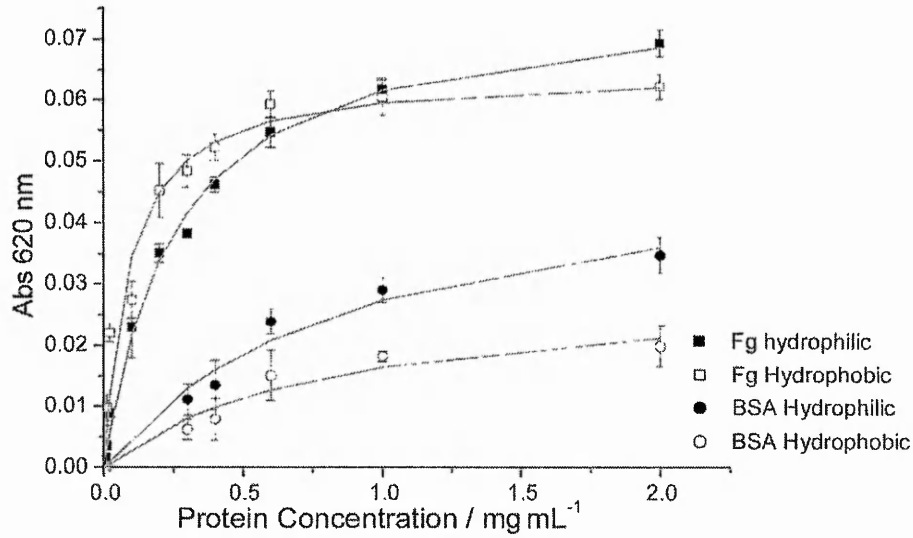

Figure 5.5. Saturation curves for fibrinogen and albumin onto 'flat' hydrophobic and hydrophilic surfaces obtained using the amido black assay.

The amido black assay, in good agreement with QCM data, showed that fibrinogen and albumin adsorbed in higher amounts to hydrophilic surfaces.

Table 5.2. Data obtained from amido black assay.

	Saturation Value /10^2 Abs 620 nm	Mass of adsorbed Protein from Fluorescence Assay /ng cm^{-2}
Fg **OH**[a]	7.743 ± 0.224	450 ± 35
Fg $\mathbf{CH_3}$[b]	6.531± 0.349	285 ± 26
BSA **OH**	5.224± 0.751	301 ± 1
BSA $\mathbf{CH_3}$	2.981± 0.597	271 ± 11

[a]**OH** and $\mathbf{CH_3}$ represent hydrophilic and hydrophobic surfaces respectively.

5.2.5.3 Nano Orange Assay

Absorbance values obtained when conducting an amido black assay of surface bound protein allows only relative amounts of protein to be assessed. Likewise, problems associated with QCM mass measurement of non-rigid systems can result in misleading or inaccurate quantitation. External calibration is therefore required when using such methods to achieve quantitative information. Solution phase protein assays can easily be calibrated by a number of common methods such as UV spectroscopy or the Bradford assay, although these are limited to solutions with concentrations above 50 $\mu g\ mL^{-1}$ and 1 $\mu g\ mL^{-1}$ respectively. An assay examining a monolayer of adsorbed protein in the range of 300-400 ng cm^{-2} would require the use of a surface area of approximately 4 cm^{-2} for the adsorbed protein quantity even to be detectable by these methods. Fluorometric assays are much more sensitive to small amounts of protein stretching the limits of detection down to ng mL^{-1}. The Nano Orange fluorescence assay can either be used as a calibration for other methods or as a stand-alone method for the detection of surface bound proteins.

Saturation curves constructed using Nano Orange show the same trends as those for QCM[3] and amido black although the surface concentration of protein can be assessed directly, Figure 5.6.

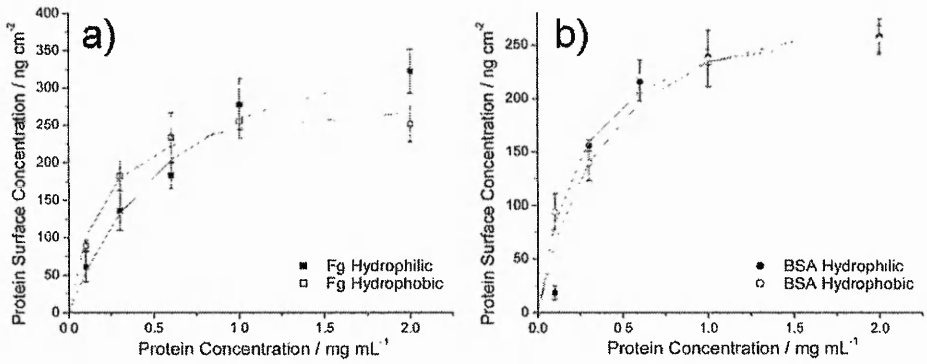

Figure 5.6. Saturation curves for a) fibrinogen and b) albumin onto 'flat' hydrophobic and hydrophilic surfaces obtained from Nano Orange assay. Solid lines show fitted Langmuir curves.

Binding affinities can be found from the shape of the fitted Langmuir curve. The '*k*' value relates to the equilibrium position between adsorbing and desorbing species, being higher with higher adsorbate-adsorbent interaction. Binding affinity values from QCM will include entrapped water mass and viscoelasctic contributions for the adsorbing layer. The non-specific nature of the amido black stain can cause variations in results due to the geometry of the surface-bound protein as discussed above. Nano Orange is not affected as much by such factors and can therefore be considered to give more accurate information with regard to binding affinity.

The binding affinities of fibrinogen and albumin adsorbing onto hydrophilic and hydrophobic surface are compared in Table 5.3. All three techniques show that both proteins tested have a higher affinity towards hydrophobic surfaces, although bind with lower saturation values. This is consistent with the hypothesis that proteins may deform to a greater extent upon binding to a surface with a high protein-surface affinity.

Table 5.3. Data obtained from Nano Orange fluorometric assay.

	QCM Binding Affinity	Amido Black Binding Affinity	Nano Orange Binding Affinity
Fg **OH**[a]	10.9	3.88 ± 0.34	1.43 ± 0.29
Fg **CH_3**[b]	36.0	11.58 ± 2.90	5.33 ± 1.01
BSA **OH**	5.3	1.10 ± 0.33	2.48 ± 1.05
BSA **CH_3**	5.4	1.23 ± 0.53	4.00 ± 0.86

[a]**OH** and **CH_3** represent hydrophilic and hydrophobic surfaces respectively.

Examination of the protein binding affinity of the different proteins to the hydrophobic versus hydrophilic surfaces was found to vary in a similar fashion, irrespective of the analysis techniques used. Thus for fibrinogen the affinity to the hydrophobic versus hydrophilic surface was found to be approximately 270 % higher from the fluorometric assay, 230 % from QCM and 200 % from the amido black assay. Albumin also showed a greater affinity towards hydrophobic surfaces.

The protein adsorption trends observed by QCM and amido black assay were verified by the Nano Orange assay, although the differences reported between the techniques highlight the possibility for mis-interpretation when using the non-quantitative techniques in isolation.

5.2.6 Porous Surfaces

Many techniques used to study protein adhesion processes cannot be employed when examining porous or very rough surfaces. QCM crystals can be coated with any number of surfaces but problems associated when using rough surfaces with QCM are well known. Liquid may become entrapped at the surface, acting as a rigid mass causing a crystal response.[31,32] Other mechanisms accounting for this differing frequency response have been proposed, including interfacial slip where the liquid slips across the surface of the crystal due to the shear mode of oscillation.[33-35] Porous materials produced from hydrophobic materials are superhydrophobic, meaning that water on the surface will not enter the pores but instead bridge across neighbouring pore walls.[36] It is also possible that entrapment of gas within the pore network is responsible for the differing QCM frequency response to mass loading.[37] Ellipsometry also cannot be used to examine porous or rough surfaces because any adsorption inside a material cannot be observed.[11]

With the recent interest in superhydrophobicity and superhydrophilicity for a number of applications,[38-40] and protein adsorption being shown to be controlled by surface topography,[3,4] porous materials are of potential interest for biomedical and biosensor applications. It is clear however that conventional quantification techniques have inherent problems when rough or porous surfaces are to be analysed. For this reason we show the use of Nano Orange for just such an investigation, comparing it to amido black staining as above.

Porous silica materials were used that can be produced as superhydrophobic surface coatings and by thermal treatment be switched to become superhydrophilic.[38]

These materials have high surface areas exceeding 300 $m^2 g^{-1}$ onto which protein adsorption may take place, Figure 5.7.

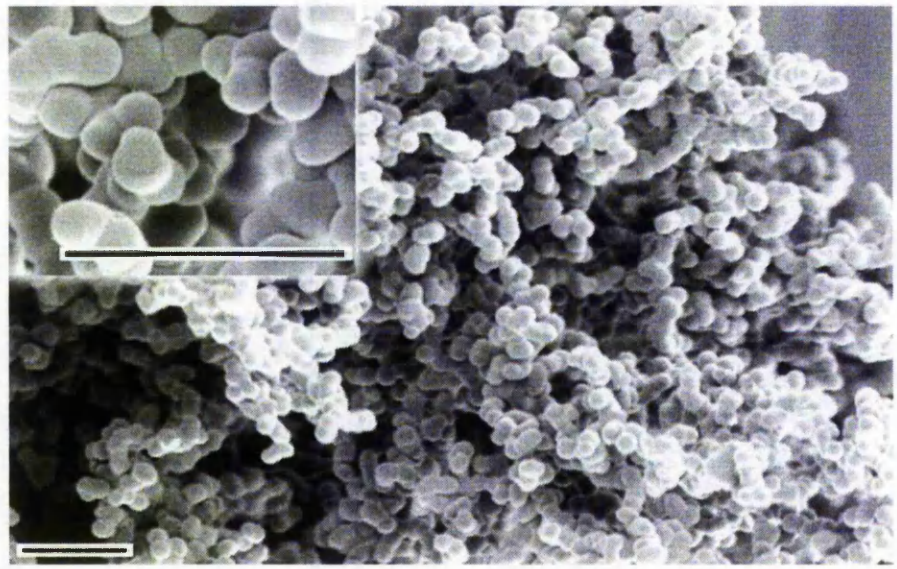

Figure 5.7. Scanning electron micrograph of porous material. Insert shows enlarged region. Scale bars indicate 10 μm.

The water contact angle on the flat hydrophobic material is 'θ_s' = 107°, whereas the porous hydrophobic material having the same surface chemistry has a water contact angle 'θ_r' = 152°. From the Cassie-Baxter relationship, Equation 5.4[39] it can be shown as water does not penetrate into the pores of the hydrophobic material, only ~16.5 % of the base of the water droplet will interact with the surface material, the remainder of the base being entrapped gas. This should restrict the available surface area for protein adsorption.

$$\cos\theta_r = f\cos\theta_s + (1-f)\cos\theta_x \qquad \text{Equation (5.4)}$$

where 'f' is the fraction of the droplet base in contact with the surface and 'θ_x' is the contact angle of water on air – assumed to be 180°.

When these porous materials are hydrophilic the surfaces are superhydrophilic, with the liquid phase readily penetrating into the pore network providing a much greater surface area for protein adsorption.

The porosity of the material used was characterised by nitrogen adsorption, having predominantly micropores that proteins would be too large to enter. The external surface area available for protein adsorption was found to be 36.0 $m^2 g^{-1}$ by the difference between total and micropore surface area. The V-t method was used wherein the micropore volume was determined by the de Boer method, involving the measurement of nitrogen adsorbed at low pressures. A t-plot is a visual representation of volume of gas adsorbed versus the statistical thickness of the adsorbed film, 't'. Using the value of 36.0 $m^2 g^{-1}$ surface area of the sample used it was calculated that each well used for protein incubation had approximately 440 times the available surface area compared to flat surfaces tested.

Data from the fluorometric analysis was normalised to available surface area per well, i.e. a much larger surface area was available for protein adsorption when using superhydrophilic compared to superhydrophobic surfaces. However, very low saturation values were observed for both proteins adsorbed onto superhydrophilic surfaces, with approximately a 100-fold decrease compared to flat surfaces, Figure 5.8a, data is summarized in Table 5.4, (compared to Table 5.2).

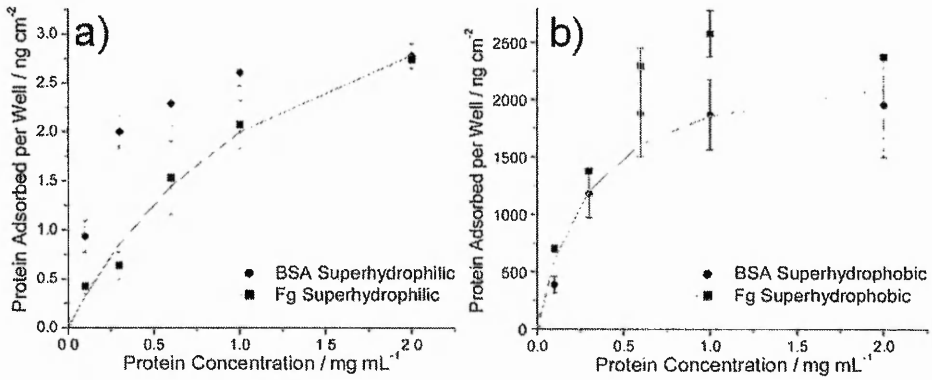

Figure 5.8. Saturation curves for albumin and fibrinogen onto a) superhydrophilic and b) superhydrophobic surfaces obtained using the Nano Orange assay. Lines show fitted Langmuir curves.

This difference in the amount of protein adsorbed may be due to differences in protein transport to the surface of the material. Transport of a protein molecule to a flat surface would depend largely on its diffusion through the liquid to the solid-liquid interface. When considering porous materials most of the surface area is within the bulk

and although the protein solution can penetrate into the porous network a longer period of time may be required for the protein adsorption process to reach equilibrium.

Table 5.4. Fibrinogen and albumin adsorption parameters onto superhydrophobic and superhydrophilic surfaces by fluorometric analysis.

	Binding Affinity	Saturation Value / ng cm^{-2}
Fg **OH**[a]	0.76 ± 0.20	4.62 ± 0.63
Fg $\mathbf{CH_3}$[b]	3.62 ± 1.32	2994 ± 319
BSA **OH**	5.08 ± 0.67	3.09 ± 0.10
BSA $\mathbf{CH_3}$	3.34 ± 1.23	2410 ± 267

[a]**OH** and $\mathbf{CH_3}$ represent hydrophilic and hydrophobic surfaces respectively.

The superhydrophobic materials show a massive increase in the surface concentration of surface bound protein when normalised to available surface area, Figure 5.8b. These values far exceed those for flat surfaces which may suggest that the protein serves as a surfactant allowing the aqueous phase to interact with a greater substrate surface area than expected (see above). The adsorbed protein layer may aid the protein solution to penetrate further into the porous coating expanding the surface area in contact with the aqueous phase and thus allow more protein molecules to adsorb. In this way the protein front may push into the pored network.

Binding constants show that fibrinogen has a greater affinity towards superhydrophobic compared to superhydrophilic surfaces. Albumin in contrast to fibrinogen is shown to have a higher affinity towards the superhydrophilic compared to superhydrophobic surface which indicates a significant difference in protein adsorption characteristics with regards to surface roughness effects on hydrophobicity and hydrophilicity.

Amido black assay was also used to assess fibrinogen and albumin adsorption onto these porous materials. Higher quantities of both proteins were found to adsorb onto superhydrophilic compared to superhydrophobic materials when data was not normalised to surface area, Figure 5.9. Due to difficulties in determining the actual surface area presented to the protein solution by the superhydrophobic material only relative amounts of protein can be assessed. Data is summarised in Table 5.5.

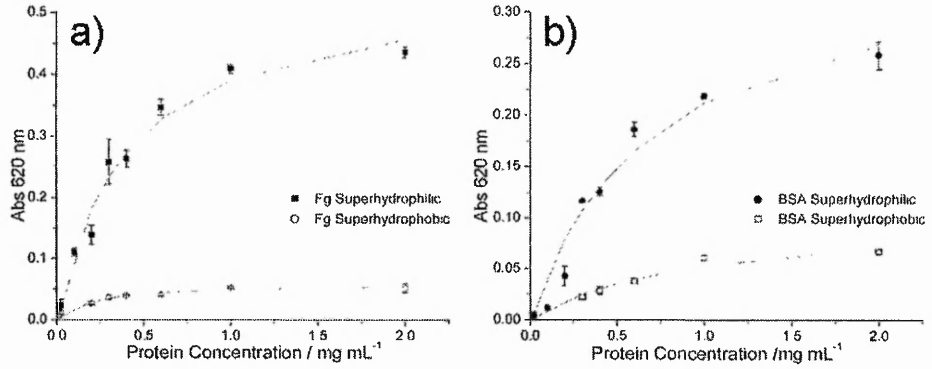

Figure 5.9. Saturation curves for a) fibrinogen and b) albumin onto superhydrophobic and superhydrophilic surfaces constructed using amido black assay. Solid lines represent fitted Languir curves.

The saturation values show an increase in the amount of protein adsorbing per well of approximately 700% when comparing to porous to flat hydrophilic surfaces, although these values are again much lower than would be expected for a material offering such a large surface area for protein adsorption.

Table 5.5. Fibrinogen and albumin adsorption parameters onto superhydrophobic and superhydrophilic surfaces by amido black assay.

	Binding Affinity	Saturation Value /10^2 Abs 620 nm
Fg **OH**[a]	2.47 ± 0.60	54.8 ± 4.9
Fg $\mathbf{CH_3}$[b]	4.60 ± 0.98	6.0 ± 3.6
BSA **OH**	1.38 ± 0.45	36.5 ± 5.4
BSA $\mathbf{CH_3}$	1.04 ± 0.32	10.4 ± 1.5

[a]**OH** and $\mathbf{CH_3}$ represent hydrophilic and hydrophobic surfaces respectively.

Binding constants were found to differ somewhat compared to those on flat surfaces. Fibrinogen again had a higher affinity towards the superhydrophobic compared to superhydrophilic material, although affinities towards both surfaces were about 40 % and 60 % lower than on the corresponding hydrophilic and hydrophobic flat surfaces respectively. Binding constants for albumin were similar to those on the flat surfaces however average values possibly indicate a slightly higher affinity towards the superhydrophilic surface, which supports data obtained by fluorometry.

5.3 Discussion

A novel use for the Nano Orange assay has been discussed, either as an external calibration for other methods or as a stand-alone method for quantifying protein adsorption. Data obtained for fibrinogen and albumin adsorbing onto flat chemically defined hydrophilic and hydrophobic surfaces was compared for QCM, amido black and fluorometric assays. The values obtained correspond well with those expected from previous reports.[29,30] These techniques were chosen to highlight the limitations of current methods used to study protein adsorption, using fluorometry as a means to quantify the amount of protein adsorbed onto various surfaces. The use of an off-the-shelf fluorescence protein quantification kit (Molecular Probes) to analyse the amount of protein adsorbed onto surfaces that can then be used to calibrate other non-quantitative methods has been demonstrated.

Results showed trends in protein adhesion parameters which were common for all three methods used, (Tables 5.1-5.3). A greater quantity of fibrinogen compared to albumin adsorbed on surfaces having the same chemistry, with both proteins generally having a higher affinity but lower saturation values on hydrophobic surfaces. This may indicate that as the protein molecules interact with the hydrophobic surface, deformation of their secondary structure occurs to minimize interaction with surrounding water, as discussed in previous chapters. Surface-protein hydrophobic bonding which is known to play a dominant role in surface-protein interactions possibly drives the adsorption process and structural change.[41]

Some differences between the methods were, however, highlighted which may be due to the non-specific binding of the fluorescent dye used due to its surfactant nature. The Nano Orange assay showed a greater difference between the amount of fibrinogen adsorbed onto hydrophilic compared to hydrophobic surfaces, which may indicate that a large proportion of the QCM frequency shift arises from the viscoelastic properties of the adsorbing protein layer. Albumin however is much smaller in size than fibrinogen and so viscoelastic effects are assumed to be lower. The proportions of albumin adsorbed onto the two surface chemistries correlate well between QCM and fluorometry, although the amido black assay results differ. Variation may be due to the specific binding of the amido black stain which could be hindered by conformation or orientational changes of the surface-bound proteins.

Binding affinities assessed by all three methods showed good correlation, with fibrinogen having a higher affinity towards hydrophobic compared to hydrophilic

surfaces, with an increase of 270 %, 230 % and 200 % being observed by fluorometric analysis, QCM and amide black assay respectively. Albumin also has a higher affinity towards hydrophobic surfaces with values reported by QCM and amido black assay being in good agreement.

The porous coatings investigated allowed protein adsorption to be assessed on superhydrophilic compared to superhydrophobic materials. It was assumed that because the aqueous phase penetrated into the hydrophilic network a much higher surface area would be available for protein adsorption, and conversely that a lower surface area was presented by the superhydrophobic material due to bridging-type wetting, as discussed above. Results showed that the surface density of protein when normalised to surface area was much less than would have been expected. This could be due to protein transport through the porous material which may extend adsorption equilibrium times dramatically. Saturation values on superhydrophilic materials were also quite different. A much greater amount of protein was observed on superhydrophobic surfaces than was expected, which may be explained by the surfactant nature of the adsorbing layer, although this is currently a hypothesis that requires further investigation.

Binding affinities for proteins adsorbing onto porous materials were also quite different from those on the flat surfaces tested. Fibrinogen showed a greater affinity towards the superhydrophobic compared to superhydrophilic materials but values were ~50 % and 70 % lower than those on flat hydrophilic and hydrophobic surfaces respectively. Albumin was found possibly to have a slightly higher affinity towards the superhydrophilic compared to the superhydrophobic surface.

5.4 Conclusions

Techniques such as QCM and ellipsometry are commonly used for the study of protein adsorption, although such methods rely on basic assumptions that may not be strictly true for protein adsorption systems. These problems can lead to the misinterpretation of data, especially when calculating the mass of protein adsorbed at a solid-liquid interface. Other methods used to compare protein adsorption onto different surfaces, such as amido black staining, only give an indication of the relative amounts adsorbed. The key issue with all these techniques is that they lack the ability to give quantitative information.

The use of fluorimetry has allowed the detection and accurate quantification of protein in solution in the order of nanograms per mL, permitting measurement of protein adsorbed onto flat surfaces of a 'usable size' for laboratory methods. The adsorption characteristics of fibrinogen and albumin onto model hydrophobic and hydrophilic surfaces have been analysed by QCM, amido black staining and results compared to those obtained by fluorometric assay. Furthermore, the use of porous coatings was investigated with results from amido black and fluorometric methods being compared. The latter investigation could not be conducted by QCM due to practical experimental difficulties involved with flowing liquids over superhydrophobic surfaces giving an unstable resonant crystal frequency, and problems associated with data interpretation as described above.

Because the results from the three methods are largely comparable over the range of protein concentrations analysed, it is possible to use the protein quantities determined by fluorometric analysis as a means of standardising or calibrating both QCM and amido black assay methods. A protocol has been developed wherein a standard off-the-shelf fluorometric assay can be used either in collaboration with other methods, acting as an external calibration, or as a stand-alone assay as a novel method for constructing protein saturation curves. The benefits of this method over current techniques are the speed and absolute quantification of protein loading, as well as the different types of surfaces which can be investigated.

This fluorometric method is three orders of magnitude more sensitive than standard colourimetric methods used to detect proteins, which means that to detect sub-monolayers of protein, considerably smaller surface areas can be used. Experimentally this is more practical when studying flat surfaces. Non-porous materials can also be used allowing protein adsorption to be further characterised on materials exhibiting superhydrophobicity and superhydrophilicity.

It was found that the presence of surface roughness affects the binding characteristics of proteins, with albumin possibly having a higher affinity towards superhydrophilic compared to superhydrophobic materials. Protein adsorption characteristics are known to be controlled by surface chemistry and topography, with many studies examining the effects of hydrophobic compared to hydrophilic surfaces. To our knowledge this is the first report examining protein adsorption onto superhydrophilic and superhydrophilic materials. Topographically textured and porous surfaces may complement surface chemistry affects, leading to the enhancement of

biomaterials and biosensor devices. Because conventional techniques that are used to monitor protein adsorption processes only give an indication of processes occurring at solid-liquid interfaces, the search for new methods that give absolute information is essential.

5.5 References

1. M. Shen; T.A.Horbett; "The Effects of Surface Chemistry and Adsorbed Proteins on Monocyte / Macrophage Adhesion to Chemically Modified Polystyrene Surfaces," *J. Biomed. Mater. Res.*, **2001**, 57(3) 336-345
2. M.J. Nam; C.S. Thaxton; C.A. Mirkin, "Nanoparticle-Based Bio-Bar Codes for the Ultrasensitive Detection of Proteins," *Science*, **2003**, 301, 1884-1886
3. P. Roach; D. Farrar; C.C. Perry, "Interpretation of Protein Adsorption: Surface-Induced Conformational Changes," *J. Am. Chem. Soc.*, **2005**, 127(22) 8168-8173
4. R. Barbucci; S. Lamponi; A. Magnani, "Fibrinogen Conformation and Platelet Reactivity in Relation to Material-Blood Interaction: Effect of Stress Hormones," *Biomacromolecules*, **2003**, 4, 1506-1513
5. A.A. Vertegal; R.W. Siegel; J.S. Dordick, "Silica Nanoparticle Size Influences the Structure and Enzymatic Activity of Adsorbed Lysozyme," *Langmuir*, **2004**, 20(16) 6800-6807
6. A. Kondo; H. Fukuda, "Effects of Adsorption Conditions on Kinetics of Protein Adsorption and Conformational Changes at Ultrafine Silica Particles," *J. Colloid Int. Sci.*, **1998**, 198(1) 34-41
7. T.A. Horbett; C.M. Cheng; B.D. Ratner; A.S. Hoffman, "The Kinetics of Baboon Fibrinogen Adsorption to Polymers: In Vitro and In Vivo Studies," *J. Biomed. Mater. Res.*, **1986**, 20(6) 739-772
8. C.Galli Marxer; M. Collaud Coen; H. Bissig; U.F. Greber; L. Schlapbach, "Simultaneous Measurement of the Maximum Oscillation Amplitude and the Transient Decay Time Constant of the QCM Reveals Stiffness Changes of the Adlayer," *Anal. Bioanal. Chem.*, **2003**, 371(3) 570-577
9. E-L, Lyle; G.L. Hayward; M. Thompson, "Acoustic Coupling of Transverse Waves as a Mechanism for the Label-Free Detection of Protein-Small Molecule Interactions," *The Analyst*, **2002**, 127, 1596-1600
10. G. McHale; R. Lucklum; M.I. Newton; J.A. Cowen, "Influence of Viscoelasticity and Interfacial Slip on Acoustic Wave Sensors," *J. Appl. Phys.*, **2000**, 88(12) 7304-7312
11. P. Tengvall; I. Lundström; B. Liedberg, "Protein Adsorption Studies on Model Organic Surfaces: An Ellipsometric and Infrared Spectroscopic Approach," *Biomaterials*, **1998**, 19, 407-422

12. F.A. Denis; P. Hanarp; D.S. Sutherland; J. Gold; C. Mustin; P.G. Rouxhet; Y.F. Dufrêne, "Protein Adsorption on Model Surfaces with Controlled Nanotopography and Chemistry," *Langmuir*, **2002**, 18, 819-828
13. A. Sethuraman; M. Han; R.S. Kane, G. Belfort, "Effect of Surface Wettability on the Adhesion of Proteins," *Langmuir*, **2004**, 20, 7779-7788
14. C. Zhou; J-M. Friedt; A. Angelova; K-H. Choi; W. Laureyn; F. Frederix; L.A. Francis; A. Campitelli; Y. Engelborghs; G. Borghs, "Human Immunoglobulin Adsorption Investigated by Means of Quartz Crystal Microbalance Dissipation, Atomic Force Microscopy, Surface Acoustic Wave, and Surface Plasmon Resonance Techniques," *Langmuir*, **2004**, 20, 5870-5878
15. X. Jiang; J. Jiang; Y. Jin; E. Wang; S. Dong, "Effect of Colloidal Gold Size on the Conformational Changes of Adsorbed Cytochrome C: Probing by Circular Dichroism, UV-Visible, and Infrared Spectroscopy," *Biomacromolecules*, **2005**, 6(1) 46-53
16. B. Sweryda-Krawiec; H. Devaraj; G. Jacob; J.J. Hickman, "A New Interpretation of Serum Albumin Surface Passivation," *Langmuir* , **2004**, 20, 2054-2056
17. C.R. Wittmer; P.R. Van Tassel, "Probing Adsorbed Fibronectin Layer Structure by Kinetic Analysis of Monoclonal Antibody Binding," *Colloids and Surfaces B: Biointerfaces*, **2005**, 41(2-3) 103-109
18. A.B.D. Cassie ; S. Baxter, "Wettability of Porous Surfaces," *Trans. Faraday Soc.*, **1944**, 40, 546-551
19. M.I. Jones; I.R. McColl; D.M. Grant; T.L.Parker, "Protein Adsorption and Platelet Attachment and Activation, on TiN, TiC, and DLC Coatings on Titanium for Cardiovascular Applications," *J. Biomed. Mater. Res.*, **2000**, 52, 413-421
20. J.D. Whittle; N.A. Bullett; R.D. Short; C.W.I. Douglas; A.P. Hollander; J. Davies, "Adsorption of Vitronectin, Collagen and Immunoglobulin-G to Plasma Polymer Surfaces by Enzyme Linked Immunosorbent Assay (ELISA)," *J. Mater. Chem.*, **2002**, 12, 2726-2732
21. A. Dieckmann-Schuppert; H-J. Schnittler, "A Simple Assay for Quantification of Protein in Tissue Sections, Cell Cultures, and Cell Homogenates, and of Protein Immobilized on Solid Surfaces," *Cell Tissue Res.*, **1997**, 288, 119-126

22. G. Sauerbrey, "The Use of Quartz Oscillators for Weighing Thin Layers and for Microweighing," *Z. Phys.*, **1959**, 155, 206-222
23. C. Tsopelas; R. Sutton, "Why Certain Dyes are Useful for Localizing the Sentinel Lymph Node," *J. Nuclear Medicine*, **2002**, 43, 1377-1382
24. D.S. Wilbur, "Formation of Sulfonamide Bonds Through Reaction of Dyes With Serum Proteins," *J. Nuclear Medicine*, **2003**, 44(9) Author Reply 1540-1541
25. B. Giordano; L. Jin; A.J. Couch; J.P. Ferrance; J.P. Landers, "Microchip Laser-Induced Fluorescence Detection of Proteins at Submicrogram Per Milliliter Levels Mediated by Dynamic Labeling Under Pseudonative Conditions," *Anal. Chem.*, **2004**, 76(16) 4705-4714
26. M.D. Harvey; V. Bablekis; P.R. Banks; C.D. Skinner, "Utilization of the Non-Covalent Fluorescent Dye, NanoOrange, as a Potential Clinical Diagnostic Tool. Nanomolar Human Serum Albumin Quantitation," *J. Chromatography, B*, **2001**, 754, 345-356
27. L.J. Jones; R.P. Haugland; V.L. Singer, "Development and Characterization of the NanoOrange Protein Quantitation Assay: A Fluorescence-Based Assay of Proteins in Solution," *Biotechniques*, **2003**, 34, 850-861
28. S. Silberblatt; R.A. Felder; T.E. Mifflin, "Optimizing Reaction Conditions of the NanoOrange Protein Quantitation Method for use With Microplate-Based Automation," *JALA*, **2001**, 6(6) 83-88
29. G.B. Sigal; M. Mrksich; G.M. Whitesides, "Effect of Surface Wettability on the Adsorption of Proteins and Detergents," *J. Am. Chem. Soc.*, **1998**, 120(14), 3464-3473
30. B.R. Young; W.G. Pitt; S.L. Cooper, "Protein Adsorption on Polymeric Biomaterials. II. Adsorption Kinetics," *J. Colloid and Int. Sci.*, **1988**, 125(1) 246-260
31. S.J. Martin, G.C. Frye, A.J. Ricco and S.D. Senturia, "Effect of surface roughness on the response of thickness-shear mode resonators in liquids," *Anal. Chem.*, **1993**, 65(20) 2910–2922
32. S.J. Martin, "Interactions of Acoustic Waves with Thin Films and Interfaces," Closing Remarks, *Faraday Discuss.*, **1997**, 107, 463–476
33. M. Thompson, A.L. Kipling, W.C. Duncan-Hewitt, L.V. Rajakovic and B.A. Cavic-Vlasak, "Thickness-Shear-Mode Acoustic Wave Sensors in the Liquid Phase. A Review," *Analyst*, **1991**, 116(9) 881–890

34. M.S. Yang; M. Thompson; W.C. Duncan-Hewitt, "Interfacial Properties and the Response of the Thickness-Shear-Mode Acoustic Wave Sensor in Liquids," *Langmuir,* **1993**, 9(3) 802–811
35. M.S. Yang and M. Thompson, "Surface Morphology and the Response of the Thickness-Shear Mode Acoustic Wave Sensor in Liquids," *Langmuir*, **1993**, 9(8) 1990–1994
36. N.J. Shirtcliffe; S. Aqil; C. Evans; G. McHale; M.I. Newton; C.C. Perry; P. Roach, "The Use of High Aspect Ratio Photoresist (SU8) for Super-Hydrophobic Pattern Prototyping," *J. Micromech. Microeng.*, **2004**, 14, 1384-1389
37. L.A. Theisen, S.J. Martin and A.R. Hillmann, "A Model for the Quartz Crystal Microbalance Frequency Response to Wetting Characteristics of Corrugated Surfaces," *Anal. Chem.*, **2004,** 76(3) 796–804
38. N.J. Shirtcliffe; G. McHale; M.I. Newton; C.C. Perry; P. Roach, "Porous Materials Show Superhydrophobic to Superhydrophilic Switching," *Chem. Commun.*, **2005**, 25, 3135-3137
39. D. Quéré, "Rough Ideas on Wetting," *Physica A-Statistical Mechanics and its Applications*, **2002**, 313(1-2) 32-46
40. A. Lafuma; D. Quéré, "Superhydrophobic States," *Nature Materials*, **2003**, 2, 457-460
41. W. Norde ; (J.D. Andarde Ed.) "*Surface and Interfacial Aspects of Biomedical Polymers*," **1985**, 2nd Ed., Plenum Press, New York

Chapter 6:

General Discussion, Conclusions and Future Work

6.1 Discussion and Conclusions

The previous chapters of this thesis examine the influence of surface parameters on protein adsorption processes. Surface chemistry has been shown to play an important role in the rate and total amount of protein adsorbed at equilibrium and in Chapter 4 the effect of surface topography in combination with surface chemistry was also considered using nano-sized surface curvature as a model system. This chapter includes a general discussion of the data presented, highlighting the key issues advances reported in this thesis. The final sections focus on areas which could be investigated further to develop a greater understanding of the principles affecting protein adsorption.

Two model surfaces were chosen allowing the investigation of protein adsorption with respect to surface wettability, comparing hydrophilic to hydrophobic surfaces. Albumin and fibrinogen are two serum proteins having contrasting sizes and shapes which are found in high concentrations at medical implant sites. These proteins were therefore chosen as model proteins to examine the influence of surface parameters with respect to medical implant surfaces. Because of the many thousands of proteins present in serum it was also useful to observe effects related to the differing size and shape of the adsorbing proteins.

Data shown in Chapter 3 strongly suggests that albumin and fibrinogen undergo differing adsorption processes due to their differing shapes. Fibrinogen is elongated and so can adsorb in two distinctly different orientations and therefore adsorbs in a two-stage process which was observed by QCM. Upon adsorption from solutions $>0.5 mgmL^{-1}$ it was found that fibrinogen adsorbed in a stepwise fashion, wherein the primary adsorption took place with the molecule most probably lying with its long axis parallel to the surface. It is suggested that rearrangement then takes place, driven by intermolecular hydrophobic bonding between neighbouring adsorbed fibrinogen molecules, resulting in the molecules standing with their long axis perpendicular to the surface. Albumin, in contrast, is a globular protein which can adsorb in many differing orientations to achieve the same surface coverage and was seen to undergo a single-stage adsorption process.

Several studies by others have implied that proteins may become denatured on some surfaces spreading as they attach, although detailed assessment of this structural change had not been conducted. Particular attention to the conformational analysis of surface-bound proteins has been made throughout the investigations reported here. The data shown in Chapter 3 show that both albumin and fibrinogen experience a stronger affinity towards hydrophobic compared to hydrophilic surfaces. This strong interaction causes a greater degree of protein deformation as confirmed by a loss of ordered secondary structure. In Chapter 4 the influence of surface chemistry was shown to be compounded by surface curvature. Onto particles with radii > 30 nm fibrinogen was found to adsorb with similar conformation to that on 'flat' surfaces, although onto smaller particles (with higher surface curvature) fibrinogen experienced greater deformation possibly due to the molecule folding around the observed surface curvature. Albumin, again due to its differing shape, was found to behave in an opposing manner, having more disordered structure on larger particles. This is possibly

due to the globular protein having a larger protein-surface interaction area on the larger particles.

The methods commonly used to study protein adsorption are directly quantitative. Many techniques such as QCM and ellipsometry rely on basic assumptions which may not be strictly true when examining protein adsorption systems. Other methods are strongly affected by the adsorbed conformation and orientation of the adsorbed protein which may lead to mis-interpretation of results. Some information on the relative amounts of protein adsorbed can be gained but such methods do not readily give absolute quantification of surface-bound protein. For these reasons Chapter 5 was dedicated to the calibration of surface analysis techniques. A fluorometric assay was employed for the absolute quantification of surface-bound protein. A protocol was established whereby any number of surfaces could be investigated.

QCM data presented in Chapter 3 was compared to an amido black assay of albumin and fibrinogen adsorbing onto hydrophilic and hydrophobic surfaces. Results show that the fluorometric assay can be used to act as either an external calibrant for other techniques or as an independent assay. The nature of QCM and ellipsometric techniques dictates that flat surfaces must be used when studying adsorption processes. This severely limits the investigation of protein adsorption onto topographically different surfaces, a surface parameter which has been shown to have a major impact on adsorption characteristics. The fluormetric method described in Chapter 5 was used to study the adsorption of fibrinogen and albumin onto very rough, porous surfaces to highlight its advantage over other techniques. Materials with contrasting wettabilities were prepared, allowing superhydrophobic and superhydrophilic coatings to be compared. Roughness enhanced wettability is an emerging area of interest in both chemistry and physics due to the interesting differences of the materials related to their flat counterparts. Results showed interesting differences compared to other protein-surface systems studied in this thesis, with albumin possibly having a higher affinity towards superhydrophilic compared to superhydrophobic materials. A much greater (10 fold) amount of protein was found to adsorb onto superhydrophobic surfaces than was expected. The data was normalised to the surface area expected to be available for protein adsorption although the adsorbed protein may act as a surfactant guiding layer allowing the protein solution to enter part-way into the surface. This would expose more surface area onto which protein adsorption may take place, thereby accounting for the increase in protein quantity observed.

From the above discussion it is clear that surface-protein interactions are governed by the nature of the underlying surface onto which they adsorb. Surface chemistry at the molecular level and topography on the nano-scale have been shown to impact on protein-surface affinity and therefore on the rates and total amounts adsorbed upon surface saturation. Once adsorbed the chemistry and topography also dictate to what extent a protein molecule is denatured and therefore how much activity will be retained. The investigation of other parameters will lead not only to a better understanding of protein-surface interactions but fine tuning of the parameters relating to a specific application, such as medical implant coatings, will bring about tailored material properties.

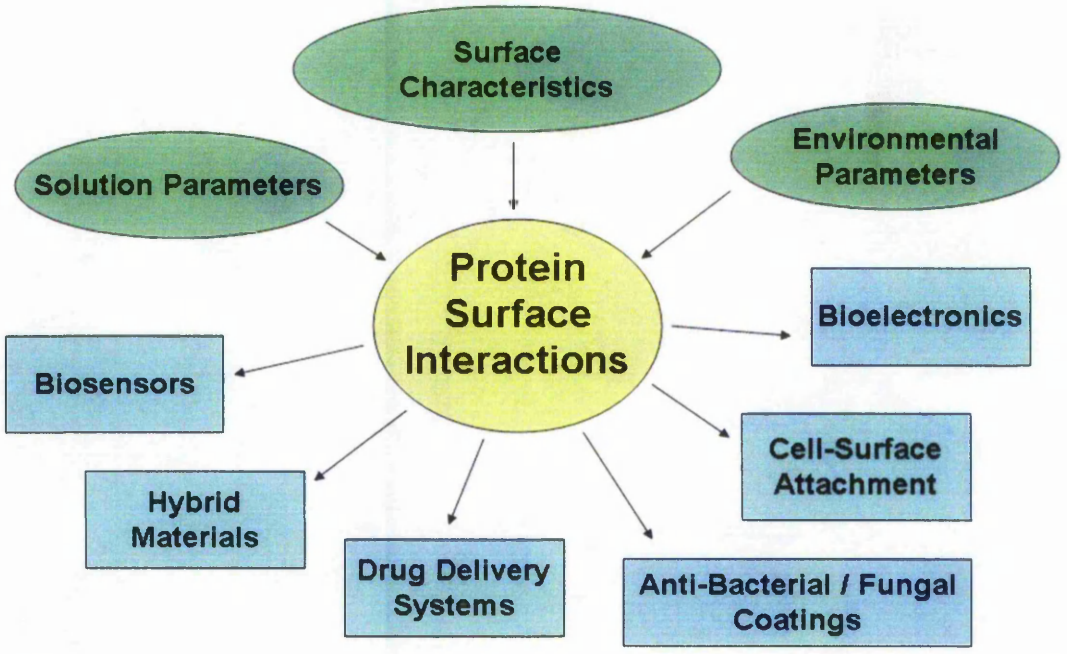

Figure 6.1. Protein-surface interactions are at the heart of many of today's leading research areas.

Once the principles underpinning the control of protein adsorption, and in particular the conformation (and thus activity) of surface-bound proteins have been established, a new era in the design of advanced materials will be possible. A new breed of so-called 'smart materials' will impact on almost every aspect of life, from medical implants with rapid and controlled healing abilities to ultra-antibacterial surface coatings, Figure 6.1.

6.2 Further Work

Some other investigations that could be carried out to further understand the importance of surface characteristics in relation to protein adsorption are listed below. These are an extension of the work reported in this thesis. Simple extensions such as the investigation onto differing chemical surfaces are not listed. Hydrophilic and hydrophobic model chemistries have been covered herein, but an obvious progression would be to examine surfaces with differing charge, such as amine or carboxylic acid terminated surfaces.

6.2.1 Infrared Experiments Supporting Chapter 3

Infrared spectroscopy has been used to assess the conformation of surface-bound proteins as described in Chapters 3 and 4, although the technique can also be used to follow the adsorption process in situ. Various surfaces could be assessed by deposition of, for example, polymer layers on the upper surface of an ATR crystal. If coatings are used that are transparent or weakly adsorbing in the infrared range of interest then an adsorbing layer of protein can be detected, although it should be noted that such coatings must not exceed the thickness of the evanescent wave penetration depth, equation 2.14. Some initial data is shown below for just such a study, comparing hydrophilic and hydrophobic surfaces. An increasing amide I or amide II band indicates a higher quantity of protein adjacent to the crystal surface, Figure 2a. Differences between the amide I/II ratios may indicate changes in orientation with respect to time, as highlighted for fibrinogen in Figure 6.2b.

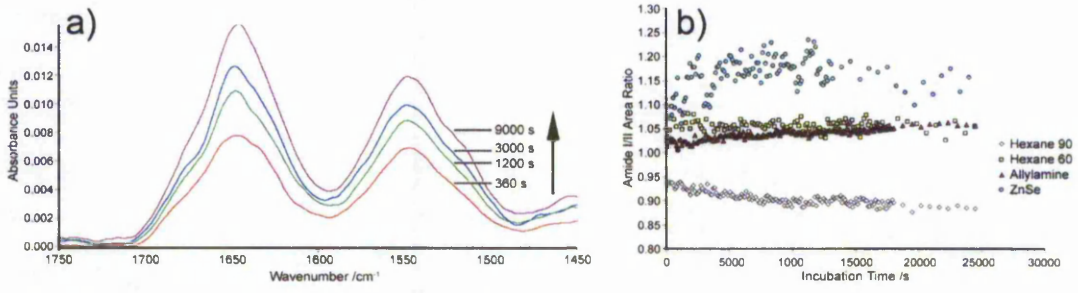

Figure 6.2. Fibrinogen adsorption followed by FTIR-ATR, a) adsorption onto a plasma deposited hexane polymer (water contact angle 90°), b) comparison of amide I/II area ratios for adsorption onto plasma deposited polymers: ◇ hexane CA 90°, □ hexane with some surface hydroxyls CA 60°, ▲ allylamine CA ~30° and ○ zinc selenide CA ~25°.

Onto successively hydrophobic surfaces fibrinogen amide I/II ratios tend to decrease. This may indicate the denaturing of the adsorbing protein. Further investigation of the spectra recorded over the varying time domains will allow conformational changes to be assessed with respect to time. I hypothesise that onto hydrophilic surfaces a gradual decrease in ordered secondary structure will be observed until the adsorbing protein molecules reach conformational equilibrium within a few minutes of attachment. Proteins adsorbing onto hydrophobic surfaces however will most probably become denatured very rapidly upon adsorption, with their ordered secondary structure steadily decreasing over time as relaxation occurs until the protein layer reaches equilibrium.

6.2.2 The Vroman Effect – Competitive Binding of Proteins

The investigations reported in this thesis examine only single protein systems, although physiological environments would be flooded with many hundreds of differing proteins, each adsorbing and desorbing at differing rates due to specific and non-specific protein-surface interactions. The Vroman effect suggests that the initial adsorbed protein layer will change over time until an equilibrium is reached, at which time some proteins will dominate the surface. Such surface enrichment, as discussed in Chapter 1, will be governed by protein-surface interactions. Surface chemistry and topography can be used to control protein-surface affinity and the conformation of surface-bound proteins. Because different proteins react differently to these changes (as reported for fibrinogen and albumin) it may be possible to use surface chemistry and topography together to control which proteins are present at an interface. I hypothesise that the Vroman effect can be shifted by changes in surface parameters.

An adaptation of the protocol described in Chapter 4 can be made to extend the investigation to monitor multi-component protein systems. Briefly, proteins can adsorb onto varying nano-sized particles with defined terminal chemistry from solutions contining protein mixtures. After a required incubation period aliquots can be taken and the proteins remaining in solution separated and quantified, Figure 6.3. The amount of each protein adsorbed can then be calculated by mass balance.

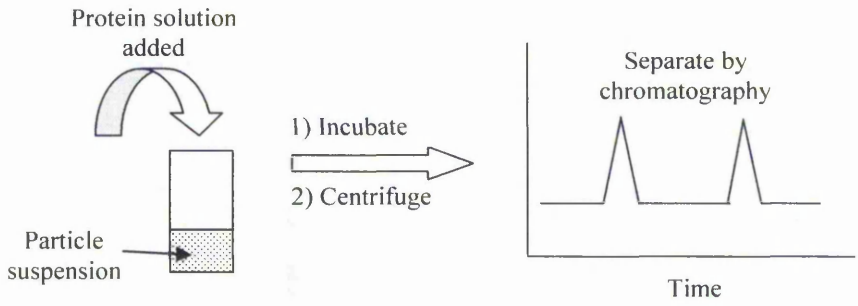

Figure 6.3. Schematic of proposed protocol to assess competitive adsorption with respect to surface chemistry and topography.

Differing incubation times can be investigated to build up a picture of the whole adsorption and enrichment process, whist a wider experiment can be conducted over a number of sized particles with a range of surface chemistries, using a long incubation time to make certain that equilibrium has been established. Simple protein mixtures in ratios which are representative of those observed in a physiological environment could be used as a starting point, although much more sophisticated mixtures could be accommodated after initial method development.

The results of such a study would have an enormous impact on the biomaterials community, highlighting the types of surfaces which could be most useful, i.e. those which guide surface enrichment of the cell adhesive proteins.

6.2.3 Cell-Surface Interactions - Nano-Topography

Protein conformations and adsorption characteristics have been investigated onto nano-sized particles. A direct extension of the work described in Chapter 4 and a progression of the experiments described in section 6.2.2 would be to examine how cells interact with proteins adsorbed on such substrates. This could be achieved by forming a close packed layer of the silica particles as shown in Figure 6.4, and incubating cells in media over these surfaces. Cell-surface attachment proceeds via interaction with the pre-adsorbed protein layer as described in Chapter 1. By examining how cells adhere and proliferate on these surfaces and comparing the observed effects to the conformations of the bound proteins, a broader picture of how surface topography impacts on biocompatibility issues can be realised.

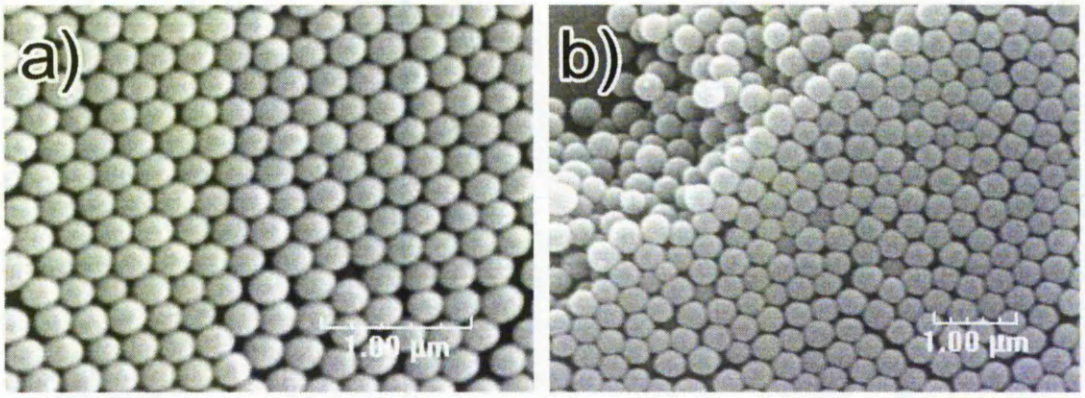

Figure 6.4. Scanning electron micrographs of close packed silica spheres on a glass substrate, a) top face of sphere array and b) a boundary showing the multi-layers of packed spheres.

The silica sphere arrays shown in Figure 6.4 were formed by a 'reverse dip-coating' process wherein the meniscus of a silica / ethanol suspension lowers as the solvent evaporates. Varying sized spheres can be used and these can be chemically modified by silylation, allowing differing surface chemistries to be investigated.

Inverse opaline surfaces can also be formed having even smaller surface features. These can be fabricated by spin coating polymers over silica sphere arrays and subsequently etching away the silica, Figure 6.5.

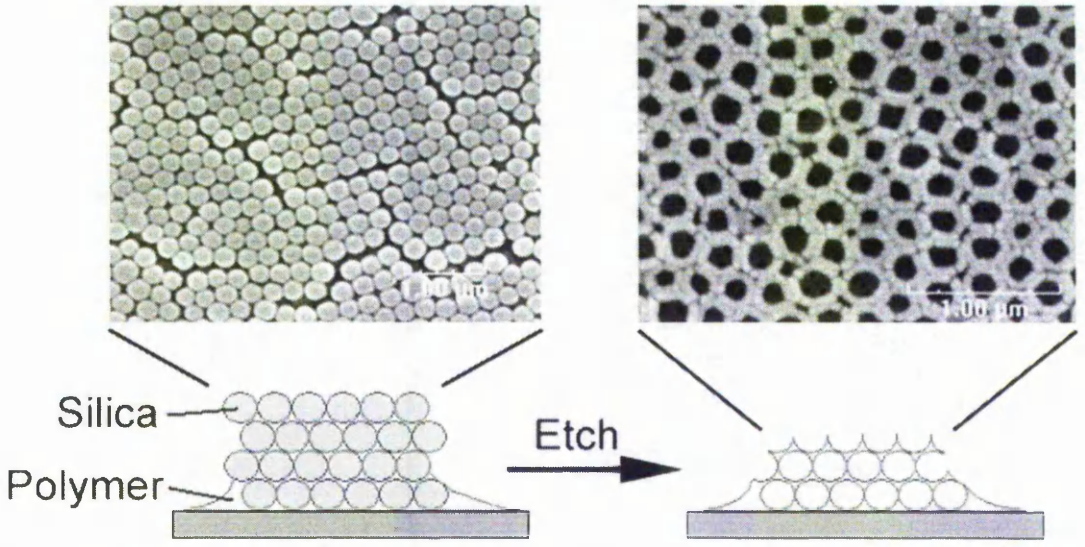

Figure 6.5. Schematic of inverse opal formation showing scanning electron micrographs of surfaces before and after etching.

In-filling of the inverse opal pores with a second material may allow alteration not only of the chemistry presented at the surface but also material properties such as elasticity, stiffness, etc.

6.3 Concluding Remarks

From the investigations reported in this thesis the impact of surface chemistry and topography on the adsorption characteristics of proteins is clear. It has been shown that protein-surface interactions differ greatly depending on the type of protein and the substrate used. The key issues highlighted here are that protein-surface affinity, and therefore the amount of specific proteins at saturation can be controlled. Furthermore it has been demonstrated that conformational changes of surface-bound proteins, which link directly to their activity, can be guided by the underlying surface. Armed with this knowledge one may investigate further to establish the criteria for enhanced materials-those which can either induce rapid cell adhesion or prevent proteins from binding at the two extremes.

Appendix: Publications and Presentations

Publications

1. P. Roach; D. Farrar; C.C. Perry, "Interpretation of Protein Adsorption – Surface Induced Conformational Changes," *J. Am. Chem. Soc.*, **2005**, 127, 8168-8173
2. N.J. Shirtcliffe; G. McHale; M.I. Newton; C.C. Perry; P. Roach, "Porous Materials Show Superhydrophobic to Superhydrophilic Transition," *Chem. Commun.*, **2005**, 24, 3135-3137 – **Chosen for front cover Illustration**
3. P. Roach; D. Farrar; C.C. Perry, "Surface Tailoring for Controlled Protein Adsorption: Effect of Topography at the Nanometre Scale and Chemistry," *J. Am. Chem. Soc.*, **2006,** 128, 3939-3945
4. P. Roach; D. Eglin; K. Rohde; C.C. Perry, "Modern Biomaterials: A Review – Bulk Properties and Implications of Surface Modifications," **2006**, *Journal of Materials Science: Materials in Medicine*, Article In Press
5. P. Roach; N.J. Shirtcliffe; D. Farrar; C.C. Perry, "Rapid Quantification of Surface-Bound Proteins By Fluorometric Assay – Comparison with QCM and Amido Black Assay," *Submitted for publication*
6. N.J. Shirtcliffe; G. McHale; M.I. Newton; C.C. Perry; P. Roach, "Superhydrophobic Phase Separated Sol-gel Films and the Use of Superhydrophobic to Superhydrophilic Transitions for Temperature, Surfactant or Alcohol Measurement," *In preparation*

Oral Presentations

1. **P. Roach**; C.C. Perry; D. Farrar, "Surface-Protein Interactions: Adsorption and Surface-Bound Characteristics," **Highlight Talk** - Federation of European Materials Societies, Euromat, Prague, Sept. **2005**

2. **P. Roach**; C.C. Perry; D. Farrar, "Surface-Protein Interactions: Effects of Chemistry and Topography," Research Day, Smith and Nephew, York, July **2005**
3. **P. Roach**; C.C. Perry; D. Farrar, "Control Over Surface-Protein Interactions," UKSB 4th Annual Meeting, Nottingham University, June **2005**
4. **P. Roach**; C.C. Perry; D. Farrar, "Surface-Protein Interactions: Effects of Chemistry and Topography," Departmental Seminar, Nottingham Trent University, May **2005**

Poster Presentations

1. **P. Roach**; C.C. Perry; D. Farrar, "Protein-Surface Interactions Surface Topography Controlled Protein Deformation," MC7: Functional Materials for the 21st Century, RSC, University of Edinburgh, July **2005**
2. **P. Roach**; C.C. Perry; D. Farrar, "Protein-Surface Interactions, A QCM and GA-FTIR Approach," UKSB 3rd Annual Meeting, University of Brighton, July **2004**
3. **P. Roach**; C.C. Perry; D. Farrar, "Protein-Surface Interactions," Chemistry and Biomaterials Workshop, Faraday Partnership/ UKSB/ RSC/EPSRC, London, Jan. **2004**
4. **P. Roach**; C.C. Perry; D. Farrar; S. Ali; D. Eglin, "Studies of Novel Biomaterials and Surface-Protein Interactions," SET for Britain: National Chemistry Week, Houses of Parliament, London, Nov. **2003**
5. **P. Roach**; C.C. Perry; D. Farrar; S. Ali; D. Eglin, "Studies of Novel Biomaterials and Surface-Protein Interactions," Federation of European Materials Societies, Euromat, Switzerland, Sept. **2003**
6. **P. Roach**; C.C. Perry; D. Farrar, "Measurement of Protein Interactions on Novel Surfaces," UKSB 2nd Annual Meeting, University of Ulster, June **2003**